Integrated Project

ABSOLUTE-Aerial Base Stations with Opportunistic Links for Unexpected & Temporary Events

Contract No. 318632

Deliverable

FP7-ICT-2011-8-318632-ABSOLUTE/D3.2.2

Evaluation of Opportunistic Relaying for Disaster Relief and Temporary Events

Contractual date:	**M30, 31/03/2015**
Actual date:	**M30 27/04/2015**
Authors/Editors:	**Wei Jiang (UDE), Leonardo Goratti (CNET), Akram Hourani (RMIT), Sathyanarayan Chandrasekaran (RMIT), Kandeepan Sithamparanathan (RMIT)**
Participants:	**UDE, RMIT, CNET**
Work package:	**WP3**
Security:	**PU**
Nature:	**Report**
Version:	**V1.0**
Total number of pages:	**123**

Abstract

As the follow-up of D3.2.1, the performance evaluation of the proposed algorithms for ABSOLUTE in the work task of "Opportunistic Relaying" have been carried out. Through theoretical analyses, Ray-tracing simulations and real-world experiments and measurements, the radio channels for the scenarios of ABSOLUTE have been investigated, and the channel models for aerial-to-terrestrial and device-to-device links of ABSOLUTE have been recommended. Based on these channel models, the performance of opportunistic relaying, such as the achieved system capacity, the link reliability, the probability of link connection, the energy efficiency, and the system coverage, have been clarified. The analytical and numerical results of performance are presented in this deliverable.

Keywords

aerial-terrestrial network, amplify-and-forward, decode-and-forward, channel model, cooperative diversity, device-to-device, space-time coding, dynamic spectrum allocation, game theory, in-band relaying, out-of-band relaying, opportunistic relaying, power control, rapid deployment

Table of Contents

Abbreviations 10

Executive summary 13

1 Introduction 14

2 Channel Models 16

2.1 ABSOLUTE model 16

2.1.1 RF planning 16

2.1.2 The development of radio model 17

2.1.3 Ray-tracing simulation 17

2.1.4 The model parameters 18

2.1.5 Numerical examples 19

2.2 Device-to-device channel models 20

2.3 D2D propagation experiments 25

2.3.1 Experiment scenarios 26

2.3.2 Experiment setup 28

2.3.3 Experiment results 28

2.4 Conclusion 31

3 Performance evaluation of D2D relaying 33

3.1 Performance of D2D relaying: Distributed power allocation 34

3.1.1 Distributed power optimal allocation 34

3.1.2 Numerical results 36

3.2 Performance of D2D relaying: The impact of feedback delay 41

3.2.1 Performance of opportunistic relaying 42

3.2.2 Performance of Generalized Selection Combining 44

3.2.3 Numerical results 45

3.3 Performance of D2D relaying: Opportunistic space-time coding 48

3.3.1 Opportunistic space-time coding 49

3.3.2 Numerical results in Rayleigh channels 51

3.3.3 Numerical results in realistic channels 53

3.4 Performance of D2D relaying: Energy efficiency 54

3.4.1 System assumptions 54

3.4.2 Energy saving by relaying 55

3.4.3 Energy saving circle 55
3.5 Performance of D2D relaying: Coverage 57
3.5.1 System model 57
3.5.2 Spatial analysis 58
3.5.3 Performance results 60
3.6 Performance of D2D relaying: Game-theoretic relay selection 61
3.6.1 Network model 62
3.6.2 The game model 62
3.6.3 Performance evaluations 64
3.7 Performance of D2D relaying: Co-channel interference mitigation 66
3.7.1 Power control 66
3.7.2 Performance evaluation 67
3.8 Summary 71
4 Protocol specifications for PLMU and D2D relaying 73
4.1 Protocol specifications 73
4.1.1 PLMU relaying 76
4.1.2 D2D relaying 77
4.2 Performance evaluation 81
4.2.1 Modelling aggregate interference 86
4.2.2 ABSOLUTE use cases 93
4.2.3 Connectivity analysis 94
4.2.4 Numerical results 105
4.3 Conclusions 114
5 Conclusions 116
Bibliography 117
Acknowledgement 123

List of Figures

Figure 1: The selected urban layout. 17

Figure 2: A simulation snapshot of RF rays. 18

Figure 3: Air-to-ground path-loss fordifferent urban environments. 20

Figure 4: Shadowing variations for different environments 20

Figure 5: Results on WINNER II channel model B4. 24

Figure 6: Results on WINNER II channel model C2. 25

Figure 7: ABSOLUTE architecture with D2D communications. 26

Figure 8: Environment 1: Structures on both sides of the road in Hewson on the left and Grundy on the right (Map data: Google, CNES/Atrium). 27

Figure 9: Environment 2: Structures on one side of the road in Follet on the left and Watts on the right (Map data: Google, CNES/Atrium). 27

Figure 10: Environment 3: Forest areas $Reserve_{S01}$ in green and $Reserve_{S02}$ in pink (Map data: Google). 27

Figure 11: Experiment setup 28

Figure 12: Measured path-loss in dB and curve-fitting for all test cases at 922MHz frequency. 30

Figure 13: Measured path-loss in dB and curve-fitting for all test cases at 2.466 GHz. 30

Figure 14: Estimated auto-correlation of shadowing for all the test areas at 922MHz and 2.466GHz. 31

Figure 15: Opportunistic relaying based on device-to-device communications and PLMN 33

Figure 16: The gains of source-relay and relay-destination in a dual-hop relaying channel, ... 35

Figure 17: A uniform quantization example of OPA factor. 35

Figure 18: The mechanism of the proposed power optimal allocation scheme in ABSOLUTE scenario 36

Figure 19: Ergodic capacity of opportunistic relaying with both optimal and equal power allocation. 37

Figure 20: Outage capacity of opportunistic relaying with both optimal and equal power allocation. The target outage probability is set to P_{out}=0.01 for calculating outage capacity. 37

Figure 21: Outage probability of opportunistic relaying with both optimal and equal power allocation over *i.i.d.* Rayleigh channels. The end-to-end target spectral efficiency is R=1 bps/Hz for outage analysis. 38

Figure 22: Outage probability of the proposed scheme by using limited feedback. The end-to-end target spectral efficiency is R=1 bps/Hz for outage analysis. 38

Figure 23: Spectral efficiencies of opportunistic relaying as a function of transmit power in (a) linear and (b) decibels, over D2D and A2T channels. The altitude of aerial base station is set to 1km, the maximum distance among terminals is 50m, and the carrier frequency is 2GHz. 40

Figure 24: Spectral efficiencies of opportunistic relaying as a function of the number of relays over D2D and A2T channels. The altitudes of aerial base station are set to (a) 1km, and (b) 10km, respectively. The maximum distance among terminals equals to 50m and the carrier frequency is 2GHz. 40

Figure 25: Spectral efficiencies of opportunistic relaying as a function of terminal transmit power over D2D and A2T channels. In (a), the altitude of aerial base station is changed to 10km; while in (b), the carrier frequency increases to 5.8GHz. 41

Figure 26: Spectral efficiencies of opportunistic relaying as a function of (a) the transmit power and (b) the number of relays over D2D and A2T channels. The altitude of aerial base station is set to 1km, the maximum distance among terminals increase to 200m, and the carrier frequency is 2GHz. 41

Figure 27: The feedback delay over Aerial-Terrestrial channel. 42

Figure 28: Outage probabilities of ORS in the presence of outdated CSI as a function of average transmit SNR. The simulated results are denoted by Markers while the analytical results by Curves. 43

Figure 29: Ergodic capacities of AF ORS in the presence of outdated CSI as a function of average transmit SNR. The simulated results are denoted by Markers while the analytical results by Curves. 43

Figure 30: Ergodic capacities of AF ORS in the presence of outdated CSI as a function of the number of relays. The simulated results are denoted by Markers while the analytical results by Curves. 44

Figure 31: Schematic diagram of GSC in Aerial-Terrestrial links of ABSOLUTE 45

Figure 32: Outage probability comparisons of GSC and ORS as a function of average transmit SNR when K=4. The simulated results are denoted by Markers while the analytical results by Curves. 46

Figure 33: Outage probability comparisons of GSC and ORS as a function of average transmit SNR when K=8. The simulated results are denoted by Markers while the analytical results by Curves. 46

Figure 34: Ergodic capacity comparisons of GSC and ORS as a function of the average SNR when K=4. 47

Figure 35: Ergodic capacity comparisons of GSC and ORS as a function of average transmit SNR when K=8. 48

Figure 36: Opportunistic space-time coding over Aerial-Terrestrial links of ABSOLUTE. 49

Figure 37: Outage probability comparisons of ORS and OSTC as a function of average transmit SNR. The simulated results are denoted by Markers while the analytical results by Curves. 51

Figure 38: Outage probability comparisons of ORS and OSTC as a function of average transmit SNR, together with GSC in the case of N=4. The simulated results are denoted by Markers while the analytical results by Curves. 52

Figure 39: Outage probability comparisons of ORS, GSC and OSTC as a function of correlation coefficient, when K=8 and SNR=20dB. The simulated results are denoted by Markers while the analytical results by Curves. 52

Figure 40: Outage probability comparisons of ORS and OSTC as a function of transmit power at the terminals over the realistic channels models. The number of relays K=15 and the target spectral efficiency is 3.5bps/Hz. 53

Figure 41: The energy saving circle. 55

Figure 42: The expected value of the energy saving gain η versus the average number of relays inside the saving zone. 57

Figure 43: Link-level success probability vs. the distance from the serving transmitter [31]. 60

Figure 44: Coverage extension of PLMU, by D2D relaying. 61

Figure 45: ABSOLUTE architecture showing the game-theoretic relay selection. 61

Figure 46: Network Model for Game-Theoretic Optimal Relay Selection. 62

Figure 47: Price-Power profile showing αi and Cost of all relays. 64

Figure 48: κi values v/s the game sequence for different R-MM-UEs. 65

Figure 49: Rewards of all R-MM-UEs over the game sequence. 65

Figure 50: Network scenario considered for D2D power control 66

Figure 51: An example of a simulated network for D2D relaying power control. 67

Figure 52: Distribution of the uplink SIR (γ) at the AeNB for the cell edge MMUE access, for varying number of D2D communication links. 68

Figure 53: Distribution of the D2D link SIR (ρ) for varying number of D2D communication links. .. 68

Figure 54: Outage probability variation in the D2D links for different path-loss exponents. 69

Figure 55: Outage probability variation for the uplink access with different LAP altitudes. 69

Figure 56: Outage probability variation in the D2D links for different LAP altitudes. 70

Figure 57: Outage probability for the D2D transmissions with and without power control. 70

Figure 58: Outage probability for the uplink transmissions with and without power control. 71

Figure 59: FME functional block diagram. 74

Figure 60: Different relaying mode configurations in ABSOLUTE architecture. 76

Figure 61: D-beacon interval for a network in D2D mode. 78

Figure 62: Modified D-beacon interval for D2D Relay Mode. 81

Figure 63: Scattering of points (or interferers) on the two-dimensional space. 86

Figure 64: Two-state channel model for the behaviour of a UE. 95

Figure 65: PLMU relaying with no CSI knowledge. Connectivity probability ω for α=2.01, Π_{on}=0.8 vs. normalized test link distance r_0 and for different values of the Matern HC distance of the spatial PLMU process. 107

Figure 66: SIT for a UE trying to attach to a PLMU relay with no CSI knowledge, α=2.01, Π_{on}=0.8 vs. normalized test link distance r_0 and for different values of the Matern HC distance for the spatial PLMU process. 107

Figure 67: PLMU relaying with no CSI knowledge. Connectivity probability ω for α=4, Π_{on}=0.8 vs. Test link distance r_0 and different values of the Matern HC distance for the spatial PLMU process. 108

Figure 68: SIT for a UE trying to attach to a PLMU relay with no CSI knowledge, α=4, Π_{on}=0.8 vs. normalized test link distance r_0 and different values of the Matern HC distance of the spatial PLMU process. 108

Figure 69: D2D and PLMU relaying with no CSI knowledge. Connectivity probability ω for the D2D network vs. normalized test link distance r_0, α=4, W=10 MHz and Matern HC distance r_m=0.03. 109

Figure 70: SIT for D2D and PLMU relaying with no CSI knowledge of a UE trying to attach to a D2D network vs. normalized test link distance (r_0), α=4, W=10 MHz and Matern HC distance r_m=0.03. 110

Figure 71: D2D and PLMU relaying with no CSI knowledge: probability ω versus the normalized test link distance (r_0) and Matern HC distance (r_m). 110

Figure 72: D2D and PLMU relaying with partial CSI knowledge for path-loss compensation. D2D network connectivity probability ω vs. normalized test link distance (r_0) with α=4, W=10 MHz and Matern HC distance r_m=0.03..... 111

Figure 73: SIT for D2D and PLMU relaying with partial CSI knowledge and path-loss compensation for a UE trying to attach to a D2D network vs. normalized test link distance (r_0), α=4, W=10 MHz and Matern HC distance r_m=0.03. 112

Figure 74: D2D and PLMU relaying with partial CSI knowledge for path-loss compensation: probability ω versus the normalized test link distance (r_0) and Matern HC distance (r_m)..... 112

Figure 75: D2D and PLMU relaying with perfect CSI knowledge for path-loss and fading compensation. D2D network connectivity probability ω vs. the normalized test link distance with α=4, W=10 MHz and Matern HC distance r_m=0.03. 113

Figure 76: SIT for D2D and PLMU relaying with perfect CSI knowledge for path-loss and fading compensation for a UE trying to attach to a D2D network vs. normalized test link distance (r_0), α=4, W=10 MHz and Matern HC distance r_m=0.03. 113

List of Tables

Table 1: Selected Urban Environments. 17
Table 2 RF model parameters 19
Table 3: A1, B4 and C2 WINNER II Channel Models [19]. 22
Table 4: Experiment Parameters 28
Table 5: Experiments' results 30
Table 6: Notations and Parameters. 59
Table 7: Simulation Parameters 64
Table 8: Numerical parameters for simulations 104
Table 9: Mapping of relays modes selected for connectivity analysis with ABSOLUTE use cases. . 114

Abbreviations

3GPP	The third generation partnership project
AAA	Authentication, authorization and accounting
ABSOLUTE	Aerial Base Stations with Opportunistic Links For Unexpected & Temporary Events
AeNB	Aerial evolved Node B
API	Application Programming Interface
AF	Amplify and forward
Cell-ID	Cell identity
CF	Compress and forward
CRN	Cognitive relay node
CSI	Channel state information
CQI	Channel Quality Indicator
CSMA/CA	Carrier sense multiple access with collision avoidance
CTS	Clear-to-send
DAS	Distributed antenna system
DeNB	Donor evolved Node B
DL/UL	Downlink/Uplinks
DSTC	Distributed space-time coding
DF	Decode and forward
DSP	Digital Signal Processing
DSA	Dynamic spectrum access
D2D	Device-to-device
eNodeB	Evolved Node B
EPC	Evolved Packet Core
EPA	Equal power allocation
FDD	Frequency Division Duplexing
FME	Flexibility Management Entity
GSC	Generalized selection combining
HAP	High Altitude Platforms
HARQ	Hybrid automatic request

LAP	Low Altitude Platforms
LNA	Low-noise amplifier
LOS	Line-of-sight
LTE	Long Term Evolution
LTE-A	Long Term Evolution Advanced
MAC	Medium Access Control
MAP	Medium Altitude Platforms
MBSFN	Multicast broadcast single-frequency network
MGF	Moment generating function
MIMO	Multiple-Input Multiple-Output
MME	Mobility Management Entity
MRC	Maximal ratio combining
NLOS	None line-of-sight
OR	Opportunistic relaying
ORS	Opportunistic relay selection
OPA	Optimal power allocation
OFDM	Orthogonal Frequency Division Multiplexing
OFDMA	Orthogonal Frequency Division Multiple Access
OSTC	Opportunistic space-time coding
PDCCH	Physical downlink control channel
PDSCH	Physical downlink shared channel
PDCP	Packet Data Control Protocol
PDF	Probability density function
PDN	Packet Data Network Gateway
PHY	Physical Layer
PLMU	Portable land mobile unit
PPDR	Public protection and disaster relief
PS	Public safety
PU	Primary user
QoS	Quality of Service
RB	Resource block
RTS	Ready-to-send

RLC	Radio Link Control
RN	Relay node
RF	Radio frequency
RRC	Radio Resource Control
RSRP	Reference Signal Received Power
RSSI	Received Signal Strength Indicator
SDR	Software-defined radio
SGW	Serving Gateway
SINR	Signal-to-interference-plus-noise ratio
SNR	Signal-to-noise ratio
SON	Self-organizing network
SS	Spectrum sensing
SU	Secondary user
TeNB	Terrestrial evolved Node B
TETRA	Terrestrial Trunked Radio
TDD	Time-Division Duplexing
TU	Typical Urban
UE	User Equipment

Executive summary

This technical report is the second deliverable of ABSOLUTE Work Task 3.2 "**Opportunistic relaying to increase PHY Layer communication resilience**", which is contractually due at M30.

In the ABSOLUTE project, opportunistic relaying has been chosen as the key technique to improve the reliability and resilience of communication links in the two defined scenarios of ABSOLUTE, i.e., Public Safety and temporary events, which are specified in detail in "D2.1: Use Cases Definition and Scenarios Description" [1]. In the first deliverable of this work task, i.e., "D3.2.1: *Initial Approaches for Opportunistic Relaying for Disasetr Relief and Temporary Events*" [2], some algorithms enabling the technique of opportunistic relaying to be applied for ABSOLUTE scenarios, including optimal relay selection, distributed power allocation, power control, co-channel interference mitigation, energy-efficient optimization, and resistance to the feedback delay, have been proposed. These algorithms can be applied for a wide range of ABSOLUTE uses cases, that is, ABS.UC.01 (according to [1]), ABS.UC.02, ABS.UC.03, ABS.UC.04, ABS.UC.05, ABS.UC.06, ABS.UC.10, ABS.UC.11, ABS.UC.13, ABS.UC.14, ABS.UC.18, ABS.UC.21, and ABS.UC.22 for the scenario of Public Safety, and ABS.UC.15, ABS.UC.16, ABS.UC.19, ABS.UC.20 and ABS.UC.23 for the scenario of temporary events. To clarify achievable performance of the proposed algorithms in the system architecture of ABSOLUTE, which is specified in "D2.5.2: Architecture Reference Model" [3], the evaluation of these algorithms has been carried out in the second phase of T3.2. Thanks to the tight and fruitful cooperation among involved project partners, the theoretical analyses, the link-level simulations, as well as some real-world experiments and measurements, have been done to shed light on the system performance of opportunistic relaying in the scenarios of Public Safety and temporary events. The obtained performance results, as well as the used radio channel models, the simulation setup and experimental procedure, and the recommendations on enhancement/modification of LTE protocols, are presented in this deliverable.

The work in this deliverable is derived from other ABSOLUTE deliverables, which includes but is not limited to:

[1] D2.1: Use Cases Definition and Scenarios Description"

[2] D3.2.1: Initial Approaches for Opportunistic Relaying for Disasetr Relief and Temporary Events

[3] D2.5.2: Architecture Reference Model

[4] D2.6.1: System-wide simulations planning

[5] D2.3: Aerial platforms study

[6] D5.1.1: LTE-A AeNodeB implementation requirement specifications for cognitive LTE extension

[7] D5.2.1: Portable land mobile rapid deployment unit specification

[8] D3.4.3: Performance Analysis of Direct Mode LTE Communications

[9] D3.1.1: Requirements and Specification for Spectrum Awareness

[10] D3.3.1: Initial approaches for Cognitive Spectrum Assignment using Distributed Artificial Intelligence

1 Introduction

The history of human beings is a history of fighting with natural disasters such as forest fire, flood, typhoon, and earthquake, as well as social conflicts such as riots and terrorist attacks. Recent history has shown that telecommunication infrastructures play a key role in the aftermath of an emergency disaster or unexpected events. In most cases, however, the legacy terrestrial infrastructure is seriously compromised and cannot guarantee reliable services for citizens and rescue teams. Although satellite communications are more reliable, the limited system capacity and the limited number of subscribers restrict the provision of high quality-of-service. In a nutshell, it is widely recognized that the current public safety networks cannot provide sufficient capacity and quality-of-service for broadband applications. The mission for research community, i.e., ABSOLUTE project, is to explore more powerful communication technologies and solutions to prevent and at least alleviate the damages from the natural disaster and emergency events.

Opportunistic relaying provides an efficient way to increase the resilience of communications links and will be of particular importance in Public Safety and temporary event scenarios, where coverage from base stations may be patchy and dynamically varying. For example, the signal coverage of AeNodeB is expected to rapidly change at the roll-out and roll-back phase, referring to ABS.UC.19 and ABS.UC.20 defined in [1]. In the ABSOLUTE project, therefore, opportunistic relaying has been chosen as the key technique to improve the reliability and resilience of communication links in the two defined scenarios of ABSOLUTE, i.e., Public Safety and temporary events, which are specified in detail in "D2.1: Use Cases Definition and Scenarios Description" [1]. In the first phase of the work task in T3.2, some algorithms enabling the technique of opportunistic relaying to be applied for ABSOLUTE have been proposed, including, optimal relay selection, distributed power allocation, power control, co-channel interference mitigation, energy-efficient optimization, and resistance to the feedback delay. The research findings have been published in several IEEE journal and conference papers, and have also been given in the first deliverable of T3.2, i.e., "D3.2.1: *Initial Approaches for Opportunistic Relaying for Disasetr Relief and Temporary Events*" [2]. In the second phase of T3.2, it is naturally to clarify the achievable performance of the proposed algorithms. Hence, the theoretical analyses, the link-level simulations, as well as the real-world experiments and measurements, have been carried out to evaluate the performance of opportunistic relaying in the scenarios of Public Safety and temporary events.

The accurate channel models are fundamental to the build-up of a wireless communication system and plays a vital role in the process of algorithm design, protocol optimization and performance evaluation. From a practical point of view, we need a model that combines all the aspects of radio channel including path loss, shadowing and small-scale fading, rather than a theoretical one such as the Rayleigh channel that only takes the small-scale fading into account. In ABSOLUTE, the propagation characteristics of radio channels are distinct from that of the conventional channels in terrestrial cellular systems, referring to "D2.6.1: System-wide simulations planning document" [4], due to the differences on antenna height, propagation distance, mobility speed, surrounding environment, and etc. Therefore, the propagation characteristics of Aerial-to-Terrestrial and Device-to-device channels are required to be clarified. By means of ray-tracing, the ABSOLUTE channel model was proposed to simulate the Aerial-to-Terrestrial (A2T) links, while WINNER II channel model was selected to be used for Device-to-Device (D2D) communications based on the theoretical analysis and

experimental measurements. The performance evaluation of the proposed algorithms has been carried out based on these models.

In ABSOLUTE, the coverage area of a rapidly-deployed Aerial eNodeB (AeNB), which was specified in "D2.3: Aerial platforms study" [5] and "D5.1.1: LTE-A AeNodeB related implementation requirement specifications for cognitive LTE extension" [6], is patchy and dynamically varying since the network planning and optimization are impossible to be carried out in the case of disaster relief and some emergency events. On the other hand, the portable and suitcase-like eNodeB, referred to as Portable Land Mobile Unit (PLMU) in ABSOLUTE, which is specified in "D5.2.1: Portable land mobile rapid deployment unit specification" [7], can be also established to provide a specific coverage for hot spots. When a multi-mode user equipment (MM-UE) cannot access the AeNB, this MM-UE could search its neighbouring MM-UEs and send its data via D2D communication links to neighbours, which are attached on the network and can help to forward this data to the infrastructure. This mechanism is called D2D relaying. The detail of D2D transmission mode can refer to "D3.4.3: Performance Analysis of Direct Mode LTE Communications" [8]. If an MM-UE is merely covered by a PLMU or the link quality from PLMU is better than from AeNB, and PLMU works as the standalone mode without direct Evolved Packet Core (EPC) connections, PLMU could relay MM-UE's signal towards AeNB, which is called PLMU relaying. If the sensor networks are applied, the gateway of the sensor networks can access to the PLMU to report the collected information, which is similar to the case of MM-UE. In summary, opportunistic relaying in ABSOLUTE can be categorized into two types: D2D relaying (applicable to the uses cases of ABS.UC.01, ABS.UC.02, ABS.UC.18, ABS.UC.19, ABS.UC.20, ABS.UC.21, ABS.UC.22, ABS.UC.23) and PLMU relaying (corresponding to ABS.UC.03, ABS.UC.04, ABS.UC.05, ABS.UC.06, ABS.UC.10, ABS.UC.11, ABS.UC.13, ABS.UC.14, ABS.UC.15, ABS.UC.16).

The rest of this deliverable is organized as follows. In Chapter 2, the channel models of A2T and D2D channels have been investigated and the proposed ABSOLUTE model and the selected WINNER II model have been given. In Chapter 3, we will first clarify the achievable performance of D2D relaying under Aerial-Terrestrial architecture of ABSOLUTE. The theoretical analyses, the simulation and the experiments have been carried out to evaluate the achievable performance. In Chapter 4, some considerations about how to modify the LTE/LTE-A standard specifications to integrate the opportunistic relaying in the practical system have been presented. And the performance results of PLMU relaying and D2D relaying in the context of LTE system have been given.

2 Channel Models

Accurate channel models are fundamental to the build-up of a wireless communication system and play a vital role in the process of algorithm design, protocol optimization and performance evaluation. From a practical point of view, we need a model that combines all the aspects of radio channel including path loss, shadowing and small-scale fading, rather than the theoretical one such as the Rayleigh distribution that only takes the small-scale fading into account. In ABSOLUTE, the propagation characteristics of radio channels are distinct from that of the conventional channels in terrestrial cellular systems due to the differences on antenna height, propagation distance, mobility speed, surrounding environment, and so on. That is to say, the Aerial-to-Terrestrial (A2T) channels between a Low-Altitude Platform (LAP) and mobile terminals on the ground and the Device-to-Device links among the terminals are required to be modelled for facilitating the performance evaluation of the ABSOLUTE system. The channel models used in this deliverable are aligned with the channel models applied for the system simulation, referring to "D2.6.1: System-wide simulations planning" [4]. Different from the system-level simulation, the simulation in this deliverable focus on the link-level, so there still exist some different aspects. That is the motivation to give an independent chapter in this deliverable to report on the channel models of such aerial-terrestrial system architecture. The first section studies the A2T channels and introduces the proposed ABSOLUTE model, while the second section discusses the D2D-related channel modelling.

2.1 **ABSOLUTE model**

In this section, we present a statistical propagation model for predicting air-to-ground path loss between a low-altitude platform and a mobile terminal. The prediction is based on the urban environment properties and is dependent on the elevation angle between the terminal and the platform. This model was partly presented in [11] and [12].

2.1.1 RF planning

To deploy an aerial network, it is important to properly estimate the required infrastructure to establish the expected services. Accordingly, Radio Frequency (RF) planning should be carried out in the target area to produce the estimation for (i) the required number of Aerial Base Stations, (ii) the optimum altitude of platforms [12], and (iii) the expected Quality-of-Service (QoS) level.

The proposed channel model in this section allows aerial network operators to perform accurate RF planning without the need to the site-specific ray-tracing simulation. In the aftermath of a disaster, it is unlike to easily obtain the 3D-model of city buildings. In this case, the RF planning could be realized based on the urban statistical parameters. As recommended by the International Telecommunication Union (ITU) [13], a standardized model with three simple parameters α_o, β_o and γ_o, can be employed to describe the general geometrical statistics of a certain urban area. These parameters are explained as below:

- α_o represents the ratio of the built-up land area to the total land area (dimensionless);
- β_o represents the mean number of buildings per unit area (buildings/km^2);

- γ_o is a scale parameter that describes the buildings' height distribution according to Rayleigh probability density function:

$$f(h) = \frac{e^{-\frac{h^2}{2\gamma^2}}}{\gamma^2} h$$

In order to cover a wide range of application scenarios, four simulation environments were selected for this model, similar to [14], i.e., (i) Suburban Environment that also covers the rural areas, (ii) Urban Environment that is the most common situation representing average European cities, (iii) Dense Urban Environment representing some types of cities where buildings are in close proximity to each other, (iv) Urban Environment with high-rise buildings, representing modern cities with skyscrapers. ITU statistical parameters are relatively straightforward to obtain from a certain city's urban style, for example, Table 1 summarizes the selected parameters for these environments.

Table 1: Selected Urban Environments.

Environments	α	β	γ
Suburban	0.1	750	8
Urban	0.3	500	15
Dense Urban	0.5	300	20
High-rise Urban	0.5	300	50

2.1.2 The development of radio model

It is well-known that a certain urban planning code and style exists for every city or suburb. So even if two cities share the same statistical parameters, this does not imply sharing the same building layout. Accordingly, a model-city plan should be adopted for allowing a valid general mathematical approximation. In the ABSOLUTE RF model, we select a virtual city environment similar to Manhattan grid as depicted Figure 1, which has an array of structures (buildings or houses) of an assumed width *W* and an inter-building spacing of *S*.

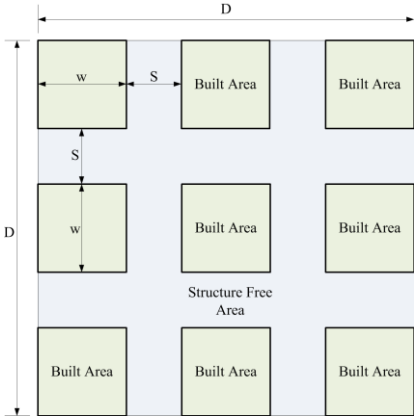

Figure 1: The selected urban layout.

2.1.3 Ray-tracing simulation

A ray-tracing simulation was conducted using the software of Wireless InSite® for three types of rays (*Direct*, *Reflected* and *Refracted*), while *transmitted* rays were neglected in order to simplify the calculations. It is important to note that the availability of *optical* line-of-sight between the LAP and a

receiver does not necessarily mean that the RF line-of-sight condition is satisfied. That is because RF signals require much wider ellipsoids than the optical light according to Fresnel Zones Concept [15].

We show a sample of ray tracing for a signal receiver in Figure 2, where the ray colour indicates the intensity of the electric field. RF rays are combined in vector manner, taking into consideration both the magnitude and the phase of the rays. In order to obtain the coverage of the LAP over the target area (1,000m×1,000m), we simulate the received power of more than 37,000 uniformly distributed receivers, where the electric field of all the captured rays is summed (complex summation) and the received power is calculated from the resulting electric field.

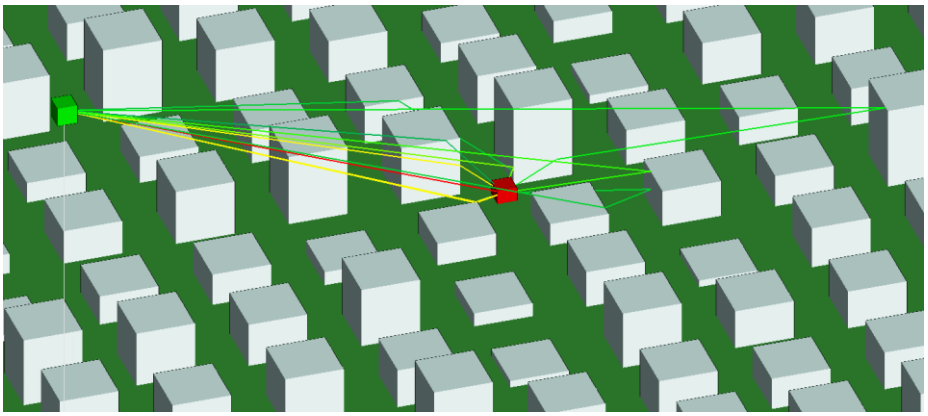

Figure 2: A simulation snapshot of RF rays.

The ray-tracing simulator yields a list of all receivers including the corresponding path loss of each receiver (we call these results as samples), and the samples are then further processed in order to obtain the excessive path loss component as we define it in the following formula:

$$\eta_n = PL_n - FSPL_n,$$

where PL_n is the path loss at the n^{th} receiver, FSPL is the free space path-loss for a certain receiver that can be derived from Friis equation and be represented as:

$$FSPL_n = 20\log\left(\frac{\Delta h}{\sin(\theta_n)}\right) + 20\log(f_{MHz}) - 27.55$$

In the next subsection, we explain the method to calculate the excessive path-loss, while the detailed derivation of the model can be found in the published paper [12].

2.1.4 The model parameters

We model the excessive path-loss as a normally-distributed random variable, i.e., $N(\mu_\zeta,\sigma_\zeta)$, where ζ is the propagation group. There are two main propagation groups ζ={G1,G2}, where each group has different statistical behaviour. Starting with μ_ζ, the mean excessive path-loss did not show a clear dependency on the elevation angle but rather a constant value, which can be obtained by averaging all samples in a certain propagation group, the results are listed inTable 2. While the general trend of the standard deviation of G1 and G2 is fitted to the following expression:

$$\sigma_\xi = a_\xi \exp(-b_\xi \theta),$$

where a_ξ and b_ξ are dependent to the carrier frequency and environment, which can be obtained by curve fitting using Damped Least-Squares (DLS) method, as listed in Table 2. It is important to note

that the proposed model here is valid only for the elevation angles larger than 15°, since low elevation angles have a very limited probability of receiving the signal from the LAP. The resulting empirical curve fitting equation for group occurrence probability (of group 1) is chosen to balance simplicity and accuracy, and it is a function of the elevation angle, given by

$$P_1(\theta) = c\,(\theta - 15)^d,$$

where θ is the elevation angle (the angle at which the AeNB is seen from a certain receiver), c and d are empirical curve fitting parameters, as listed in Table 2 as well. Group 2 occurrence probability is simply the complement of the probability of group 1, i.e., $P_2(\theta) = 1 - P_1(\theta)$.

Table 2 RF model parameters

	700 MHz			
	Suburban	**Urban**	**Dense Urban**	**Highrise Urban**
μ_1	0.0	0.6	1.0	1.5
μ_2	18	17	20	29
(a_1,b_1)	(11.53, 0.06)	(10.98, 0.05)	(9.64, 0.04)	(9.16, 0.03)
(a_2,b_2)	(26.53, 0.03)	(23.31, 0.03)	(30.83, 0.04)	(32.13, 0.03)
(c,d)	(0.77, 0.05)	(0.63, 0.09)	(0.37, 0.21)	(0.06, 0.58)

	2,000 MHz			
	Suburban	**Urban**	**Dense Urban**	**Highrise Urban**
μ_1	0.1	1.0	1.6	2.3
μ_2	21	20	23	34
(a_1,b_1)	(11.25, 0.06)	(10.39, 0.05)	(8.96, 0.04)	(7.37, 0.03)
(a_2,b_2)	(32.17, 0.03)	(29.6, 0.03)	(35.97, 0.04)	(37.08, 0.03)
(c,d)	(0.76, 0.06)	(0.6, 0.11)	(0.36 , 0.21)	(0.05, 0.61)

	5,800 MHz			
	Suburban	**Urban**	**Dense Urban**	**Highrise Urban**
μ_1	0.2	1.2	1.8	2.5
μ_2	24	23	26	41
(a_1,b_1)	(11.04, 0.06)	(10.67, 0.05)	(9.21, 0.04)	(7.15, 0.03)
(a_2,b_2)	(39.56, 0.04)	(35.85, 0.04)	(40.86, 0.04)	(40.96, 0.03)
(c,d)	(0.75, 0.06)	(0.56, 0.13)	(0.33, 0.23)	(0.05, 0.64)

2.1.5 Numerical examples

As illustrated in Figure 3, the difference between utilizing the conventional log-distance path-loss model and the proposed aerial path-loss model. The average path-loss is calculated as

$$PL_{ATG} = PL_1 P_1 + PL_2 P_2\,,$$

where PL_1 is the mean path-loss of propagation group (1) that corresponds to receivers favouring line-of-sight condition or near-line-of-sight condition, while the second propagation group (2) generally corresponds to receivers with no LAP line-of-sight but still receiving coverage via strong reflection and refraction. It is noted that free-space path loss model cannot be used to represent air-to-ground channel. We also compare with the extended version of the FPSL, which is the log-distance model:

$$PL = 10\,\alpha \log(d) + C,$$

where α is the propagation exponent and C is a constant, selecting $\alpha = 2.5$ and $C = 20\,log(f) - 27.55$, and $f = 2.6\,GHz$. We can clearly notice log-distance model cannot represent the air-to-ground channel as well.

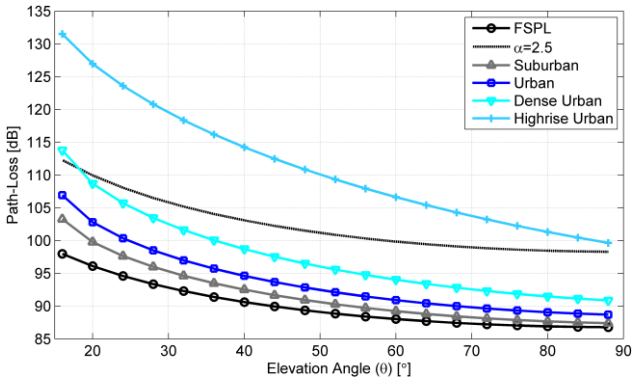

Figure 3: Air-to-ground path-loss fordifferent urban environments.

The previous example compared the mean received power of the different urban scenarios. Next, we visualize the effect of shadowing variations by plotting the heat-map of the coverage generated beneath an AeNB in Figure 4, increasing path-loss starting from Suburban, Urban, Dense Urban, towards High-Rise Urban, and the transmit power is assumed to be 0 dBm.

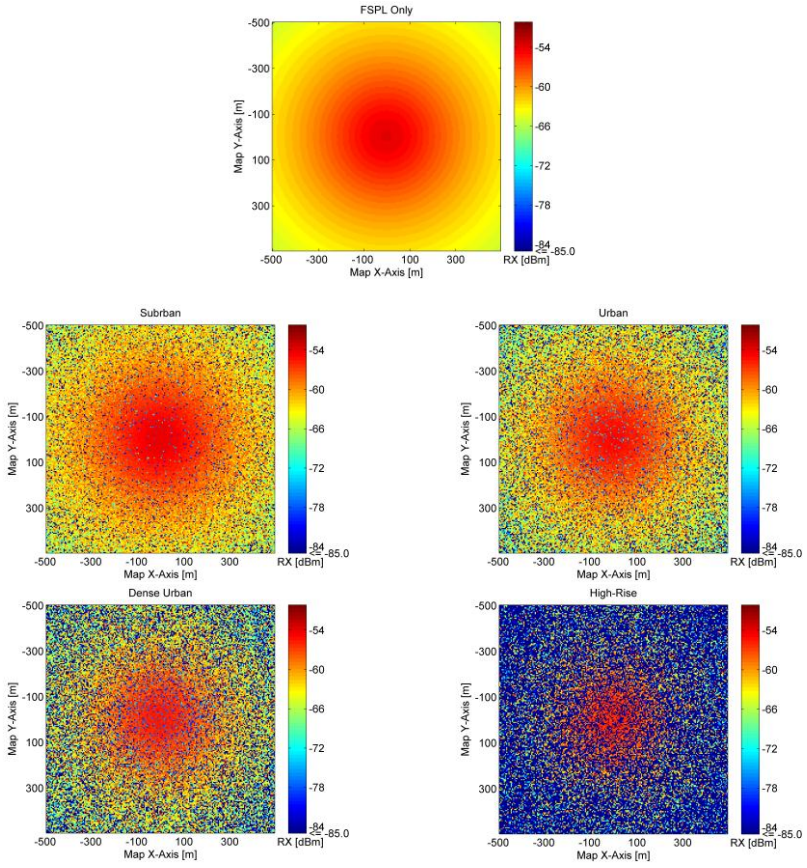

Figure 4: Shadowing variations for different environments

2.2 **Device-to-device channel models**

The previous section has depicted the channel modelling that is relevant to the link between the aerial base station and the mobile terminals. The other important one that is necessary to explore is the device-to-device channels, where the mobile terminals communicate with one another in a direct

mode. Besides, the so-called Portable Land Mobile Unit (PLMU), which is an element of the ABSOLUTE system providing additional coverage and capacity, can be regarded as a special equipment of D2D communications. That is because the portable suitcase-like base stations will be rapidly deployed on the ground or be placed on the top of trucks. The antenna height of PLMN in these cases is typically from 1 to 10 meters, which is very similar to the mobile terminal.

Basically, the most important factors to affect the channel characteristics are the carrier frequency, the propagation distance, the height of antenna, the propagation environment, and the movement of transmitter and receiver. As we all know, a plenty of channel models, such as COST, SCME and WINNER II, have been generated during the research and development of cellular communication systems in the past decades. However, these models are specifically developed for the radio channels between the terrestrial base stations and the terminals. The following factors contribute to the specific propagation characteristics of D2D channels:

(1) The antenna heights of terrestrial base station are normally ranged from 25m to 50m for urban macro-cell, 10m for urban micro-cell, and 3-6m for indoor hot spots. In D2D communications, the antenna heights of both transmitter and receiver should be around 1.5m, even the PLMU's antenna height is typically up to 10 meters.

(2) In general, the scatters are close to the terminal while locating far away from base station. Both the transmitter and receiver in D2D channels are surrounded by the scatters, leading to different channel characteristics especially in multi-antenna scenarios.

(3) As we know, the movement of transmitter or receiver cause Doppler spread. Although the terrestrial base stations are always static, the terminals at both ends of D2D link are highly possible to be in motion.

(4) As given in a survey of Intel [16], the rough estimated distance between two terminals connecting D2D link in a dense urban area is merely about 10m, which is much shorter than the typical distance observed in cellular systems.

After a careful investigation of all the existing channel models, we revealed the following conclusion. For the D2D communication links, we can take advantage of Scenario A1 of WINNER II channel models. The antenna heights of both BS and MS are ranged from 1 to 2.5 meters, which are quite similar to the propagation environment encountered by D2D communications. The applicable frequency range is also from 2 to 6 GHz. Similarly, the scenarios B4 and C2 of WINNERII model will be used here to evaluate the link between PLMU and UE.

The WINNER II project developed channel models suitable for different propagation environments, including indoor and outdoor, Line-of-Sight (LOS) and non-LOS (NLOS). In particular, WINNER II is based on a stochastic geometric modelling approach in which the radio signal is made of rays that are assumed to arrive in clusters. Each cluster corresponds to a path in the multipath environment with each cluster (or path) made of several rays (or sub-paths). Referring to the documentation explaining the MATLAB implementation of each WINNER II model [17], there are up to 24 paths with a fixed number of rays equal to 20. The models allow taking into account several propagation parameters (number of stations, number of links, antenna height, indoor/outdoor, room and street environments, etc), as well as different RF parameters (antenna type MIMO or SISO, delay, power, angle-of-arrival and angle-of-departure of each ray). Typical outputs that can be collected with WINNER II software is the RMS delay spread of the received signal.

In D3.2.1 "*Initial Approaches for Opportunistic Relaying for Disaster Relief and Temporary Events*" [18], the scenario A1 of WINNER II has been employed to simulate the D2D channels. Similarly, the study carried out here evaluates the capacity of a communication link between PLMU and a UE focusing on the achievable link capacity for scenarios B4 and C2. B4 is particularly suitable for outdoor NLOS environments, whereas C2 can be used to obtain results for urban environment in NLOS conditions. Relevant parameters for B4 and C2 channel models derived from the WINNER II Interim Report are also provided in Table 3.

Table 3: A1, B4 and C2 WINNER II Channel Models [19].

Scenario	**Definition**	**LoS/NLoS**	**Mobility [km/h]**	**Frequ-ency [GHz]**	**CG[1]**	**Note**
A1	Indoor small office /residential	LOS/ NLOS	**0-5**	**2-6**	**LA**	
B4	Outdoor to indoor/ Outdoor typical urban	NLoS	0-5	2-6	MA	B1 or C2 to the wall/window
		$PL = PL_b + PL_{tw} + PL_{in}$ where $PL_b = PL_{B1}(d_{out} + d_{in})$ $PL_{tw} = 14 + 15(1 - \cos(\theta))^2$, $PL_{in} = 0.5 d_{in}$ $PL_{NLoS} = PL_{LoS}(d_1[m]) + 20 -$ $12.5 n_j + 10 n_j \log_{10}(d2[m])$, with $n_j = \max(2.8 - 0.0024 d_1[m], 1.84)$ Shadow fading std: $7dB$ $3\,m \le d_{out} + d_{in} \le 1000\,m$ $h_{BS} = 10\,m$ $h_{MS} = 3n_{FL} + 1.5\,m$				
C2	Typical urban macro-cell	NLoS	0-120	2-6	MA WA	

1 CG stands for Concept Group in which LA, MA and WA denotes Local Area, Metropolitan Area and Wide Area, respectively.

		$PL = [44.9 - 6.55\log_{10}(h_{BS}[m])\log_{10}(d[m])]$ $+ 34.46 + 5.83\log_{10}(h_{BS}[m])$ $+ 20\log_{10}(f[GHz]/5.0)$ Shadow fading std: $8dB$ $50\,m \le d \le 5\,km$ $h_{BS} = 25\,m$ $h_{MS} = 1.5\,m$				

Let $\boldsymbol{H}(t)$ denote the channel matrix which is obtained after running MATLAB simulations and let $s(t) = \sqrt{P_t}\,p(t)$ denotes the transmitted signal, P_t denoting the transmitted power and $p(t)$ is a suitable way of representing and OFDM signal with normalized unit power. The received signal $r(t)$ can thus be written as

$$r(t) = s(t) \otimes \mathbf{H}(t) \qquad (1)$$
$$P_R = P_T \left|\mathbf{H}(t)\right|^2 = P_T \sum_{l=1}^{L} \left|h_l(t)\right|^2,$$

where $8 \le L \le 24$ is the total number of multipath components, P_R is the received power of the signal, h_l denotes the channel impulse response of the lth path in a cluster, and $\otimes$ is the convolution operation. Relying on [20] for numerical values, the achievable capacity evaluated in terms of the number of bits per transmission dimension (b) is computed as

$$b = \frac{1}{2}\log_2\left(1 + \frac{P_R}{N_0 W}\right) \quad \text{[bits/dimension]}, \qquad (2)$$

where W denotes the signal bandwidth of LTE system, $N_0/2$ is the two-sided power spectral density of the Additive White Gaussian Noise (AWGN), and P_R is the received power. To obtain numerical results, the preferred system parameters include W=10MHz, P_R=23 dBm and N_0=-174 dBm/Hz.

Numerical results for WINNER II channel model B4 are shown in Figure 5. The figure shows the received power and the achievable bits/dimension. The antenna height of the PLMU is assumed equal to 10m, while that of UE is 1.5m. The speed of user is assumed to be 1.1m/s and the number of traversed floors is one. It shows that the simulated distance separating transmitter and receiver is up to 100m and the achievable bits/dimension decreases as the distance increase. For short distances, the communication links can use even a 64QAM (b=6), whereas it reduces to a QPSK (b=2) approaching 100m. Interestingly such a decrease is in line with the information conveyed by the Channel Quality Indicator (CQI), which can be used to select a higher Modulation and Coding Scheme (MCS) in correspondence to a higher CQI value that could occur more likely for shorter distance separations between the transmitter and the receiver.

Numerical results for the WINNER II channel model C2 are shown in Figure 6. The figure shows the received power and the achievable bits/dimension. Since channel model C2 is suitable for wider areas, higher speed is considered here as well. The antenna height of the PLMU is assumed equal to 25 m, while that of the UE is 1.5 m. The speed of the user is assumed here equal to 14 m/s and the simulated distance separation between transmitter and receiver is up to 800 m. Conclusions similar to those already presented in Figure 6 can be derived also for this case. In general, as anticipated in [18],

increasing the antenna height with respect to channel model B4 has a positive effect since it allows keeping approximately the same number of bits/dimension for higher distance values.

It is finally worth reminding that simulation results of WINNER II channel models A1 for D2D communication mode were showed already in D3.4.3 "*Performance Analysis of Direct Mode LTE Communications"* [21] and similarly can be reused for the case of D2D relay although not showed here.

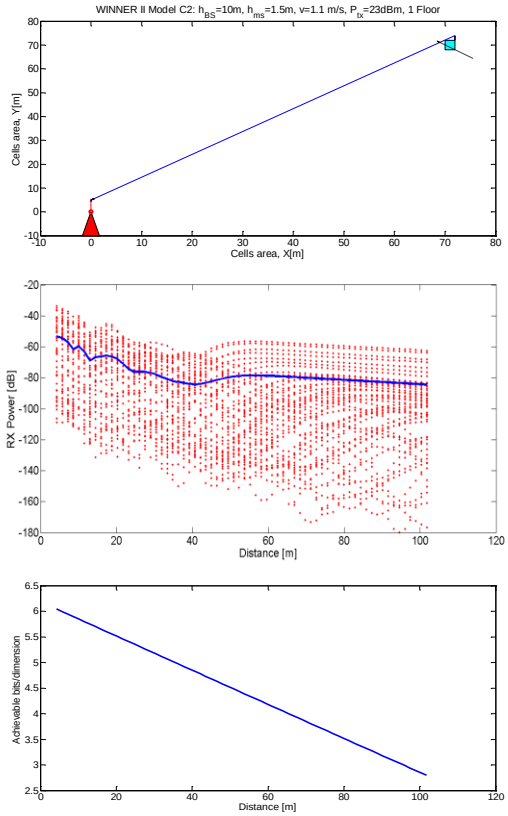

Figure 5: Results on WINNER II channel model B4.

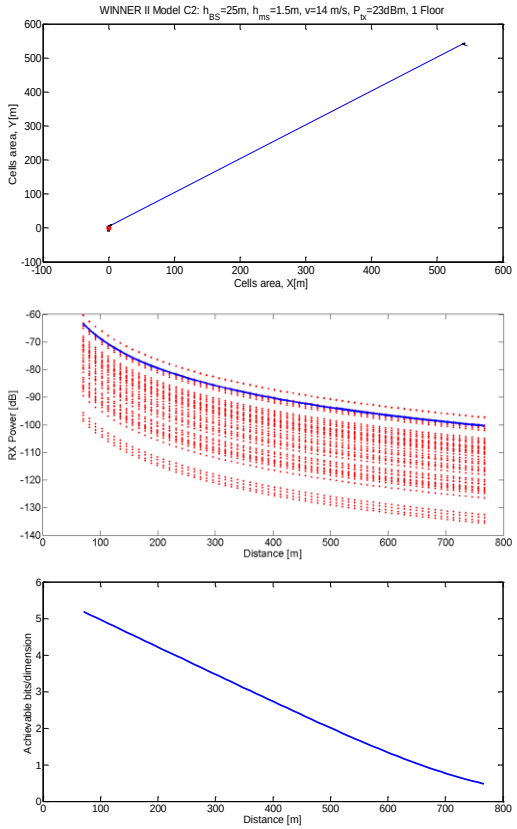

Figure 6: Results on WINNER II channel model C2.

2.3 **D2D propagation experiments**

D2D technology has shown tremendous promise to add significant gains to the communications network. The envisioned benefits are the coverage extension, capacity improvement and higher energy efficiency. D2D is the main technology that enables peer to peer communications without the need for centralized infrastructure to support communications. Hence, this technology proves to be important in the context of public safety networks. Figure 7 shows the ABSOLUTE architecture (referring to D2.5.2 "*System Architecture reference model"*) where D2D communications will be used between the mobile terminals as shown by the red dotted circle.

Mainly Due to the lower transmitter height, the D2D channel varies greatly from the conventional terrestrial channel used to model cellular communications where the transmitters are mounted on rooftops or on towers. There has been various propagation measurements conducted to model D2D channels in the literature. They have measured the channel for different frequencies in different channel conditions and have suggested different models. Some of the related works are mentioned below. In [22], [23], [24], the author has characterized the D2D channel for different environments and different frequencies. In [11], the authors have studied the path-loss behaviour of D2D channel in an urban environment for millimetre-wave frequencies. In [24], the author has studied the effect of shadowing caused by human body in cellular D2D communications. However, we are not aware of any previous works to model the D2D channel in a rural area. It is important to characterize the D2D channel in a rural area for ABSOLUTE with respect to the forest fire scenario, earthquake, and flood considered in D2.1 "*Use cases definition and scenarios description"*. Hence, we performed

experiments in a rural area in Australia to characterize the D2D channel in terms of path loss exponents and the standard deviation of shadowing. We also present to the shadowing correlation analysis. We performed the experiments for two ISM (license-exempt) bands 922 MHz and 2.466 GHz, which are close to the target frequency bands of 700MHz and 2.6GHz for ABSOLUTE, as specified in D3.1.1 "*Requirements and Specification for Spectrum Awareness"*.

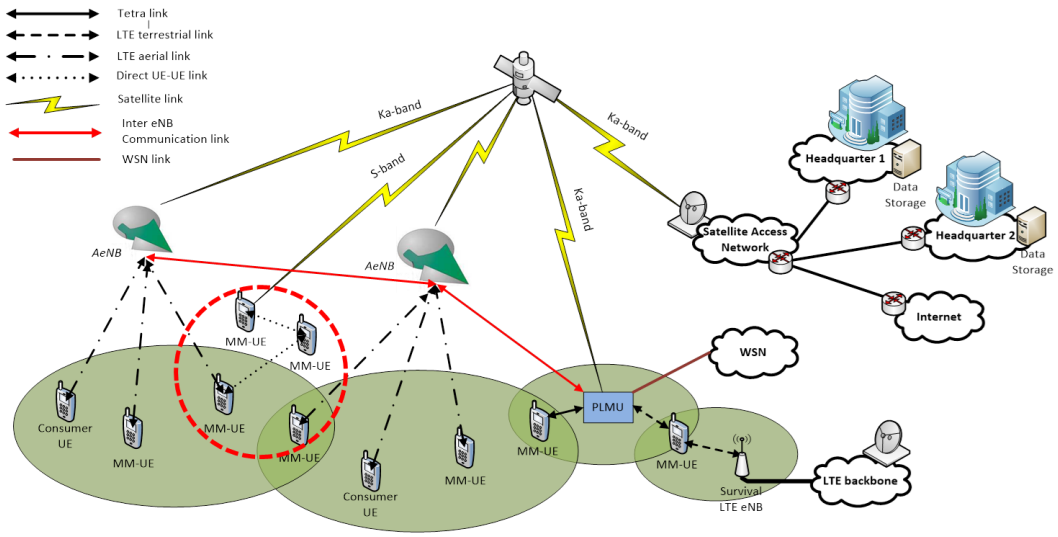

Figure 7: ABSOLUTE architecture with D2D communications.

2.3.1 Experiment scenarios

In this section, we detail the selected environments, the procedure and the experiment setup used to conduct the measurements. Three different environments in a rural area of Australia were selected, which can be classified as:

- **Structure on both sides of the road:** Figure 7 depicts the test areas selected for the first environment, i.e., Hewson and Grundy, the transmitters' locations and the path taken during the experiments. As can be seen from this figure, man-made structures are present on both sides of the road. The width of the street is around 5 meters for both the test areas. The taken path is around 450 metres in Hewson and 400 metres in Grundy. Both areas had a limited pedestrian and vehicular traffic. There was no inclination in the street level for the Grundy test area. However, for Hewson test area, there was a downward slope after 160 metres away from the transmitter location.

Figure 8: Environment 1: Structures on both sides of the road in Hewson on the left and Grundy on the right (Map data: Google, CNES/Atrium).

- **Structure on one side of the road:** Figure 9 depicts the test areas selected for the second environment, i.e., Follet and Watts, the transmitters' locations and the path taken during the experiments. As can be seen from this figure, man-made structures are present only on one side of the road and the other side is vegetation. The width of the street is around 4 meters for both the test areas. The taken path was around 450 metres in Follet and 550 metres in Watts. Both areas had a limited pedestrian and vehicular traffic. There was no inclination in the street level for both the test areas.

Figure 9: Environment 2: Structures on one side of the road in Follet on the left and Watts on the right (Map data: Google, CNES/Atrium).

- **Forest:** Figure 10 depicts the test areas selected for a forest, $Reserve_{S01}$ and $Reserve_{S02}$, the transmitters' locations and the path taken during the experiments. This environment emulates the scenario considered for the use case of Forest Fire, as specified in D2.1 of ABSOLUTE "*Use cases definitions and scenarios description*". The forest contained tall trees and half-to-one metre bushes. The green line in Figure 10 shows the path taken during the experiment for $Reserve_{S01}$ and the pink line for $Reserve_{S02}$. $Reserve_{S01}$ had partial line-of-sight conditions whereas $Reserve_{S02}$ had non-line-of-sight conditions. The path taken for $Reserve_{S01}$ was around 160 metres and for $Reserve_{S02}$ was around 130 metres from their respective transmitter locations.

Figure 10: Environment 3: Forest areas $Reserve_{S01}$ in green and $Reserve_{S02}$ in pink (Map data: Google).

2.3.2 Experiment setup

Figure 11 shows the experiment setup used to conduct the measurements. The used transmitter was a continuous wave wide-band transmitter capable of producing a maximum output power of 10dBm. The transmitter was mounted on a telescopic mast at a height of 1.5 metres emulating a victim carrying an UE. The transmitter was connected to a transmit antenna with -10.2dBi gain at the carrier frequency of 922MHz and 2.75dBi gain at 2.466GHz. The receiver used in the experiments was a handheld spectrum analyser (Agilent FieldFox) connected to a receive antenna which had similar parameters as that of the transmit antenna. A laptop was connected to the spectrum analyser that recorded the measurements using MATLAB. The laptop was also connected to GPS device, which provided the receiver's location. The receiver was condensed into a portable form and was carried by a person maintaining a height of 1.5 metres at all times during the experiment. Table 4 shows the experiment parameters used during measurements. In every test area, each sample recorded contained the following:

- The received power of the channel being measured.
- GPS coordinates of the location of the receiver.

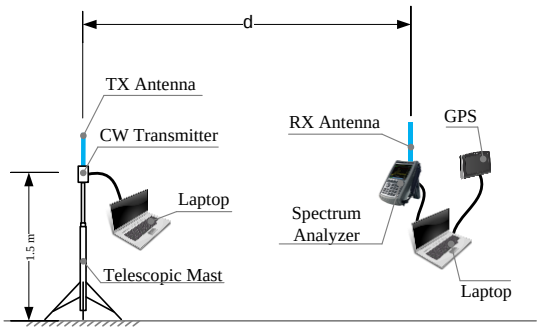

Figure 11: Experiment setup

Table 4: Experiment Parameters

Parameters	Values
Frequency	922MHz and 2.466GHz
Integration Bandwidth	5kHz
Cable Loss	2.33dB at 922MHz and 4.44dB at 2.466GHz
Transmit and Receive Antenna Gain	-10.2dBi at 922MHz and 2.75dBi at 2.466GHz
Transmit and Receive Antenna Height	1.5metres

2.3.3 Experiment results

Based on the experiment setup, we have conducted the experiments in all the test areas and recorded the measurements for 922MHz and 2.466GHz. The samples recorded were post processed in MATLAB. The received channel power was compensated for the gains/losses of all the equipment used in the experiment. The distance between the transmitter and receiver was calculated using the GPS coordinates recorded in the sample points. The received power was quantised and averaged over a bin-width of 1 metre. This was performed to give equal weightage to the sample points during linear

fitting. We present the experiment results in terms of path-loss exponents, standard deviation of shadowing phenomenon and shadowing correlation analysis, as follows.

- Path-loss exponent. We adopt the widely accepted log-normal shadowing model [25], given by,

$$PL(d) = PL(d_0) + 10\alpha \log_{10}\left(\frac{d}{d_0}\right) + X_\sigma,$$

where $PL(d)$ is the path-loss in dB at a distance d from the transmitter, $PL(d_0)$ is the reference path-loss in dB at a distance d_0 metres from the transmitter, α is the path-loss exponent, and X_σ is the zero-mean Gaussian distributed random variable with a standard deviation of σ dB, which signifies the shadowing phenomenon of the received signal. To find the path-loss exponent and the standard deviation of shadowing, we perform linear fitting of the measured sample points. Figure 12 and Figure 13 show the measured path-loss and the calculated path-loss exponents α for different test cases at 922MHz and 2.466GHz respectively. It can be observed that the path-loss exponent for the third environment (i.e., Forest) is much higher than other environments.

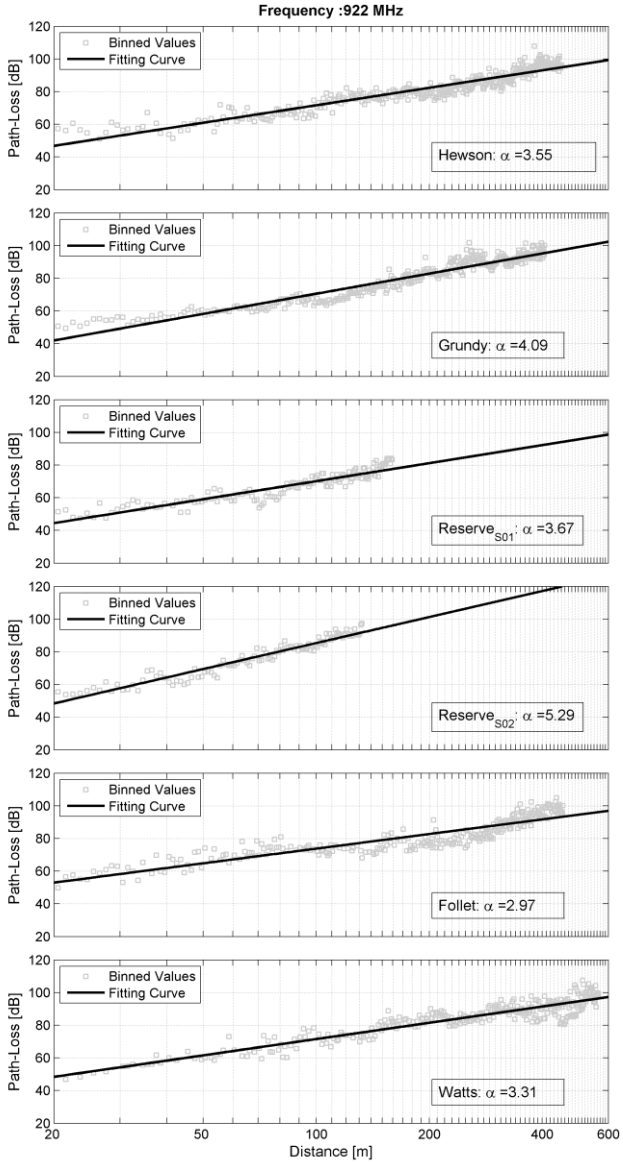

Figure 12: Measured path-loss in dB and curve-fitting for all test cases at 922MHz frequency.

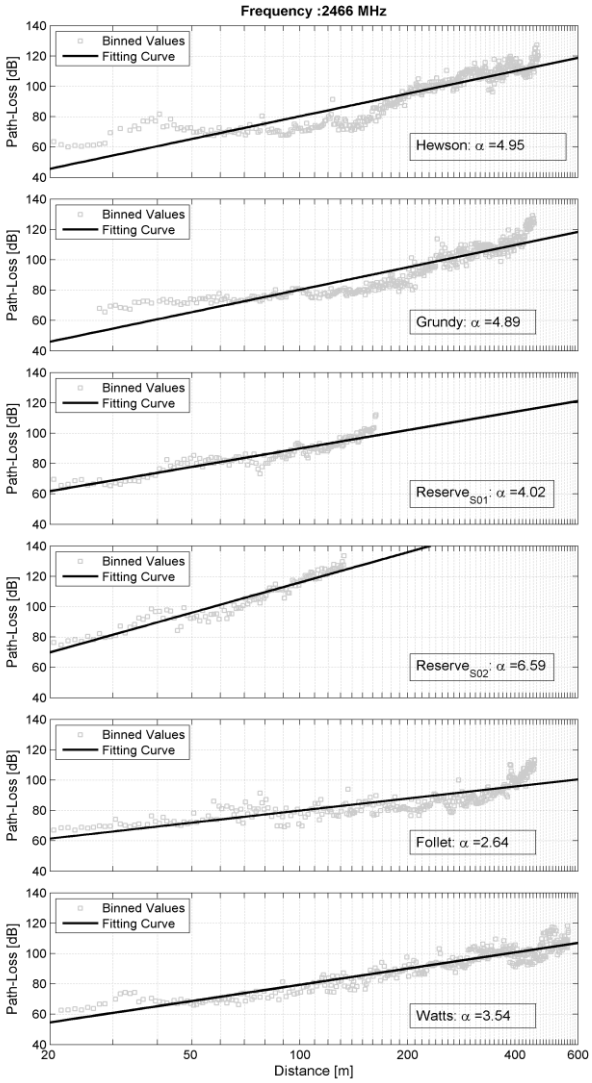

Figure 13: Measured path-loss in dB and curve-fitting for all test cases at 2.466 GHz.

- Standard deviation of Shadowing: It was get by calculating the standard deviation of the measured path-loss with respect to the linearly fitted line. Table 5 shows the standard deviation obtained in different test areas at 922 MHz and 2.466 GHz. The table also notes the path-loss exponents and $PL(d_0)$ obtained for different test areas.

Table 5: Experiments' results

Environments	**922 MHz**			**2.466 GHz**		
	$\boldsymbol{PL(d_0)}$	$\boldsymbol{\alpha}$	$\boldsymbol{\sigma\ (dB)}$	$\boldsymbol{PL(d_0)}$	$\boldsymbol{\alpha}$	$\boldsymbol{\sigma\ (dB)}$
Hewson	46.81	3.55	4.32	45.70	4.95	7.10
Grundy	41.99	4.09	4.36	46.07	4.89	7.41
Reserve$_{S01}$	44.49	3.67	4.89	61.83	4.02	5.63
Reserve$_{S02}$	48.43	5.29	4.86	69.82	6.59	5.81
Follet	52.96	2.97	5.39	61.44	2.64	6.62
Watts	48.40	3.31	4.70	54.63	3.54	5.11

- Shadow correlation analysis: the auto-correlation function of the shadowing component X_σ is investigated. The shadowing component was estimated using

$$\widehat{X_\sigma} = PL(d) - \overline{PL(d)},$$

where $PL(d)$ is the measured path-loss at distance d and $\overline{PL(d)}$ is the computed path-loss by using the path-loss exponent value α. Assuming $\widehat{X_\sigma}$ as a wide sense stationary process, the auto-correlation function is given by

$$\widehat{R_X} = \left|E\left[\widehat{X_\sigma}(d+\Delta d)\right]\left[\widehat{X_\sigma}(d)\right]\right|$$

The auto-correlation analysis was done for all test areas for a displacement distance Δd=1 and the results are shown in Figure 14. We can observe that the correlation rapidly reduces over 10's of meters in all cases. Especially, for Reserve_{S01}, Reserve_{S02} and Watts, it reduces to zero around 20 metres [26], [27].

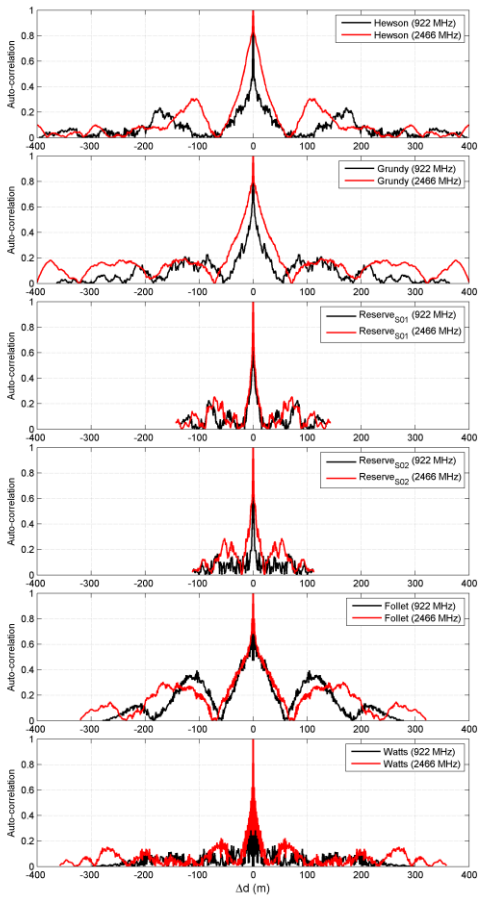

Figure 14: Estimated auto-correlation of shadowing for all the test areas at 922MHz and 2.466GHz.

2.4 **Conclusion**

According to the scenarios and use cases defined in D2.1 [1] and the system architecture in D2.5.2 [3], together with the channel models used for the system-level simulations in D2.6.1 [4], we have identified two kinds of channels that should be modelled for the link-level simulation of opportunistic relaying. The propagation characteristics of Aerial-to-Terrestrial and Device-to-device channels are required to be clarified. Aerial-to-Terrestrial path-loss behaves in a different manner compared to the conventional terrestrial propagation models. By means of ray-tracing, we have presented an empirical

A2T stochastic channel model, named the ABSOLUTE channel model to simulate the Aerial-to-Terrestrial (A2T) links. Besides, we have carried out the real-world experimental measurements, and obtained the experimental results of the D2D channel for rural areas at 922MHz and 2.466GHz in terms of path-loss exponents, the standard deviation and correlation of shadowing. The experimental sites are the typical "Callania" scenario defined in D2.1. Then, the WINNER II channel model was selected to be used for Device-to-Device (D2D) communications based on the theoretical analysis and experimental measurements. These channel models will be applied to evaluate the opportunistic relaying for ABSOLUTE in the following chapters.

3 Performance evaluation of D2D relaying

Recalling the ABSOLUTE system architecture specified by D2.5.2 "*System Architecture reference model"* within WP2 (see [3]), we have derived an architecture of opportunistic relaying, as shown in Figure 15. In the ABSOLUTE system, the coverage area of a rapidly-deployed AeNB is patchy and dynamically varying since a network planning and optimization necessary for a commercial network are impossible to be carried out in the case of disaster relief and some emergency events such as terrorist attacks. A large number of terminals may be out of AeNB's coverage, e.g., victims trapped inside destroyed buildings or villages in remote mountain areas in an earthquake. Moreover, although some mobile terminals can establish communication links with the AeNB, it is still possible that the received signal is very weak due to the blockage of buildings. In these cases, the mechanism of opportunistic relaying can be applied to improve the system's resilience and robustness. When a MM-UE cannot directly access the network, such as the use case of ABS.UC.22, this MM-UE would firstly send its data via device-to-device communication links to neighbouring terminals, which are attached on the network and help to forward this data to the infrastructure. In some use cases, one or several portable eNodeBs, referred to as PLMU in ABSOLUTE; can be also established to provide a stronger coverage for a hot spot. If a UE is merely covered by a PLMU or the link quality from PLMU is better than from AeNB, which always happens in the practical scenario, PLMU could relay UE's signal towards the destination. As shown in Figure 15, the opportunistic relaying system in ABSOLUTE can be categorized into two types: D2D relaying and PLMU relaying.

In this chapter, we will first clarify the performance of D2D relaying under Aerial-Terrestrial architecture of ABSOLUTE, and then results of PLMU relaying will be given in the next chapter. The results of D2D relaying is related to the ABSOLUTE use cases of ABS.UC.01, ABS.UC.02, ABS.UC.18, ABS.UC.19, ABS.UC.20, ABS.UC.21, ABS.UC.22, and ABS.UC.23.

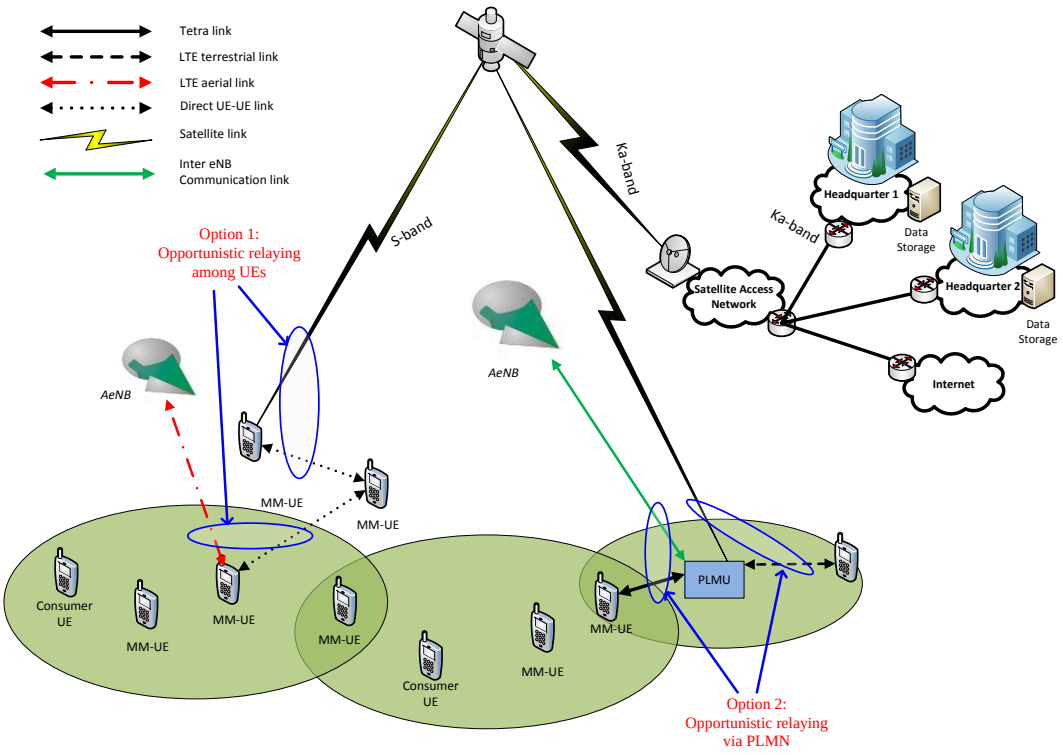

Figure 15: Opportunistic relaying based on device-to-device communications and PLMN

3.1 **Performance of D2D relaying: Distributed power allocation**

In opportunistic relaying, radio signals in the uplink have to go through two hops: (i) from the source terminal to an opportunistically selected relay, i.e., a neighbouring terminal in D2D relaying, and (ii) from the relay to an aerial base station, and vice versa in downlink. Specific to ABSOLUTE, the propagation distances among neighbouring terminals are far smaller than the distance between the terminal and AeNB. According to an investigation by a research group from Intel [28], the statistically average communicating distance between two terminals is about 10 meters in a typical urban area. However, the distance between a terminal on the ground and an AeNB mounted on low-altitude platform is often on the order of kilometres. As we know, the difference in the path loss between two hops of such an unbalanced relaying channel in ABSOLUTE's terrestrial-aerial scenario might be up to 100dB. Obviously, it is very inefficient to neglect the effect of power allocation, so that just using the same power at the first and second hops. Therefore, we propose an optimal power allocation scheme for opportunistic relaying, especially for this terrestrial-aerial network in the scenario of ABSOLUTE. The mechanism of the proposed scheme is briefly overviewed below, and the whole works have been published in [29] and [30].

3.1.1 Distributed power optimal allocation

Conditioned on a flat-fading channel realization h_{xy}, $x, y \in \{s, i_b, d\}$, where *s* is the source, i_b the best relay, and *d* the destination, the maximum rate of reliable communication supported by this channel is computed by $C_{xy} = \log_2(1+\left|h_{xy}\right|^2 \lambda\gamma)$, where $\gamma = P/\sigma^2$ denotes the end-to-end transmit SNR. As shown in **Erreur ! Source du renvoi introuvable.**, in a dual-hop relay channel, the end-to-end system capacity is determined by *the minimal one*, i.e., $C = \min(\mathrm{C}_{si_b}, \mathrm{C}_{i_b d})$. Thus, this system is very vulnerable, since if either hop falls into a deep fade it will substantially degrade the performance. Obviously, it will be gainful to allocate more transmit power to the bottleneck in order to achieve a balanced capacity between source-relay and relay-destination channels. The end-to-end capacity can be maximized if and only if

$$C_{si_b} = C_{i_b d}$$

Then, the OPA factor can be given by

$$\lambda_{i_b} = \frac{|h_{i_b d}|^2}{|h_{si_b}|^2 + |h_{i_b d}|^2},$$

where channel gains h_{si_b} and $h_{i_b d}$ are already known at the best relay simply from channel estimations. Therefore, this scheme actually operates in a distributed manner without any network coordination among terminals for getting the global CSI.

However, λ_{i_b} is a real number ranged from 0 to 1, i.e., $\lambda_{i_b} \in (0,1)$, which cannot be transmitted information-lossless with a finite number of bits in digital communications. According to the principle of limited feedback [31], λ_{i_b} is better to be quantized into a few power-control bits prior to the signalling. As an example, we give a uniform quantization method:

$$\hat{\lambda}_{i_b} = \frac{\lfloor \lambda_{i_b} N \rfloor + 0.5}{N},$$

where *b* represents the number of feedback bits, $N = 2^b$ is cardinality of the quantized set $\{\lambda_{i_b}\}$, and $\lfloor \cdot \rfloor$ stands for the floor function. For example, the case of $b = 1$ corresponds to $N = 2$ and $\lambda_{i_b} \in \{0.25, 0.75\}$, as illustrated in Figure 17.

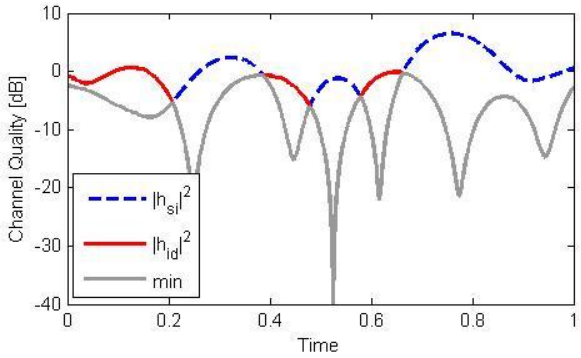

Figure 16: The gains of source-relay and relay-destination in a dual-hop relaying channel,.

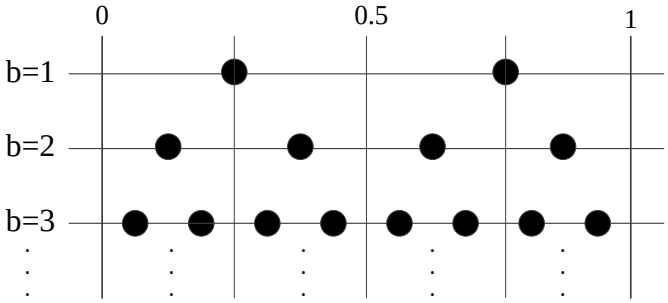

Figure 17: A uniform quantization example of OPA factor.

Recalling that the best relay will broadcast a flag packet to announce its presence after the timer expires. It is convenient to combine power-control bits with the flag, taking advantage of the existing feedback channel instead of bringing an extra signalling message. To specify this scheme more clearly, the main steps are listed as follows.

- First, i^{th} relay gets instantaneous CSIs of h_{si_b} and $h_{i_b d}$ based on the pilots, e.g. the reference symbols embedded in LTE radio frames.
- Second, i^{th} relay evaluates its path quality h_i. After received a pilot from the destination, each relay immediately starts a timer with duration inversely proportional to h_i.
- Reusing the local CSI at the best relay, the OPA coefficient λ_{i_b} can be figured out according to **Erreur ! Source du renvoi introuvable.**, and further quantized into several power-control bits. Once the timer expires, the best relay transmits *a combined flag packet* containing the flag as well as power-control bits $\hat{\lambda}_{i_b}$. Accordingly, the source and the best relay adjust their power to $\hat{\lambda}_{i_b} P$ and $(1-\hat{\lambda}_{i_b})P$, respectively, at the follow-on data transmission.

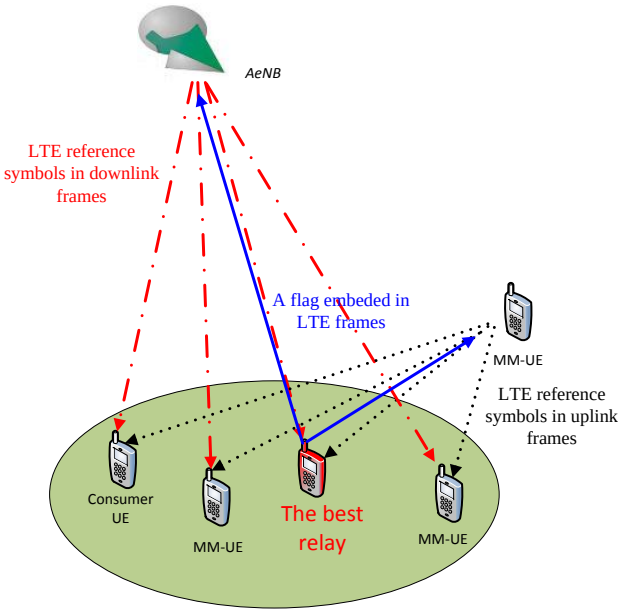

Figure 18: The mechanism of the proposed power optimal allocation scheme in ABSOLUTE scenario

3.1.2 Numerical results

To corroborate benefits of using the distributed power allocation between the source and best relay, we set up simulations to obtain numerical results with respect to channel capacity and outage probability of decode-and-forward opportunistic relaying. Monte-Carlo simulations, where a single source-destination pair under the help of *M* relays, have been established. Rayleigh fading with 10^6 independent realizations and a normalized channel gain of 1 are applied to each link. The outage behaviours are analysed under the assumption of an end-to-end target spectral efficiency of R=1bps/Hz. It is noted that corresponding target rate of either link in dual-hop relaying should be doubled, i.e., 2bps/Hz, due to the half-duplex transmission mode. In fairness to compare, all power allocation schemes are based on the same end-to-end power constraint of an average transmit SNR of 0~24dB.

Figure 20 shows ergodic capacity of DF opportunistic relaying with both OPA and Equal-Power Allocation (EPA). As we can see, more than 1dB SNR improvement can be acquired by the proposed scheme when M=2 relays at spectral efficiency level of 5bps/Hz. Despite the SNR improvement slightly decreases with the increase number of relays, more than 0.5dB are still available even in M=16. The proposed scheme can be also applied to the single relay system M=1 where no relay selection is involved, and a SNR gain of 1.5dB achieved. Figure 20 illustrates outage capacity results with an outage probability of P_{out}=0.01. At spectral efficiency level of 2bps/Hz, the proposed scheme outperforms EPA about 2dB in the case of M=2 or 4.

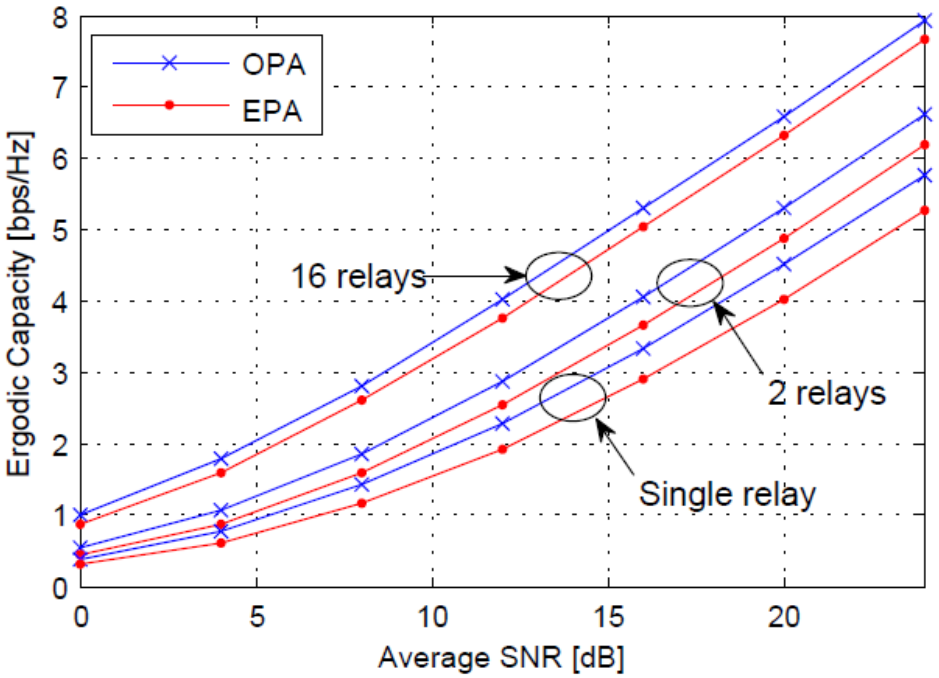

Figure 19: Ergodic capacity of opportunistic relaying with both optimal and equal power allocation

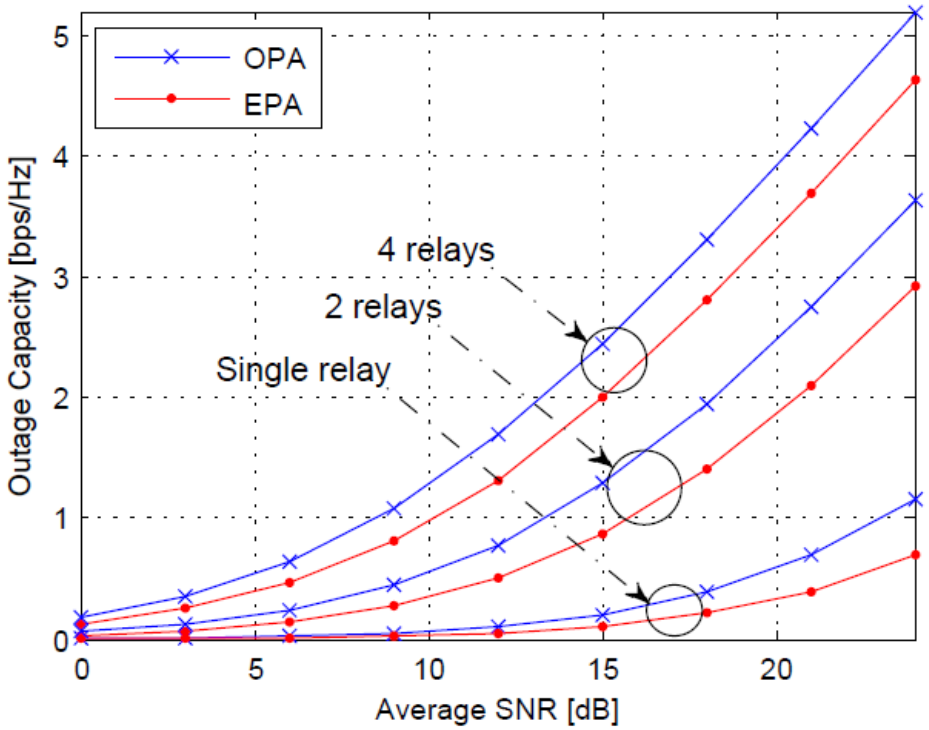

Figure 20: Outage capacity of opportunistic relaying with both optimal and equal power allocation. The target outage probability is set to P_{out}=0.01 for calculating outage capacity.

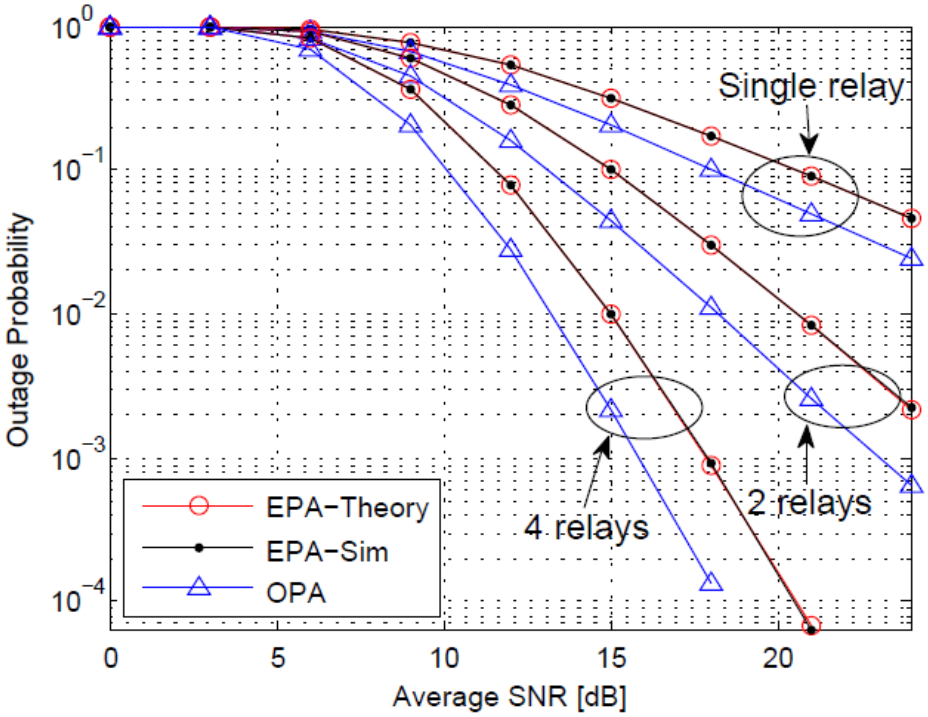

Figure 21: Outage probability of opportunistic relaying with both optimal and equal power allocation over *i.i.d.* Rayleigh channels. The end-to-end target spectral efficiency is R=1 bps/Hz for outage analysis.

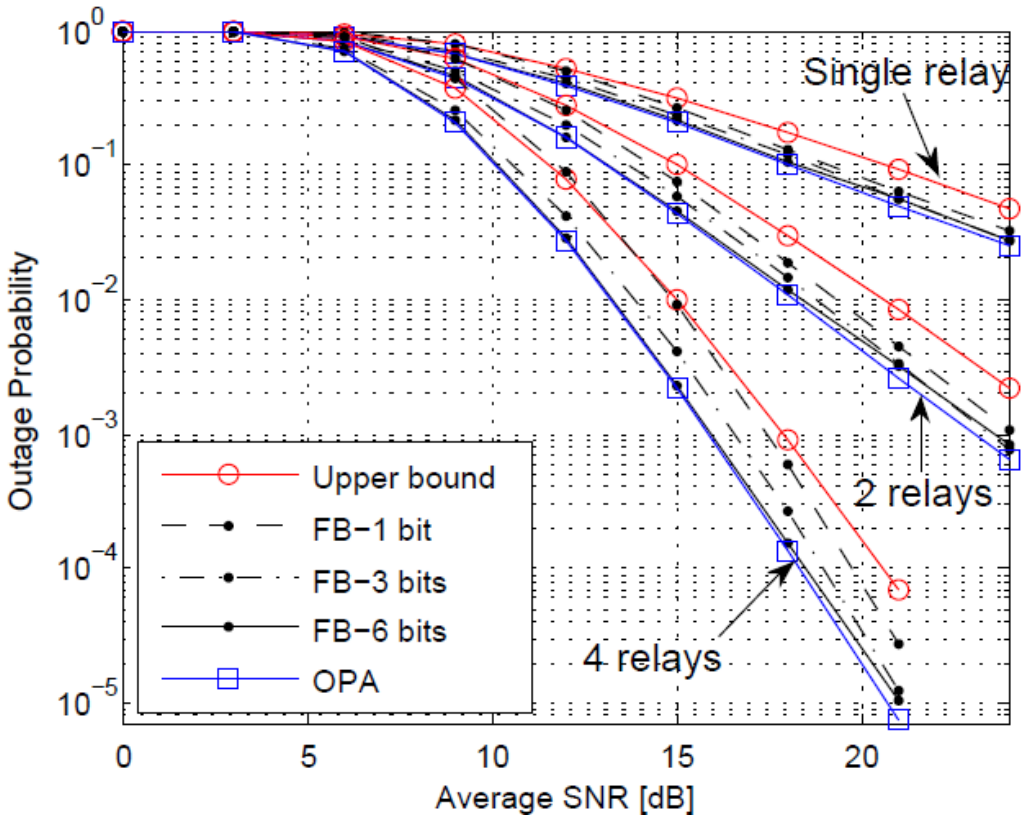

Figure 22: Outage probability of the proposed scheme by using limited feedback. The end-to-end target spectral efficiency is R=1 bps/Hz for outage analysis.

The outage probabilities of two power allocation schemes are compared in Figure 21. *The analytical results* of EPA given by a closed-form expression of equation (32) in [29] are also presented. It can be observed that analytical curves tightly agree with numerical results, which justify our theoretical analysis. As depicted in *Theorem 1*of [29], the performance of OPA is upper-bounded by that of EPA, which is also verified by these numerical results. To be specific, around 2dB gain is obtained with the utilization of distributed power control, and a considerable improvement is also appeared in the single relay system.

To identify the impact of the number of power-control bits on performance, the outage probability with limited feedback of $b \in \{1,3,6\}$ has been investigated. As illustrated in Figure 22, feeding back 6 bits can achieve a performance tightly approached the optimal performance with ideal OPA factor. Using only 3 bits can reap most of the potential gains, which is very encouraging in practice.

In order to make a clear understanding of the performance of opportunistic relaying in the aerial-terrestrial network, a performance evaluation with respect to spectral efficiency based on the realistic D2D and A2T channel models mentioned in the previous chapter is conducted. A Monte-Carlo simulation, where a single source-destination pair under the help of K relays, is established. Channel realizations with 10^6 independent samples are applied for each link. A power spectral density of white noise equals to $-174dBm/Hz$, and a signal bandwidth of 10MHz is utilized.

Figure 23a shows the spectral efficiency of opportunistic relaying as a function of transmitted power up to 200mW. Recalling that the total transmit power is denoted by P, thus, the source and relay equally transmit a power of 0.5P using EPA. In the case of OPA, the total power P is allocated between the source and relay based on instantaneous channel gains. Similarly, curves of spectral efficiencies as a function of transmit power in decibels are given in Figure 23b. As we can see in the figures, transmitting with the maximum power of 23dBm at the source and relay, the spectral efficiency of 9bps/Hz can be achieved by EPA when K=1, and is improved to more than 11bps/Hz when the number of relay increase to K=16. Let a signal bandwidth of 10MHz as an example, an uplink data rate of about 100Mbps can be achieved by opportunistic relaying over D2D and A2T channels. To highlight the benefit of OPA, Figure 24a gives a direct comparison of spectral efficiencies achieved by EPA and OPA as a function of the relay number. It is observed that an approximate 3dB power gain, corresponding to an increase of spectral efficiency of 1bps/Hz, can be acquired by OPA over EPA. Although the spectral efficiency will increase when a more number of relays cooperate each other, the performance gain from the power allocation only slightly fluctuates with the number of relays.

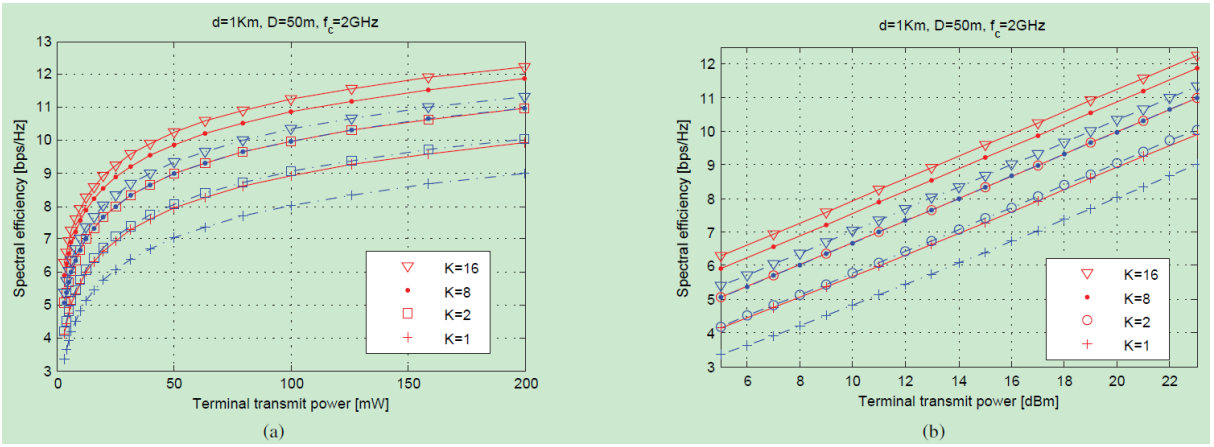

Figure 23: Spectral efficiencies of opportunistic relaying as a function of transmit power in (a) linear and (b) decibels, over D2D and A2T channels. The altitude of aerial base station is set to 1km, the maximum distance among terminals is 50m, and the carrier frequency is 2GHz.

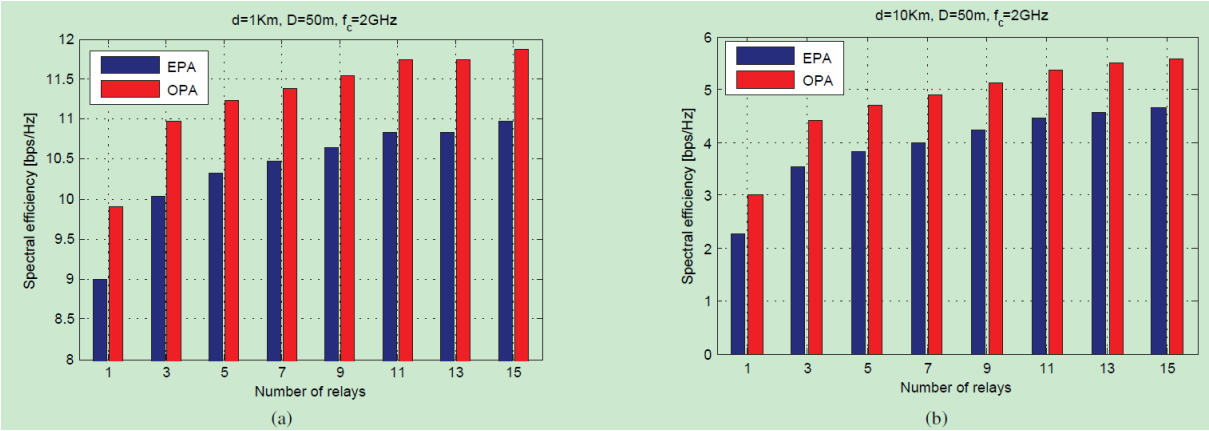

Figure 24: Spectral efficiencies of opportunistic relaying as a function of the number of relays over D2D and A2T channels. The altitudes of aerial base station are set to (a) 1km, and (b) 10km, respectively. The maximum distance among terminals equals to 50m and the carrier frequency is 2GHz.

In order to observe the impact of the altitude of LAP on the system performance, we further set an altitude of d=10km. As shown in Figure 25a, the achieved spectral efficiencies fall into a range of 2 to 6bps/Hz. That is to mean the increased path loss since the signal has to propagate a longer distance of 9km from the transmitter to receiver will cause a data rate decrease up to 7bps/Hz. Without any doubt, as illustrated in Figure 24b, the spectral efficiency is proportional to the number of relays, while OPA outperforms EPA with a spectral efficiency of slightly less than 1bps/Hz regardless of the number of relays.

To observe the effect of carrier frequency on the system performance, we further select a frequency of 5.8GHz to get another performance evaluation. In general, the path loss increases with the increment of carrier frequency due to the decrease of antenna aperture, which is proportional to the electromagnetic wavelength. Therefore, the received signal strength will decrease when the carrier frequency increase from 2GHz to 5.8GHz with the same propagation distance. As shown in Figure 25b, with the maximum transmit power of 23dBm, the spectral efficiency falls into a range from 5 to 9bps/Hz, which has a performance loss of approximately 4bps/Hz compared to that of 2GHz.

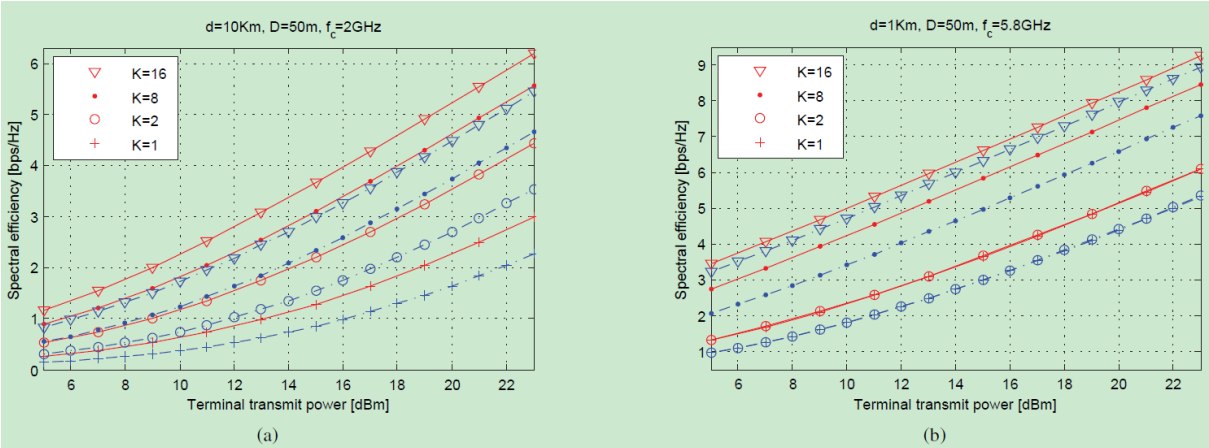

Figure 25: Spectral efficiencies of opportunistic relaying as a function of terminal transmit power over D2D and A2T channels. In (a), the altitude of aerial base station is changed to 10km; while in (b), the carrier frequency increases to 5.8GHz.

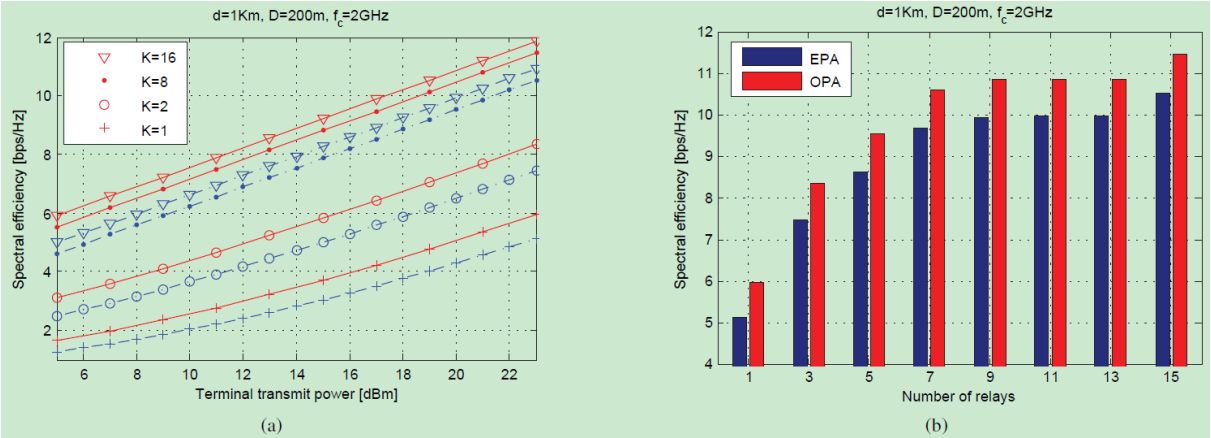

Figure 26: Spectral efficiencies of opportunistic relaying as a function of (a) the transmit power and (b) the number of relays over D2D and A2T channels. The altitude of aerial base station is set to 1km, the maximum distance among terminals increase to 200m, and the carrier frequency is 2GHz.

Furthermore, the maximum distance of D2D communication link is increased to D=200m. It can be observed in Figure 26a that the achieved spectral efficiencies is comparable to the performances in the case of D=50m, i.e., up to 12bps/Hz. That is because the performance of opportunistic relaying is limited by the bottleneck hop with the worse channel condition rather than the hop with better condition, which coincides with the theoretical analysis. Interestingly, as shown in Figure 26b, the spectral efficiencies improve more rapidly with the increase of cooperating relays. Moreover, we can see that the benefit from the utilization of OPA is shrunk to 2dB. That is to say, the distributed power allocation will receive more gain in the unbalanced channel links. Generally speaking, the larger in channel unbalance the more gain that can be achieved by the distributed power allocation.

3.2 **Performance of D2D relaying: The impact of feedback delay**

It is noted that the opportunistic relaying has two necessary steps, i.e., the relay selection based on the instantaneous channel state information (CSI) and the follow-on data transmission. From a practical point of view, however, the CSI at the instant of relay selection may substantially differ from the actual CSI as a result of the channel fading and feedback delay. Retransmitting the original signals via the best relay selected according to *the outdated CSI* will degrade the system performance. Especially in the ABSOLUTE, the propagation delay over the terrestrial-aerial links may be more serious since the propagation distance from the terminals on the ground to the aerial base stations may be larger than that of the conventional terrestrial cellular systems. On the other hand, the AeNodeB mounted on the balloon will be constantly moving due to the winds and the antenna system is unstable itself, both of which will speed up the fading rate of the radio channels. Intuitively, the radio channels in ABSOLUTE will change faster than the conventional terrestrial communication system where the base stations are fixed.

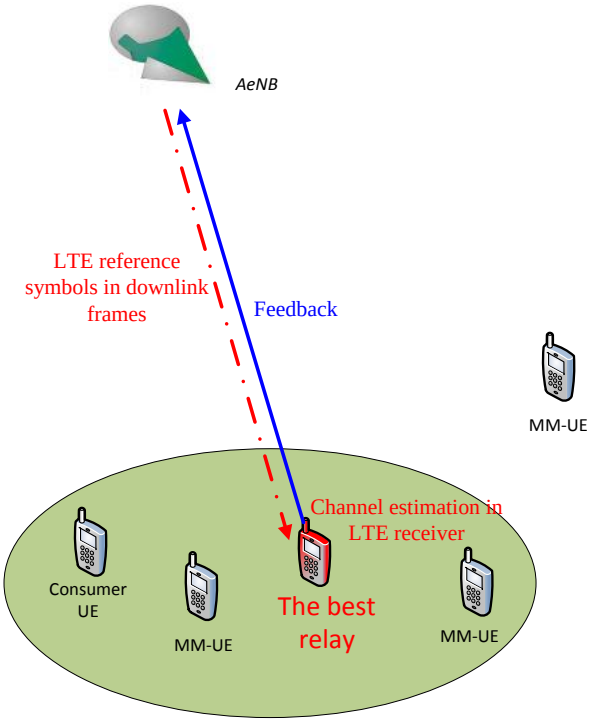

Figure 27: The feedback delay over Aerial-Terrestrial channel.

3.2.1 Performance of opportunistic relaying

In this section, we use the numerical results from Monte-Carlo simulations to verify the correctness of the closed-form expressions. Note that in all the below figures, the numerical results are denoted by **Markers** while the analytical **Curves** are figured out [32]. As we can see, the numerical results completely agree with the analytical curves, which just corroborate our theoretical analysis.

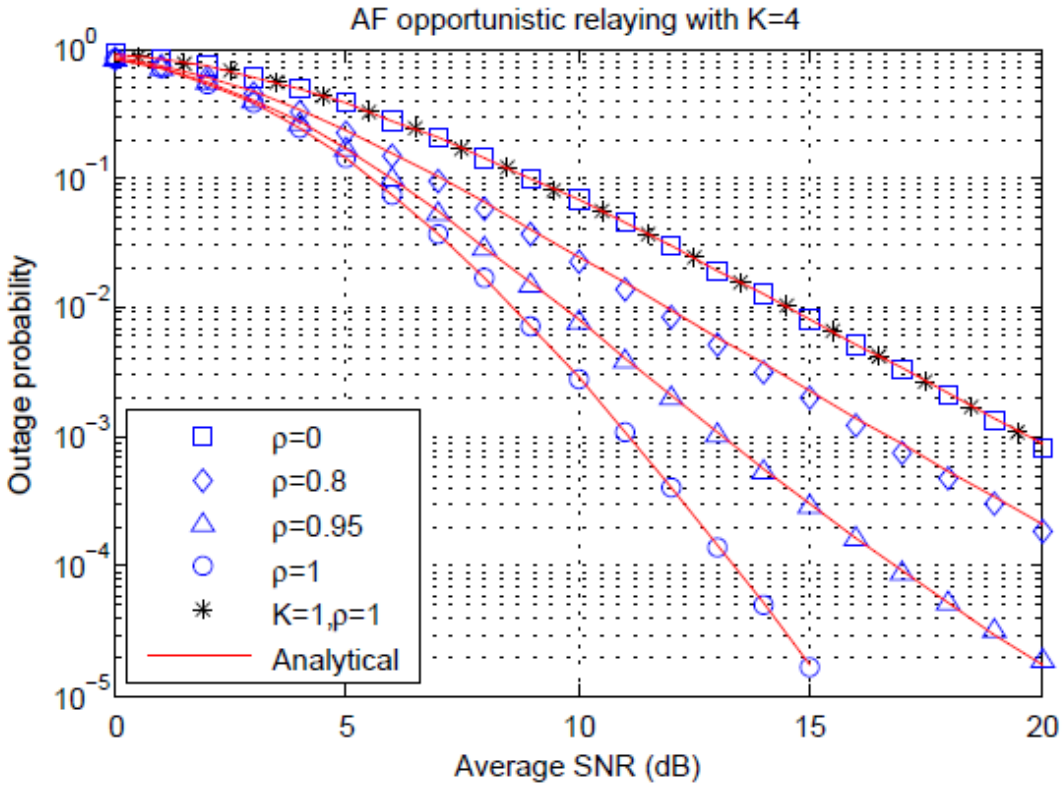

Figure 28: Outage probabilities of ORS in the presence of outdated CSI as a function of average transmit SNR. The simulated results are denoted by Markers while the analytical results by Curves.

We will investigate how the outdated CSI affects the performance of AF ORS in terms of outage probability. Consider a scenario of K=4 relays and the target spectral efficiency of R=1bps/Hz. For simplicity, all links use i.i.d. Rayleigh channels with a normalized gain $\Omega_{AB}=1$. The simulated results are obtained by iterating 10^6 channel realizations for each link, and all nodes transmit or retransmit the signal with equal power of P. When using perfect CSI $\rho=1$, as shown the above figure, the curve of outage probability decays as $1/\bar{\gamma}^5$, which implies a full diversity order of K+1 is achieved. For comparison, we also provide the performance of the single relay K=1 with perfect CSI $\rho=1$, which decays as $1/\bar{\gamma}^2$ and is marked by * in the figure.

In the presence of outdated CSI, on whatever value of correlation coefficient, such as $\rho=0,0.8$ and 0.95 in this figure, their curves are parallel with that of the single relay K=1 in high SNR regime. Therefore, the outage probabilities of AF ORS decrease with the average SNR only in $1/\bar{\gamma}^2$ and no diversity gain is available. When $\rho=0$, the curve of K=4 overlaps with that of the single relay K=1. In this case, the best relay is selected in a random manner and the benefit get from opportunistic relay selection is thoroughly vanished. Clearly, all analytical and numerical results are tightly matched, which verifies the correctness of our MGF-based performance analysis.

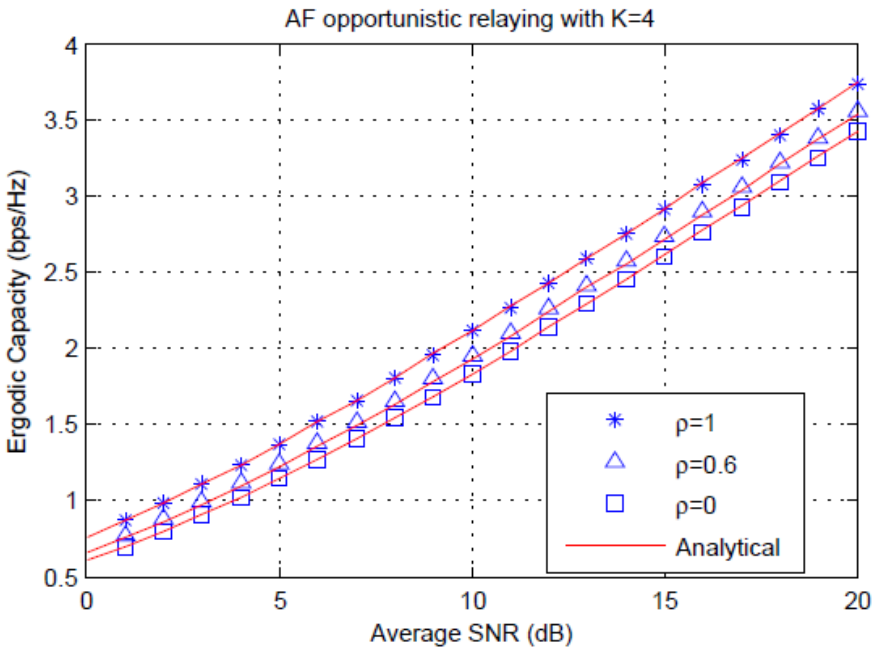

Figure 29: Ergodic capacities of AF ORS in the presence of outdated CSI as a function of average transmit SNR. The simulated results are denoted by Markers while the analytical results by Curves.

Figure 29 illustrated the ergodic capacity of AF ORS with outdated CSI. Different values of correlation coefficient, i.e., $\rho\in\{0,0.6,1\}$ are utilized. To be specific, the performance in case of K=4

relays as a function of the average SNR $\bar{\gamma}$ is given. Setting $\bar{\gamma} = 15dB$, we show the performance curves as a function of the number of relays K in Figure 30. When $\rho = 0$, the capacity of AF ORS is independent with the number of relays K, therefore no any benefit can be achieved from the opportunistic relay selection. As we can see in both figures, all numerical results from Monte-Carlo simulations tightly agree with the analytical curves.

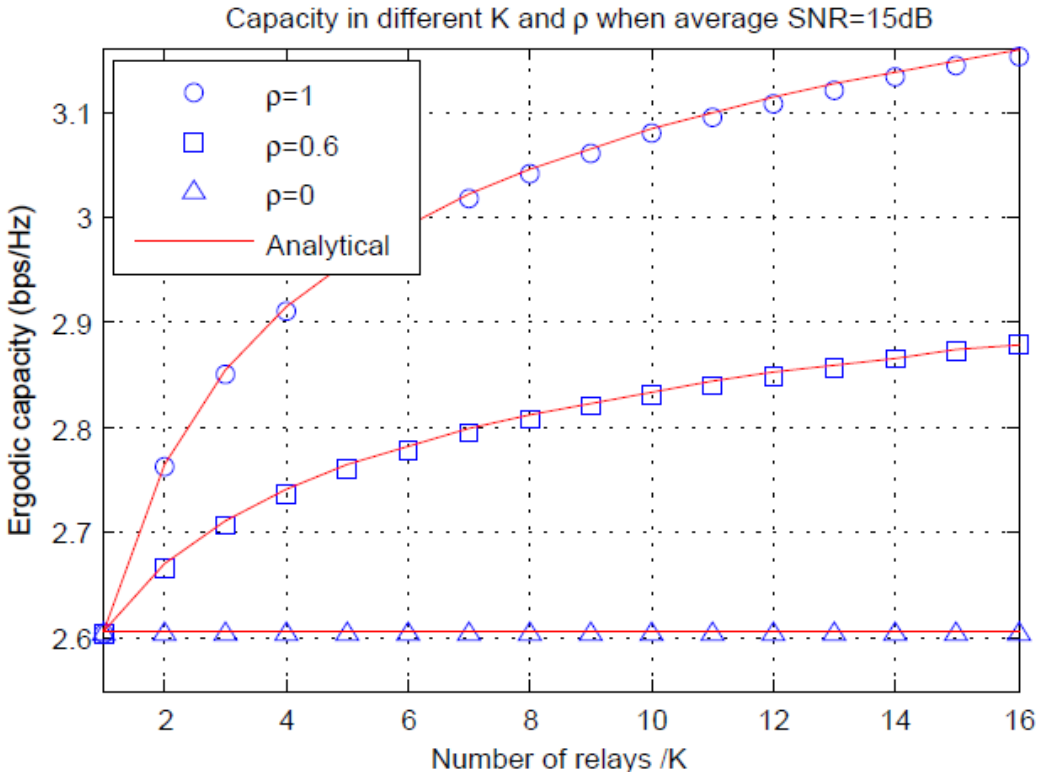

Figure 30: Ergodic capacities of AF ORS in the presence of outdated CSI as a function of the number of relays. The simulated results are denoted by Markers while the analytical results by Curves.

In this section, we investigated the performance degradation of opportunistic relaying in the effect of outdated CSI, which may be severe due to the long distance of signal propagation from the terminal on the ground to the aerial base station at the altitude of several kilometres. The theoretical analyses and numerical results from Monte-Carlo simulations revealed that the feedback delay will cause a substantial performance loss to opportunistic relaying in ABSOLUTE. To combat the effect of feedback delay from the terrestrial-aerial links in ABSOLUTE, in the following two sections, we will propose two novel relay selection methods, i.e., General Selection Combining and Opportunistic Space-Time Coding, in order to satisfy the high link-reliability and resilience requirements of ABSOLUTE.

3.2.2 Performance of Generalized Selection Combining

From a practical point of view, however, the channel state information (CSI) at the instant of relay selection may substantially differ from the actual CSI as a result of the channel fading and feedback delay. Retransmitting the original signals via the best relay selected according to *the outdated CSI* will degrade the system performance, which has been studied in the previous section. Therefore, it is meaningful to find or design the technical methods to combat the effect of feedback delay. In this section, we introduce a relay selection strategy called Generalized Selection Combining (GSC) and

investigate its performance over the terrestrial-aerial network of ABSOLUTE. Compared to the relay selection method, GSC will achieve a substantial performance gain and performs well in the practical ABSOLUTE network taking into account the feedback delay in terrestrial-aerial links.

Generalized selection combining (GSC) [33] [34] is previously designed as a diversity scheme to fight the multipath fading. The performances of GSC applied in the cooperative networks with DF and AF protocol have been analysed in [35] and [36], respectively, when using perfect CSI. However, the performance analysis of GSC in the presence of outdated CSI is still not available in the literature. Therefore, we will analyse the performance of GSC in cooperative network. Moment generating function (MGF) of the end-to-end signal-to-noise ratio (SNR) for GSC over independent and identically distributed (i.i.d.) Rayleigh channels is given. Then, the closed-form expressions of ergodic capacity and outage probability are derived directly from this MGF without any involvement of probability density function (PDF) to avoid the mathematical intractability. To compare the performance, the MGF-based analysis for ORS is also presented. Besides, Monte-Carlo simulations are set up to verify the theoretical analyses.

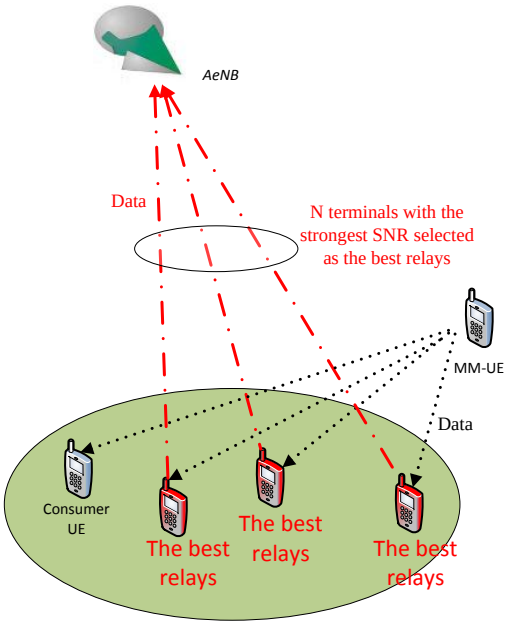

Figure 31: Schematic diagram of GSC in Aerial-Terrestrial links of ABSOLUTE

3.2.3 Numerical results

In this part, we will present the numerical results from Monte-Carlo simulations to corroborate the validity of the closed-form expressions. The performances of GSC and ORS are compared in terms of the ergodic capacity and the outage probability. Note that in all the below figures, the numerical results are denoted by markers, while the analytical results [37] are expressed as curves. It can be observed that all performance curves strictly agree with the corresponding markers, which verify our theoretical analysis above.

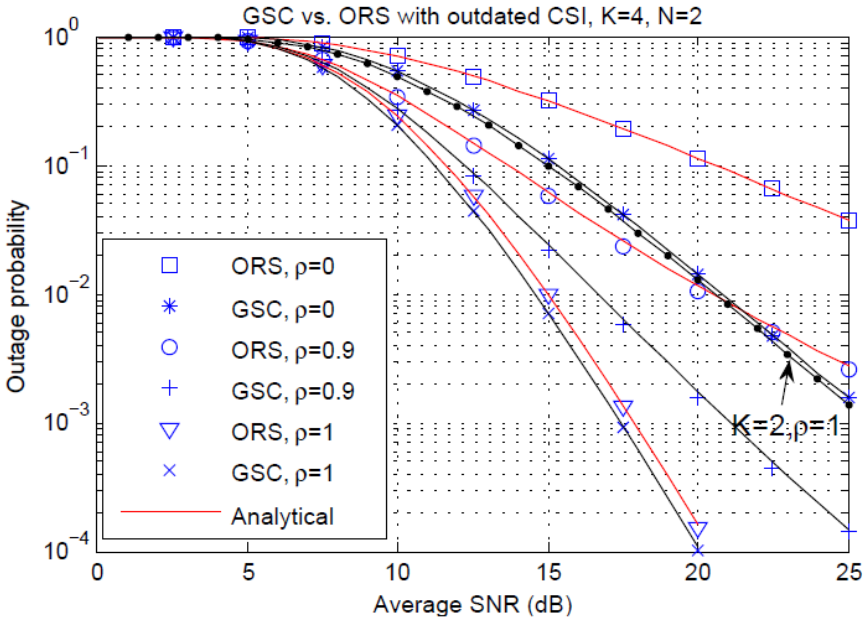

Figure 32: Outage probability comparisons of GSC and ORS as a function of average transmit SNR when K=4. The simulated results are denoted by Markers while the analytical results by Curves.

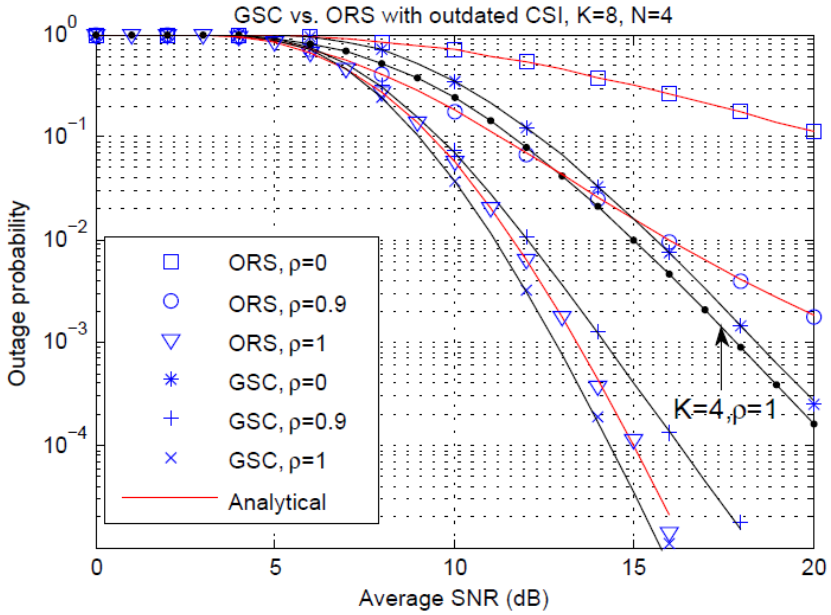

Figure 33: Outage probability comparisons of GSC and ORS as a function of average transmit SNR when K=8. The simulated results are denoted by Markers while the analytical results by Curves.

The numerical results are obtained by iterating 10^6 channel realizations of i.i.d Rayleigh fading with a normalized gain, and a target rate of R=1bps/Hz is used for the outage analysis. In fairness to compare, applying an end-to-end transmit power of P and a source power of Ps=0.5P for both ORS and GSC. In addition, the power among activated relays is equally allocated, thus, P/2N for each relay in GSC and 0.5P for the best relay in ORS.

We first investigate how the outdated CSI affects the performance of ORS and GSC in terms of outage probability. Figure 32 shows the cooperative network with K=4 relays and N=2 relays are selected for GSC, while the results of K=8 and N=4 are given in Figure 33. When using perfect CSI

$\rho = 1$, as shown in both figures, GSC slightly outperforms over ORS. Their curves decay at the same rate, i.e., $1/\bar{\gamma}^4$ and $1/\bar{\gamma}^8$ in Figure 32 and Figure 33, respectively. Therefore, a full diversity on the number of cooperating relays K is achieved by GSC as well as ORS. With outdated CSI, such as $\rho = 0$ and 0.9 illustrated in both figures, the performance of ORS drastically degrades while GSC is robust. When $\rho = 0$, the relay selection is performed in a random manner, where the performance curves fall at a rate of $1/\bar{\gamma}$. It can be observed that, the performance curves of ORS when $\rho = 0.9$ are parallel with $\rho = 0$ at high SNR regime. That is to mean no diversity can be achieved by ORS with outdated CSI, regardless of how many cooperating relays. For comparison, we also provide the performances of ORS in the case of K=2 and K=4 with perfect CSI $\rho = 1$, which decay as $1/\bar{\gamma}^2$ and $1/\bar{\gamma}^4$, respectively, as *the reference curves*. As we can see, the curves of GSC are parallel with the reference curves in high SNR regime. That is to mean a diversity order of N is achieved by GSC in the presence of outdated CSI.

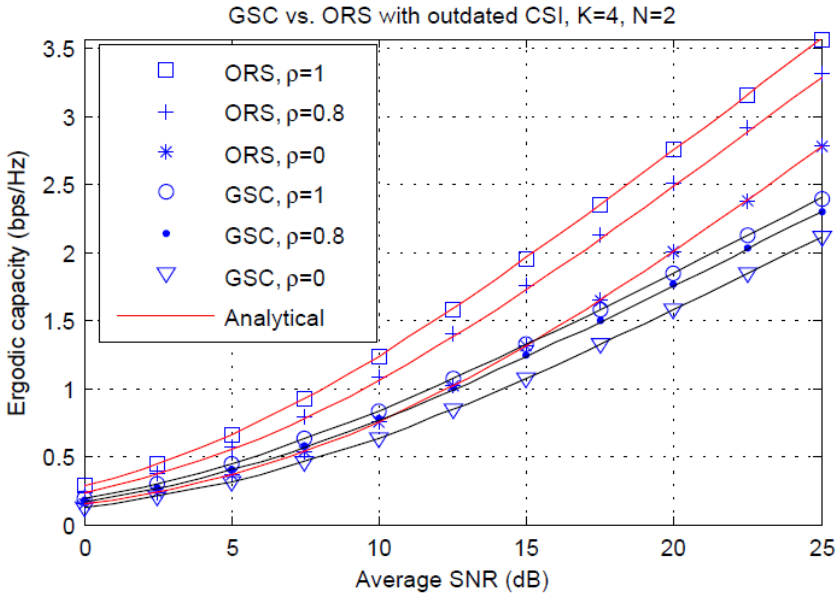

Figure 34: Ergodic capacity comparisons of GSC and ORS as a function of the average SNR when K=4.

The ergodic capacity of GSC and ORS with the number of relays K=4 and K=8 are presented in Figure 34 and Figure 35, respectively. Comparing the performance of $\rho = 1$ and $\rho = 0$ of ORS in Figure 34, the required SNR increases from 15dB to 20dB at a given spectral efficiency of 2bps/Hz. Namely, the outdated CSI causes a SNR loss up to 5dB while this loss is about 2.5dB in GSC. As we can see in Figure 35, the SNR loss increases to more than 6dB for ORS and decrease to about 1dB for GSC, respectively. Therefore, we can draw a conclusion that ORS is very vulnerable to the outdate CSI, while GSC performs in a more robust manner. However, the channel capacity of GSC remarkably decreases since N orthogonal channels are required to retransmit the signals over relay-destination links. In a nutshell, the diversity gain of GSC comes at the price of sacrifice in spectral efficiency, which decreases to 2/(N+1) compared with that of ORS.

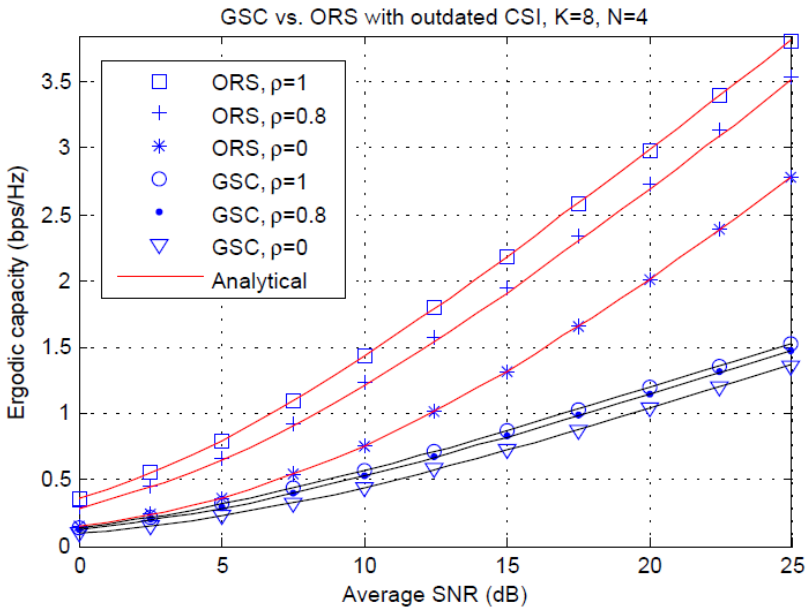

Figure 35: Ergodic capacity comparisons of GSC and ORS as a function of average transmit SNR when K=8.

In this section, we introduced Generalized Selection Combining to the terrestrial-aerial network of ABSOLUTE taking into account the presence of feedback delay. The closed-form expressions of ergodic capacity and outage probability are derived directly from their respective MGF. Monte-Carlo simulations are set up to corroborate the validity of our theoretical analysis. The analytical and numerical results reveal that GSC can effectively combat the effect of feedback delay. Although the high link reliability and resilience requirements can be effectively achieved for the *practical* ABSOLUTE network by the use of GSC, the price of sacrifice in the channel capacity have to be paid. Therefore, in the following section, we will propose a new relay selection method for opportunistic relaying, called Opportunistic Space-Time Coding, to achieve both the high link reliability and the transmission date rate.

3.3 **Performance of D2D relaying: Opportunistic space-time coding**

As depicted in the previous two sections, in practice, the channel state information (CSI) at the instant of relay selection may substantially differ from the actual CSI as a result of the channel fading and feedback delay. Retransmitting the original signals via the best relay selected according to *the outdated CSI* will degrade the system performance. Generalized Selection Combining (GSC) [38] can be used to effectively combat the impact of feedback delay. However, these schemes require at least multiple orthogonal channels to transmit the regenerated signals from the selected relays to the destination, resulting in a decrease of the spectral efficiency.

In this section, therefore, we propose a novel scheme coined opportunistic space-time coding (OSTC) to combat the effect of imperfect CSI, while avoiding the unnecessary decrease of spectral efficiency. A pair of relays (terminals or PLMU in the context of ABSOLUTE), rather than a single relay in the conventional ORS system, is opportunistically selected according to the instantaneous CSIs of relay-destination links. The Alamouti scheme [39], a unique space-time code achieving both

full-rate and full-diversity, is applied to encode the regenerated signals at this pair of relays. The main contributions can be summarized as follows:

- The proposed scheme achieves a full diversity on the number of cooperating relays when using perfect CSI. With outdated CSI, a diversity order of 2 is achieved without any decrease in the spectral efficiency. To obtain a higher diversity of N, only N/2 orthogonal channels over relay-destination links are used by OSTC. The spectral efficiency of OSTC improves 100% compared to GSC, where N channels are required.
- The closed-form expression of outage probability for OSTC is derived based on the moment generating function (MGF).
- Monte-Carlo simulations are set up, and the numerical results corroborate the theoretical analysis.

3.3.1 Opportunistic space-time coding

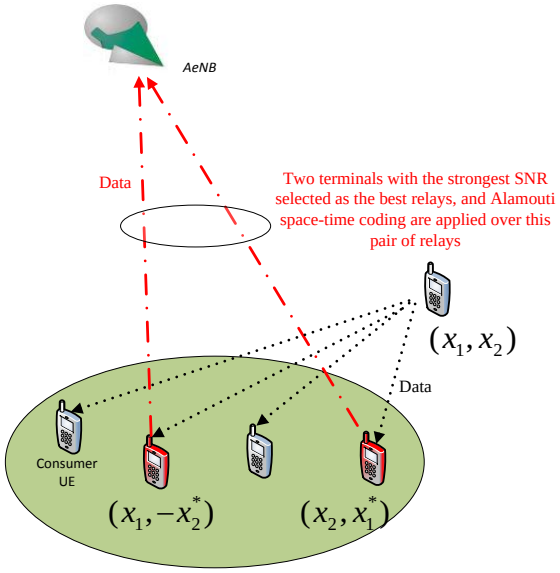

Figure 36: Opportunistic space-time coding over Aerial-Terrestrial links of ABSOLUTE.

The name of *opportunistic space-time coding* is coined from the basic idea that relays are *opportunistically* selected and then the regenerated signals are retransmitted by the selected relays using *space-time coding*.

Because of severe signal attenuations in radio channels, the relays with a single antenna should operate in half-duplex transmission mode to avoid the harmful self-interference between the circuits of transmitter and receiver. Without loss of generality, the time-division multiplexing can be applied for analysis hereinafter and therefore the signal transmission is divided into two slots. In the first slot, the source transmits and those of relays who can decode the signal correctly are defined as *decoding subset DS* of source-relay link

$$DS \triangleq \left\{k : \frac{1}{2}\log_2(1+\gamma_{s,k}) \geq \mathrm{R}\right\} = \left\{k : \gamma_{s,k} \geq 2^{2R} - 1\right\}, \quad (0)$$

where R is the end-to-end target rate for the dual-hop cooperative network. Note that the required rate for each link increases to 2R due to the half-duplex transmission mode. In the conventional opportunistic relaying, the best relay $\dot{k}$ is selected from *DS* following

$$\dot{k} = \arg\max_{k \in DS} \hat{\gamma}_{k,d}, \tag{0}$$

where $\hat{\gamma}_{k,d}$ is the SNR of relay-destination link *at the instant of relay selection*, which may be outdated compared to the actual SNR $\hat{\gamma}_{k,d}$ during the data transmission.

In the DSTC system, no relay selection will be performed and *all relays* in DS will join the transmission of regenerated signals with the use of space-time coding. The dimension of the DSTC equals to the cardinality of decoding subset, i.e., |DS|. However, in addition to the best relay, the proposed scheme will select another relay with the second strongest SNR, i.e.

$$\ddot{k} = \arg\max_{k \in DS - \{\dot{k}\}} \hat{\gamma}_{k,d}, \tag{0}$$

In the first slot, as shown Figure 36, the source broadcasts a pair of symbols (x_1, x_2) to all relays at two consecutive symbol periods, during which the channel gain is regarded as constant. Relying on the instantaneous SNR of relay-destination links, a pair of relays from the decoding subset is opportunistically selected as (0) and (0).

The regenerated signals (x_1, x_2) are encoded according to Alamouti scheme

$$(x_1, x_2) \rightarrow \begin{bmatrix} x_1 & -x_2^* \\ x_2 & x_1^* \end{bmatrix} \tag{0}$$

where the superscript * denotes the complex conjugate. In the second slot, a relay transmits two symbols $(x_1, -x_2^*)$ while another relay transmits (x_2, x_1^*) *simultaneously at the same frequency*, similar to Alamouti scheme over two co-located antennas. At the destination, the received signals (y_1, y_2) at two consecutive symbol periods can be written as

$$\begin{aligned} y_1 &= h_{\dot{k},d} x_1 + h_{\ddot{k},d} x_2 + z_1 \\ y_2 &= h_{\ddot{k},d} x_1^* - h_{\dot{k},d} x_2^* + z_2 \end{aligned} \tag{0}$$

According to [39], the transmit symbols (x_1, x_2) can be recovered simply through a linear combining of (y_1, y_2) as

$$\begin{aligned} \tilde{x}_1 &= h_{\dot{k},d}^* y_1 + h_{\ddot{k},d} y_2^* \\ \tilde{x}_2 &= h_{\ddot{k},d}^* y_1 - h_{\dot{k},d} y_2^* \end{aligned} \tag{0}$$

Substituting (0) into(0), we have

$$\begin{aligned} \tilde{x}_1 &= \left(\left| h_{\dot{k},d} \right|^2 + \left| h_{\ddot{k},d} \right|^2 \right) x_1 + \tilde{z}_1 \\ \tilde{x}_2 &= \left(\left| h_{\dot{k},d} \right|^2 + \left| h_{\ddot{k},d} \right|^2 \right) x_2 + \tilde{z}_2 \end{aligned} \tag{0}$$

Given $\left|h_{\dot{k},d}\right|^2$ and $\left|h_{\ddot{k},d}\right|^2$ acquired by the channel estimation at the receiver, it can be observed from (0) that the transmit signals are successfully recovered. Denoting the transmit power of $\dot{k}$ and $\ddot{k}$ are $P_{\dot{k}}$ and $P_{\ddot{k}}$, respectively, the instantaneous channel capacity of OSTC scheme is given by

$$C_{ostc} = \log_2\left(1+\frac{\left|h_{\dot{k},d}\right|^2 P_{\dot{k}}}{\sigma^2}+\frac{\left|h_{\ddot{k},d}\right|^2 P_{\ddot{k}}}{\sigma^2}\right) \quad (0)$$

3.3.2 Numerical results in Rayleigh channels

In this part, the outage probability of OSTC, ORS and GSC with outdated CSI over i.i.d. Rayleigh channels are compared. The numerical results are obtained by iterating 10^6 channel realizations into Monte-Carlo simulations, and the target rate is set to R=1bps/Hz. Note that in all the below figures, the simulated results are denoted by Markers, while the analytical Curves are calculated according to [40]. It can be observed that all Markers strictly match the corresponding Curves, which corroborate the theoretical analysis.

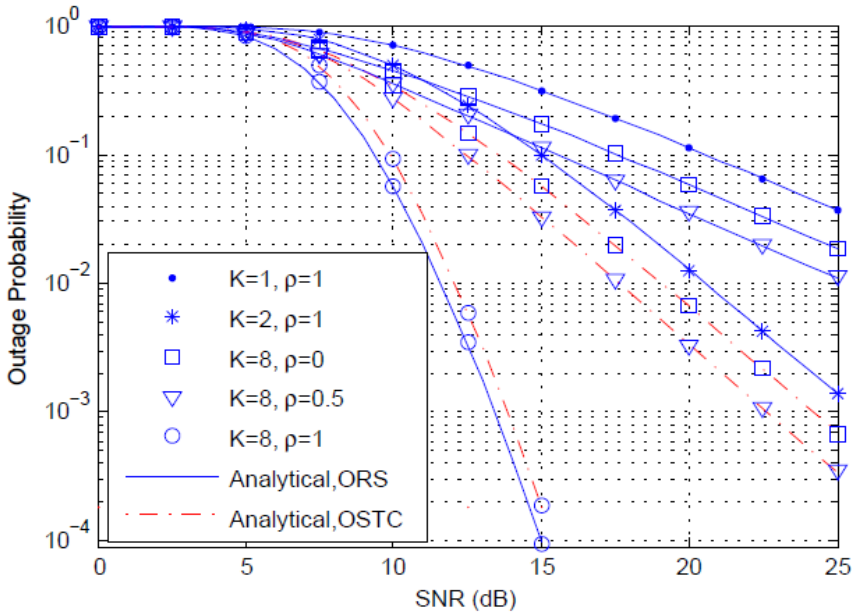

Figure 37: Outage probability comparisons of ORS and OSTC as a function of average transmit SNR. The simulated results are denoted by Markers while the analytical results by Curves.

We first investigate the impact of the outdated CSI on the outage probability of a cooperative network with K=8 relays. When using perfect CSI $\rho = 1$, as shown in Figure 37, OSTC suffers from a little bit performance loss compared to that of ORS. That is because the best relay with the strongest SNR transmits the regenerated signal in ORS, while a pair of relays with the strongest and second SNR is utilized in OSTC. Clearly, the relay with the second SNR brings some performance loss. However, the slopes of both curves are the same, which imply that a diversity order of 8 is achieved by OSTC as well as ORS and their outage probability decays both as $1/\bar{\gamma}^8$ at high SNR regime. In the presence of outdated CSI, such as $\rho = 0$ and 0.5 illustrated in this figure, the performance of ORS drastically degrades while OSTC performs far more robustly. For comparison, we also provide the performance

curves of K=1 and K=2 with $\rho = 1$. As we can see, the diversity order of ORS reduces to 1 while an order of 2 is achieved by OSTC with outdated CSI.

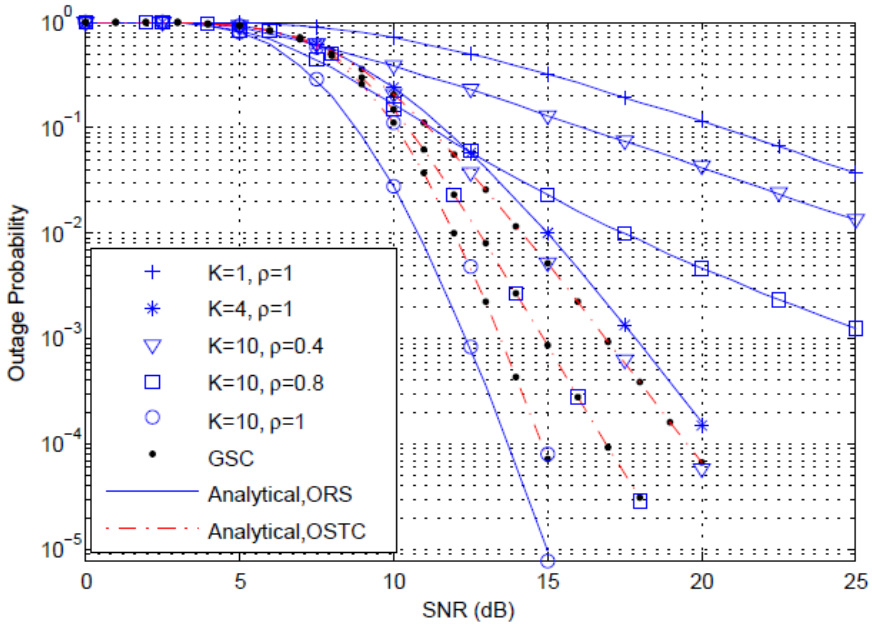

Figure 38: Outage probability comparisons of ORS and OSTC as a function of average transmit SNR, together with GSC in the case of N=4. The simulated results are denoted by Markers while the analytical results by Curves.

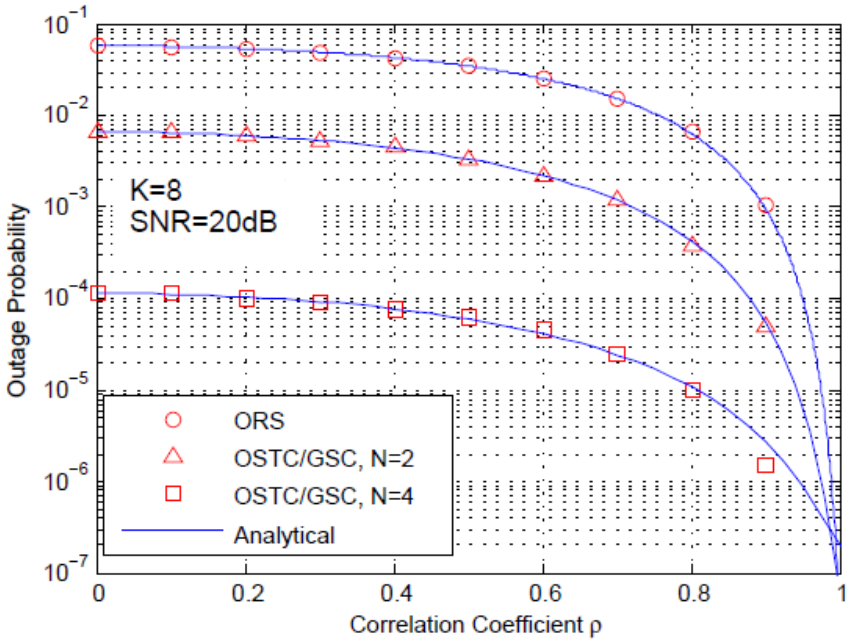

Figure 39: Outage probability comparisons of ORS, GSC and OSTC as a function of correlation coefficient, when K=8 and SNR=20dB. The simulated results are denoted by Markers while the analytical results by Curves.

To achieve a higher diversity order of 4, the regenerated symbols (x_1, x_2) are retransmitted by two pairs of relays over two orthogonal channels. Either pair of relays transmits (x_1, x_2) using Alamouti scheme independently on a channel. At the destination, the signals from 4 independent paths are

linearly combined together. Besides, we present the performance of GSC with N=4, namely, a regenerated symbol x is forwarded by 4 selected relays repeatedly over 4 orthogonal channels. As Figure 38 illustrated, a performance loss of OSTC at $\rho = 1$ is slightly increased compared with that of Figure 37. That is because the transmit power is evenly allocated among 4 relays in OSTC/GSC, while the whole power for relays is used by the best relay with the strongest SNR in ORS. However, a diversity order of 10 is observed by the proposed scheme through comparing the slopes of curves. For comparison, we also provide the performance curves of K=1 and K=4 with $\rho = 1$. Then, we find that the outdated CSI reduces the diversity order of ORS to 1, i.e., no diversity, while OSTC/GSC can still achieve an order of 4. At a given spectral efficiency of 10^{-2}, OSTC/GSC remarkably outperforms ORS with a SNR gain about 12dB. As verified by the numerical results, GSC and OSTC achieve the same performance. But please keep in mind that only 2 orthogonal channels are used by OSTC, in contrast to 4 channels by GSC. That is to mean the spectral efficiency of OSTC is two times of that of GSC in the presence of outdated CSI.

The analytical and numerical results for ORS and OSTC as a function of ρ are given in Figure 39, together with the performance of GSC. It can be observed that OSTC and GSC achieve the identical performance under all values of ρ. Given K=8 and SNR=20dB, OSTC/GSC outperforms ORS about an order of magnitude in the case of N=2. While a performance gain more than 3 orders of magnitude can be available in a high diversity mode of N=4. With perfect CSI, OSTC/GSC achieves a performance closely approaching that of ORS.

In summary, the proposed scheme can achieve a full diversity on the number of cooperating relays when using perfect CSI, only suffering from a very slight performance loss. In the presence of outdated CSI, the diversity order of ORS reduces to 1, while OSTC/GSC remarkably outperforms ORS with an order of N. However, OSTC's spectral efficiency is double of GSC given the same outage probability and diversity order.

3.3.3 Numerical results in realistic channels

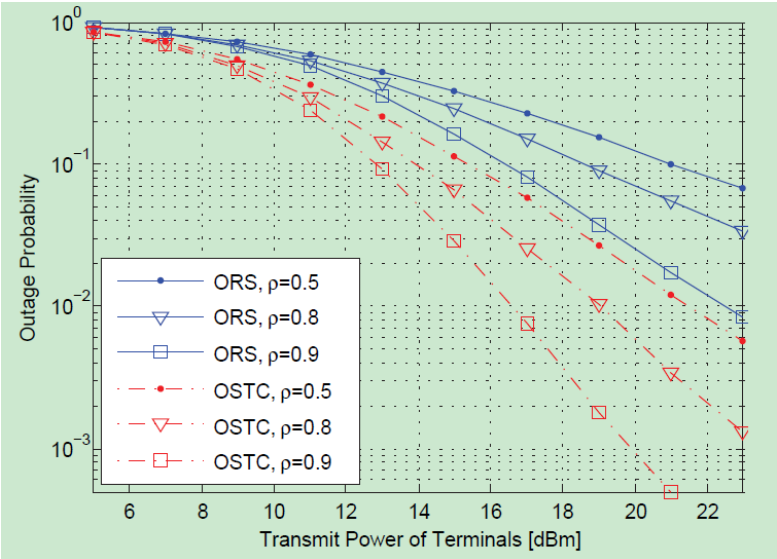

Figure 40: Outage probability comparisons of ORS and OSTC as a function of transmit power at the terminals over the realistic channels models. The number of relays K=15 and the target spectral efficiency is 3.5bps/Hz.

The numerical results in the above subsection are based on only the small-scale fading, which didn't take into account the path loss and the shadowing. In order to make clear the practical performance of ORS and OSTC in Aerial-Terrestrial network, the simulation using the realistic D2D and A2T channel models is carried out [41]. The carrier frequency is selected to 2GHz because of its popularity of utilization in most cellular systems. The altitude of LAP is assumed to 1km and the maximum distance among terminals is set to 50m. As we know, the power spectral density of white noise equals to $-174dBm/Hz$, and here an example of signal bandwidth of 10MHz is utilized. The number of available relays is assumed to K=15 and the target rate is R=3.5bps/Hz to make the curves in the figure more readable. Figure 40 shows the outage probabilities of ORS and OSTC as a function of terminal transmit power from 5dBm to 23dBm. In the cases of ρ =0.5, 0.8 and 0.9, as we can see in this figure, an improvement of approximate 6dB in transmit power can be achieved by the utilization of OSTC. Moreover, the curves of OSTC drop more rapidly than ORS with the increase of transmit power. That is because the diversity order of ORS reduces to 1 while an order of 2 is achieved by OSTC in the presence of outdated CSI.

3.4 **Performance of D2D relaying: Energy efficiency**

This section evaluates the energy efficiency of D2D relaying. We derive closed-form expressions for describing the geometrical zone where relaying acts in an energy-efficient way. In addition, we obtain the probabilistic distribution of the energy saving introduced by relays that are randomly distributed according to a spatial Poisson point process. Results reveal that a significant energy saving can be achieved when D2D relaying is adopted for distances below a certain threshold.

The detail can be found in [42], and the main contributions are summarized below:

- We introduce the concept of *relay energy saving zone* between a communicating pair (MMUE-MMUE), and we derive a mathematical approximation to describe its geometry. Inside this zone, a relay would be *energy efficient*.
- We obtain the stochastic distribution of the energy saving introduced by D2D relaying. In this case, the communicating devices have the choice to select the relay candidate that provides the best energy saving.
- We obtain a closed-form expression for the maximum theoretical limit of energy efficiency enhancement that could be achieved by D2D relaying.
- We find the distance threshold, beyond which no energy-efficient relaying can take place. Also, we study the effect of D2D relays in extending this threshold.

3.4.1 System assumptions

To account for the path-loss, the received signal power is calculated based on the following relation:

$$P_r = \frac{P_t}{L_o} d^{-\alpha},$$

where P_t is the transmit power, L_o a constant that depends on the carrier frequency and the antennas gain, d is the distance between the transmitter and the receiver, and α is the path-loss exponent. Here,

we assume that the source is capable of adjusting the transmit power in order to maintain a certain level of signal-to-interference-plus-noise ratio (SNIR). The SNIR is defined as

$$SNIR_o = \frac{P_o}{P_I + P_N},$$

where P_I is the total interference power at the receiver, and P_N is the noise power. If a signal is transmitted over a period T_m, the consumed energy can be given by

$$\varepsilon = \mu d^{\alpha} + E_{rx},$$

where E_{rx} is the minimum energy required to decode the signal at the destination. The physical interpretation of the constant $\mu = SNIR_o(\bar{P}_I + P_N)L_o T_m$ is the amount of energy required to deliver a signal to the receiver located at a reference distance, with the aim of achieving a desired $SNIR_o$. We call ε the *energy cost* of delivering the signal between a communicating pair.

3.4.2 Energy saving by relaying

Here we provide a mathematical analysis for the possible energy saving of D2D relaying. We first determine the geometrical region where an assisting relay can be utilized efficiently, i.e., can save energy when used. Secondly, we look into the probability of getting a certain energy saving gain if a single MMUE-relay is placed randomly inside this saving zone. Finally, we extend the one-relay model to an arbitrary number of relays within the saving zone, and then we deduce the expectancy of energy saving gain if relays are randomly deployed according to Poisson point process.

3.4.3 Energy saving circle

Without loss of generality, we assume a communicating pair in the 2D space where a sender S is located at the Cartesian coordinates (-d/2, 0) and a destination D at (-d/2, 0). Furthermore, we assume a relay R is located at a general point location (x, y), as illustrated in Figure 41.

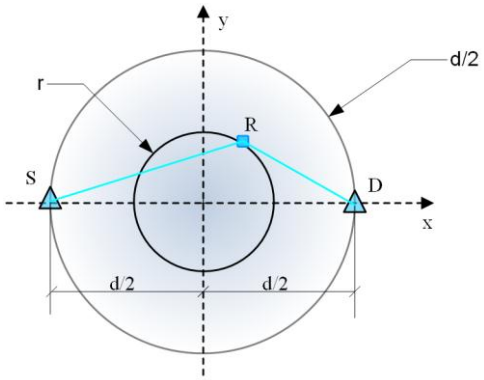

Figure 41: The energy saving circle.

The relaying is efficient if its consumed energy is less than that of directly sending a message between point S and point D. We can write

$$Sr^2 + Rr^2 \leq SD^2,$$

which is valid for the case of $\alpha = 2$ only. The above equation constitute a circle of radius R=d/2. We define the energy saving factor as the normalized energy difference between the direct path and the relay path:

$$\eta = \frac{\epsilon_D - \epsilon_R}{\epsilon_D}$$

Accordingly, the energy saving gain η can be calculated as:

$$\eta = \frac{1}{2} - \frac{2r^2}{d^2}$$

We can notice from the above relation that all points located at a certain circle of radius r can perform the same energy saving gain. Also that the upper bond of the energy saving is equal to $\eta = 0.5$ corresponding to the best case when relay-MMUE is located at the origin r=0, while the lower bond of the energy saving is equal to $\eta = 0$ representing the worst case when UE is located at the edge of the saving zone (r=d/2). Our target is to find the probability distribution function (PDF) of η if a single relay-MMUE is randomly placed inside the saving zone. In order to do so, we will first obtain the cumulative distribution function (CDF). Assuming that at least one UE is located inside the saving zone of radius d=2, with a uniform spatial probability. Accordingly, the CDF of finding the relay-MMUE inside a search radius of r, can be given as:

$$F_R(r) = p_o \pi r^2,$$

where p_o is the probability density per unit area. Following the assumption that a single relay-MMUE exists inside the saving zone, thus,

$$p_o \pi \left(\frac{d}{2}\right)^2 = 1$$

Hence, we can deduce that

$$F_H(\eta) = 2\eta$$

If the number of relay-MMUEs inside the saving region is n, we can easily extend the above relation by finding the maximum value of an *i.i.d* random vector, as follows

$$F_H(\eta, n) = F_H(\eta)^n$$

The PDF of η can be expressed as

$$f_H(\eta, n) = 2n\ (\eta)^{n-1}$$

It can be proved that if the relay-MMUEs are homogeneously distributed according to a Poisson point process, the average energy saving factor is

$$\bar{\eta} = \frac{N + e^{-N} - 1}{2N},$$

where $N = \lambda\, \pi\, \left(\frac{d}{2}\right)^2$ is the mean number of points inside the energy saving zone. We can deduce from Figure 42 that it is sufficient to have an average of 20 nodes inside the saving zone, to reach the 95% of the optimal energy efficiency.

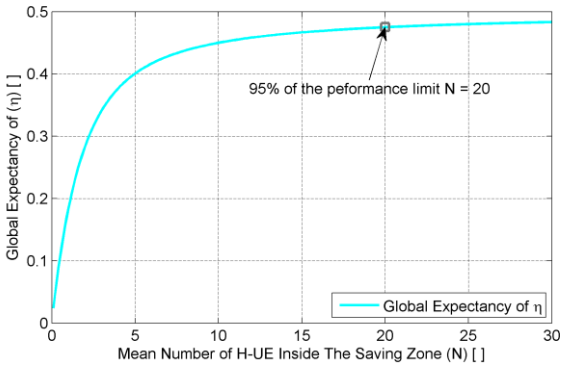

Figure 42: The expected value of the energy saving gain η versus the average number of relays inside the saving zone.

3.5 **Performance of D2D relaying: Coverage**

In addition to the coverage provided by ABSOLUTE aerial base stations, there is a vital role played by the MMUE in extending the terrestrial coverage originated from both AeNB and PLMU. In this section, we evaluate the cellular network's performance during massive infrastructure failure, where MM-UE can play the role of low-power relay nodes to assist remote terminals out of the PLMU's coverage via multi-hop communication links. The details can be referred to [43]. In summary, the main highlights of this approach are listed below:

- It provides an analytical method for studying the effect of single- and multi-hop D2D relaying with respect to extending the coverage of PLMU.
- It introduces a novel expression describing the network-level service success probability, when multi-hop relaying is adopted to extend the coverage.

3.5.1 System model

Our study focusses on Frequency-Division Duplex (FDD) implementation of LTE-A, where the downlink and the uplink utilize a pair of frequency bands denoted here as f_{UL} and f_{DL}. It is well-known that LTE-A is based on Orthogonal Frequency Division Multiple Access (OFDMA) technology that allows the utilization of a unity frequency reuse. In order to allow this high reuse scheme, several interference mitigation techniques are implemented in LTE-A, exploiting the ability of OFDMA in assigning adjacent and granular portions of the radio resource to different users. Accordingly, for an overlapped area between two cells (that is the most affected area by the inter-cell interference), base stations use coordinated frequency-time radio resources assignments for UEs inside these areas in order to mitigate inter-cell interference [44]. Several techniques are introduced in LTE-A under the name enhanced Inter-cell Interference Coordination (eICIC) [45], that further mitigates the possible interference in heterogeneous networks due to the unity frequency reuse. In this section, we use the term *interference mitigation factor* η to denote the virtual reduction of the interfering base stations power due to the interference mitigation techniques.

3.5.2 Spatial analysis

We define a successful service as that a specific UE locates in the coverage of PLMU, which is required to have both a successful uplink service and a successful downlink service. Thus, we can represent the link-level cellular service successful probability as

$$P_c = P_{DL} \, . P_{UL} \text{ (3.2.2.1)},$$

where P_{DL} and P_{UL} are the probabilities of having a successful downlink connection and a successful uplink connection, respectively.

According to [46] (Eq. (35)), we can derive the link success probability in a Poisson network as:

$$P_s = \exp\left(-\frac{{r_o}^{\alpha}\Theta W}{P_T}\right) \times exp\left[-\frac{\pi\lambda\Gamma\left(2-\frac{2}{\alpha}\right)}{1-\frac{2}{\alpha}}\left(\frac{P_I}{P_T}\,{r_o}^{\alpha}\Theta\right)^{2/\alpha}\right]$$

We succinctly express this function as [43]:

$$P_s(P_T, \alpha, P_I, \lambda, W, \Theta, r_o) \, ,$$

where we can numerically calculate the corresponding link-level success probability by the parameters $P_T, \alpha, P_I, \lambda, W, \Theta, r_o$. It is important to note that the link-level success probability depends on the distance to the serving transmitter r_o, and it does not represent the overall network-level service success probability, which is investigated in the following sections. In light of the above, we can describe the P_{DL} and P_{UL} as the following [43]:

$$P_{DL} = P_s\left(P_T = \frac{P_b}{L_{o_c}}, \alpha = \alpha_c, P_I = \frac{P_b}{L_{o_c}}\eta_b, \lambda = \lambda_b, W = W_m, \Theta = \Theta_m, r_o\right)$$

$$P_{UL} = P_s\left(P_T = \frac{P_m G_b}{L_{o_c}}, \alpha = \alpha_c, P_I = \frac{P_m G_b}{L_{o_d}}\eta_m, \lambda = \lambda_m, W = W_b, \Theta = \Theta_b, r_o\right)$$

Note that the applied reduction factor to the interference power is the result of the interference mitigation techniques explained as follows:

- Downlink: Although the frequency reuse factor is one in LTE-A, the neighbouring PLMU exchange scheduling information amongst each other in order to avoid assigning similar downlink radio resources to MMUEs located in the cell edge. We approximate the reduction in the downlink interference due to this ICIC capability by the factor λ_b and assume that it is constant throughout the network.
- Uplink: We assume that the PLMU has the capability of assigning the uplink resources to MMUEs in an orthogonal manner, thus trying to reduce the uplink interference coming from other MMUEs. This mechanism leads to a virtual reduction in the uplink interference power, approximated in the factor $\lambda_m$that is constant throughout the network.

On the other hand, a successful D2D link requires two-way successful communication, and can be directly written as [43]:

$$P_{MMUE-MMUE} = P_s^2\left(P_T = \frac{Pm}{L_{o_d}}, \alpha = \alpha_d, P_I = \frac{Pm}{L_{o_d}}\eta_r, \lambda = \gamma\lambda_r, W = W_m, \theta = \theta_m, r_o\right),$$

where λ_r is the density of relay nodes, and $\gamma \in (0, 1]$ is a scalar factor representing the portion of the D2D relaying devices that are concurrently transmitting. The value γ=1 represents the worst case when all MMUE pairs are engaged in active transmission simultaneously, on which we focus. It is

important to mention that the presented model does not account for the possible limitation in traffic handling capability of the PLMU, but rather it assumes that network nodes can serve as many MMUE as needed. Accordingly, no blockage due to radio resources limitation is accounted. This assumption is fairly reasonable in a disaster recovery situation, where coverage rather than capacity is highly important for the search and rescue operations. However, they might not be negligible when the traffic load increases, accordingly, our model will lose its accuracy in such case.

Applying the numerical values in Table 6 to the above equations, we can plot the link-level success probability as shown in Figure 43. The plot shows both the non-fading and the Rayleigh cases where the negative effect of fading can be clearly noticed. In addition, we can notice the sharp decay in the success probability profile of D2D link, which can be referred to the limit imposed by the thermal noise. On the other hand, the smooth decay of the PLMU service success probability profile indicates an interference limited network.

Table 6: Notations and Parameters.

Symbol	Numerical Value	Explanation
α_c	3.52	Propagation exponent PLMU-MMUE
α_d	3.68	Propagation exponent of D2D link
L_{o_c}	23.4dB	Cellular propagation reference path loss
L_{o_d}	26.7dB	D2D propagation reference path loss
h	-	Rayleigh fading with unity mean
Θ_b	5dB	Service threshold at the PLMU (Uplink)
Θ_m	10dB	Service threshold at the MMUE (Downlink)
G_b	14dBi	PLMU antenna directivity
P_b	(46+G_b)dBm	PLMU EIRP power
P_m	(23+0)dBm	MMUE EIRP power
λ_b	1 km^{-2}	PLMU density
λ_b	200 km^{-2}	MMUE density
λ_r	25% λ_b	D2D-relays density
W_b	-99dBm	PLMU thermal noise
W_m	-105dBm	MMUE thermal noise
η_b	-30dB	D2D interference mitigation factor
η_m	-60dB	MMUE-PLMU interference mitigation factor
η_r	-60dB	D2D interference mitigation factor

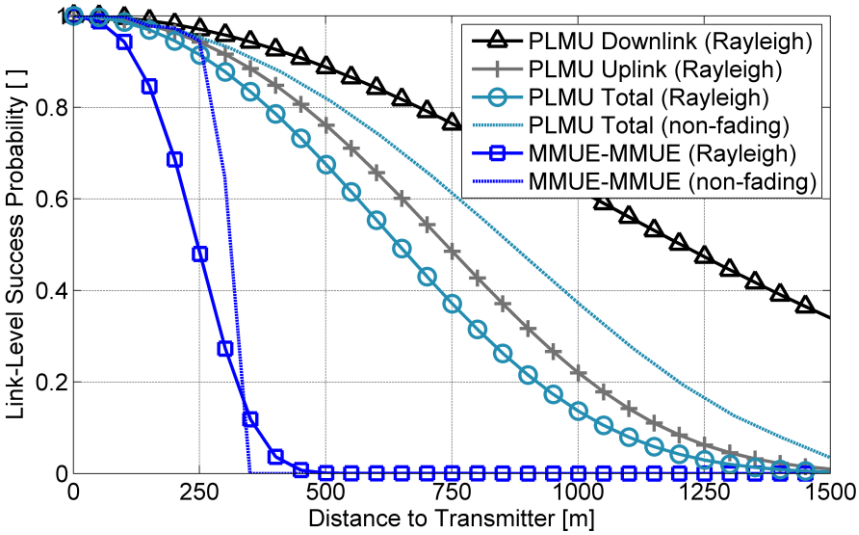

Figure 43: Link-level success probability vs. the distance from the serving transmitter [43].

3.5.3 Performance results

So far we have focused on the link-level success probability, where the distance between the serving transmitter and the receiver is known. However, in order to evaluate the average link-level performance, we need to calculate the expectancy of the link-level probability over the spatial distribution of the distance between a receiver and its serving transmitter. In an Euclidian 2D space, the probability to find at least one member X of a Poisson process Θ, i.e. $X \in \Phi$, within a search disc of radius R is well defined in the literature as the nearest neighbour or the contact distance probability, which has CDF as [47]:

$$F_{\Phi}(R) = 1 - \exp(-\lambda \pi R^2)$$

It represents the probability that a certain MMUE to find a serving transmitter (from a set of PLMU stations or set of MMUE-Relays), within a search radius R. Accordingly, we can deduce the PDF of such probability that represents the distribution of the contact distance between a UE to the serving transmitter as

$$f_{\Phi} = \frac{d}{dr} F_{\Phi}(r) = 2\lambda\pi r \exp(-\lambda \pi r^2)$$

Our main target is to obtain the average link-level success probability for both the PLMU link and for the D2D links. Accordingly, we calculate the mathematical expectancy (mean) of the service success probability in accordance to the PDF of the distance probability. Mathematically speaking, we perform the following integration [43]:

$$\kappa_o = E[P_c] = \int P_c(r)\, f_c(r)\, dr\,,$$

where f_c is the contact distance PDF between a MMUE and its nearest serving PLMU. Similarly, the average link-level D2D relaying success probability will be

$$H_o = E[P_{MMUE-MMUE}] = \int P_{MMUE-MMUE}(r)\, f_{P_{MMUE-MMUE}}(r)\, dr$$

Figure 44 shows the simulation results of applying D2D relaying to extend PLMU's coverage.

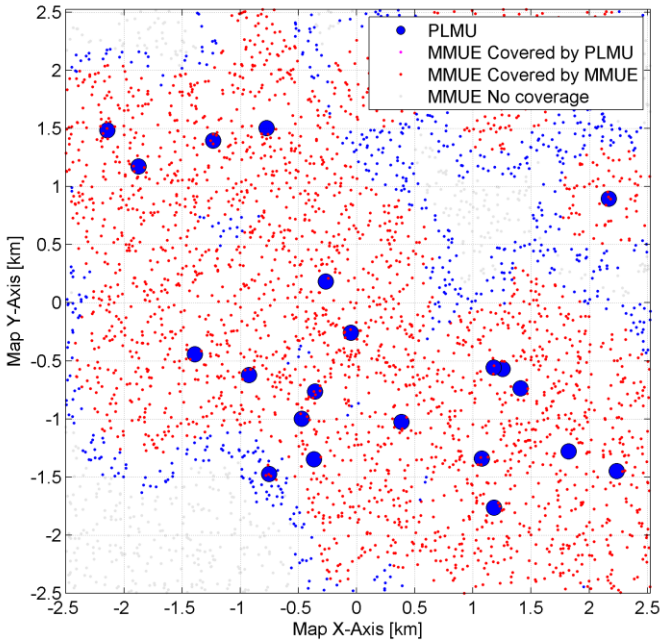

Figure 44: Coverage extension of PLMU, by D2D relaying.

3.6 **Performance of D2D relaying: Game-theoretic relay selection**

Considering public safety networks, it is very important to allow a MM-UE with low battery energy to communicate with headquarter via the AeNB. Therefore, we study a scenario where a MM-UE with low battery energy and a bad communication channel wants to communicate with the AeNB by means of cooperating with the neighbouring MM-UEs. We propose a game-theoretic model in which an optimal relay is selected to minimize the energy consumption and the delay with a given BER constraint. Figure 45 shows the scenario in which the game-theoretic model proposed here will be used to select the optimal relay MM-UE.

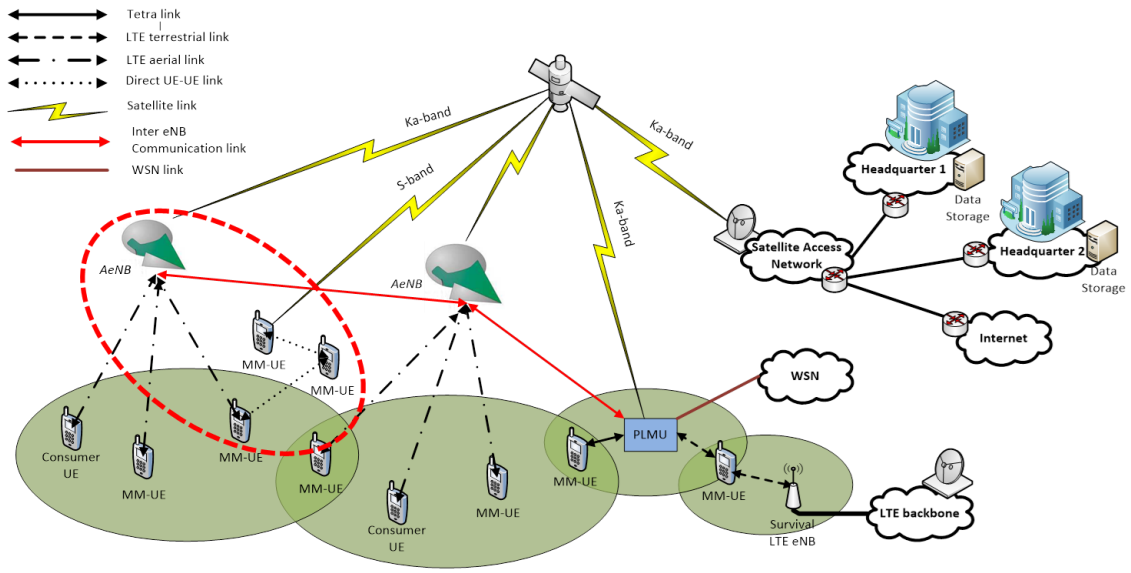

Figure 45: ABSOLUTE architecture showing the game-theoretic relay selection.

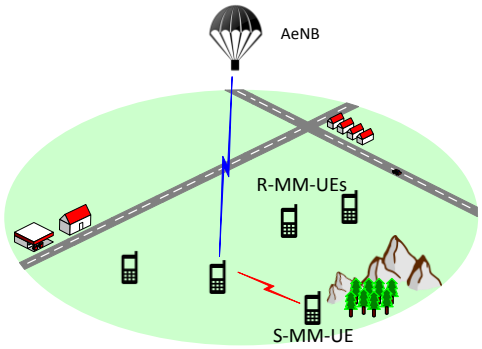

Figure 46: Network Model for Game-Theoretic Optimal Relay Selection.

3.6.1 Network model

Figure 46 shows the network model considered in this work. The MM-UE which has a bad communication channel and low residual energy sends a cooperation request to its neighbouring MM-UEs. The MM-UE asking for cooperation is henceforth called as the Source MM-UE denoted as S-MM-UE and the MM-UEs considering helping the S-MM-UE are called Relay MM-UEs denoted as R-MM-UEs. The channel for the aerial link between R-MM-UEs and the AeNB considers Rician fading in addition to the ABSOLUTE path-loss model suggested by [12] detailed in Section **Erreur ! Source du renvoi introuvable.** of this deliverable and the channel for the terrestrial link between S-MM-UE and R-MM-UEs considers Rayleigh fading in addition to log-normal shadowing [25]. It is assumed that the S-MM-UE is always in the second group (NLOS) with respect to the ABSOLUTE channel model, in other words, has a bad communication channel to the AeNB. This is one of the reasons why S-MM-UE asks for cooperation from the R-MM-UEs. It is assumed that the R-MM-UEs have their own traffic to be sent to the AeNB. Therefore, it grants only opportunistic secondary access to the S-MM-UE to send its information.

3.6.2 The game model

The background to the proposed game model in this work is presented in [48]. The game considered is a procurement auction game given by $G = < I, A, \Omega >$ where I is the set of players in the game which includes all the R-MM-UEs and the S-MM-UE, $A = A_1 \times A_2 \ldots \times A_N \times A_S$ is the Cartesian product of the set of actions available to each player where A_i is the set of actions available to player i, and Ω is the set of reward functions. We consider the game to be repeated in which multiple cooperation requests will be sent by the S-MM-UE. Therefore, the players can revise their bids over the repeated games to gain higher reward. The game considered is a first-price auction in which the player who bids the lowest wins the game. The game starts with the S-MM-UE sending a cooperation request to all the neighbouring R-MM-UEs with a BER constraint. We now analyse how the R-MM-UEs calculate their bids that need to be sent to S-MM-UE. The bid sent by R-MM-UEs is a triplet $< \widehat{P_S^t}, \widehat{\alpha_i}, \gamma_i >$ where $\widehat{P_S^t}$ is the power that needs to be transmitted by the S-MM-UE to R-MM-UE, $\widehat{\alpha_i}$ is the price asked by the R-MM-UE for cooperation and γ_i is the probability of meeting a delay threshold.

To calculate the $\widehat{\alpha_i}$, the R-MM-UEs calculate the power required to be sent to the AeNB with respect to the power sent by the S-MM-UE considering the BER constraint and then calculate their bid using,

$$\alpha_i(P_S^t) = \Lambda \kappa_i P_{R_i}^t(P_S^t)$$

where Λ is the base cost in Euros/bit/Watt which is assumed to be known to all players in the game, κ_i is the pricing index which is decided by individual R-MM-UEs and known only to themselves and not to any other player in the game and $P_{R_i}^t$ is the power transmitted by R-MM-UE to the AeNB which depends on the power transmitted by the S-MM-UE given by P_S^t due to the BER constraint. This price of α_i with respect to P_S^t is called the price-power profile (illustrated in the simulation results section). When the pricing index $\kappa_i = 1$, then the R-MM-UE receives neither profit nor loss by cooperating with the S-MM-UE. Each R-MM-UE calculates the minimum ${\kappa_i}^{min}$ using the residual battery energy and the delay metric γ_i which is given in [49]. κ_i is altered by using reinforcement learning by the R-MM-UEs which will be explained in subsequent sections. For public-safety scenarios considered in ABSOLUTE, each R-MM-UE will keep the pricing index $\kappa_i = 1$ such that it neither gains nor loses because of cooperation. However, in the case of temporary events, κ_i will be updated using reinforcement learning.

We assumed before that the S-MM-UE accesses R-MM-UE opportunistically (secondary access). To calculate the probability of meeting the delay threshold given by γ_i, R-MM-UE checks its own traffic characteristics and uses the equation provided in [49]. Assuming that the R-MM-UEs know the strategy used by the S-MM-UE for selection, which is explained in subsequent sections, they select $\widehat{\alpha_i}$ from the price-power profile and send their bids to S-MM-UE.

We now analyse the reward functions of the S-MM-UE and R-MM-UEs. The reward gained by S-MM-UE is given by,

$$\Omega_S = \Lambda P_o - C_i$$

Where, P_o is the power required to directly transmit the information from S-MM-UE to the AeNB and C_i is the economic cost to be paid by S-MM-UE to use the R-MM-UE to reach the AeNB which is given by,

$$C_i = \frac{1}{\gamma_i}(\Lambda P_S^t + \alpha_i)$$

The S-MM-UE can try to minimize the power or price depending on its policy, however, in this work we consider that S-MM-UE minimizes the price that needs to be paid to R-MM-UEs. It is assumed previously that this local policy implemented by the S-MM-UE is known to the R-MM-UEs to select their bids.

The reward gained by R-MM-UE which wins the game can be given by,

$$\Omega_i = \Lambda(\kappa_i - 1)P_{R_i}^t$$

And the reward gained by R-MM-UEs which lose the game is zero ($\Omega_i = 0$). To maximize its rewards, R-MM-UEs utilize reinforcement learning in which it alter the κ_i value in each iteration of the repeated game. The R-MM-UE which wins the j^{th} game increases its κ_i by ω_i^+ for the $j + 1^{th}$ game and R-MM-UEs which lose the j^{th} game decreases its κ_i by ω_i^- for the $j + 1^{th}$ game. However, the R-MM-UEs do not decrease their κ_i values below ${\kappa_i}^{min}$. In this way, the R-MM-UE which is advantaged by the channel conditions maximizes its reward by increasing its κ_i value. However, this increase is bounded by the competition between the R-MM-UEs such that at some point the R-MM-UE in question here will lose the game and will note this value of κ_i as ${\kappa_i}^{max}$ and henceforth will not

exceed this $\kappa_i{}^{max}$ value. Thus, the game will reach its equilibrium. It is to be noted that all κ_i values need to be reset if the channel conditions change and a new equilibrium needs to be reached by the game.

3.6.3 Performance evaluations

The simulation parameters are given in Table 8.

Table 7: Simulation Parameters

Parameters	**Values**
Aerial Channel Model	ABSOLUTE model [12] + Rician Fading
Terrestrial Channel Model	Log-Normal Shadowing + Rayleigh Fading
Rice Factor for Aerial Channel	2 dB
Path-Loss Exponent in Terrestrial Channel	2.5 – 3.0
BER	10^{-3}
Frequency	2 GHz
Data Rate from S-MM-UE	400 kbps
Data Rate from R-MM-UE	1000 kbps
Number Of Relays	3

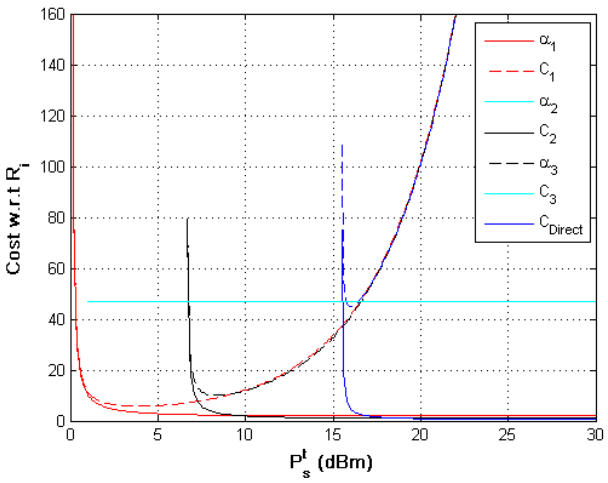

Figure 47: Price-Power profile showing α_i and Cost of all relays.

Figure 47 shows the price-power profile for all R-MM-UEs with respect to the S-MM-UE. The solid lines are the α_i of R-MM-UEs with respect to the transmit power of the S-MM-UE (P_S^t) and the dashed lines are the C_i of R-MM-UEs with respect to P_S^t. The figure also shows the cost for the S-MM-UE to directly communicate with the AeNB.

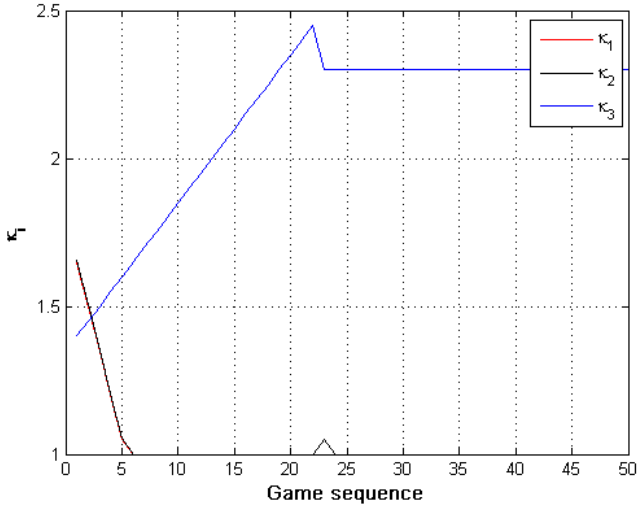

Figure 48: κ_i values v/s the game sequence for different R-MM-UEs.

Figure 48 shows the κ_i values for R-MM-UEs over the course of the repeated games including the reinforcement learning. We can clearly observe from the figure that the advantaged R-MM-UE increases its rewards by increasing its κ_i until it loses one game to another R-MM-UE. At that point, it notes down the κ_i value as κ_i^{max} and never goes above that value.

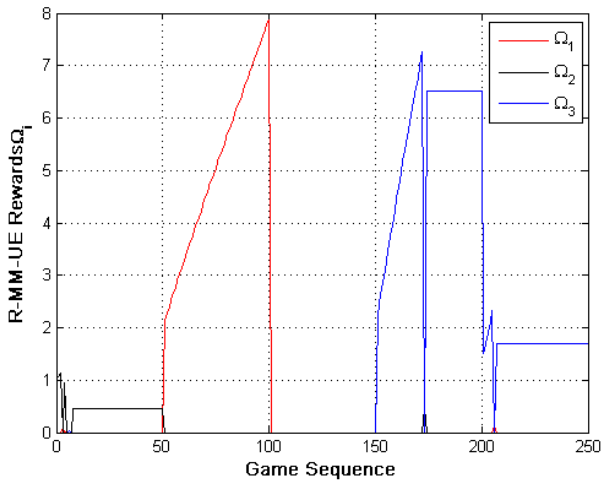

Figure 49: Rewards of all R-MM-UEs over the game sequence.

Figure 49 shows the rewards obtained by the R-MM-UEs over the game sequence. Five different channel realizations were simulated such that the fading changes and the mean path loss and locations of the R-MM-UEs and S-MM-UE remain unchanged per channel realization. For each channel realization, 50 iterations of the game were played. We can see from the figure that during the first channel realization, R-MM-UE 2 reaches the equilibrium by playing the repeated game. During the second realization, the fading channel changes and now R-MM-UE 1 starts winning the game. The equilibrium will be reached if the number of rounds were to be increased. In the third realization, we can observe that none of the R-MM-UEs received any rewards. This is due to the fact that the direct link between the S-MM-UE and the AeNB proved to be more cost-efficient than using the R-MM-UEs. In the fourth and fifth channel realizations, we can observe that R-MM-UE 3 has the advantage and wins the game reaching equilibrium.

3.7 **Performance of D2D relaying: Co-channel interference mitigation**

Power control in wireless communications is crucial to maintain a prescribed quality of service and at the same time to suppress the co-channel interference to others devices. The literature in this field is very rich and could find many techniques [50] [51] [52] [53] addressing different types of power control issues. In the recent years, power control is also used for improving the energy efficiency of transmissions especially in wireless communications [54]. In this section, we consider the power control for D2D relaying when the same carrier frequency is shared between the D2D communications and MMUEs to AeNB links. Although some preliminary works have been done in the literature for D2D power control [55] [56], we present a D2D power control taking into account an aerial-terrestrial network for the ABSOLUTE scenarios.

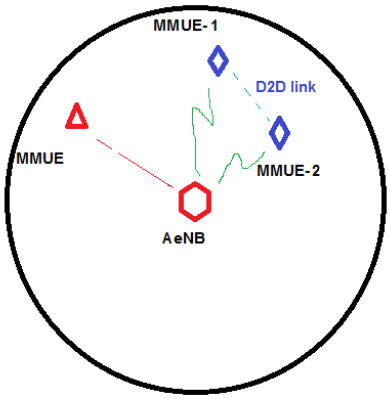

Figure 50: Network scenario considered for D2D power control

As shown in Figure 50, two terminals on the ground MMUE-1 and MMUE-2 established a D2D connection. Let the total set of uplink channels available in the access network is given by $\mathbf{U} = \{u_n\}, n = 1,2 \ldots . N$. The MMUE's participating in the D2D communication randomly select two distinct channels $u_i$and u_j from the uplink channel set **U**. The channel selection scheme for the D2D is performed in a distributed manner in which case the same channels could be selected by other MMUEs. The transmitter and the receiver associated with any D2D connection always select different channels to each other and make sure the MMUEs sense the spectrum for any existing usage of the channels in its vicinity prior to selecting them. Let us assume that K number of MMUEs select the same channel u_n for their respective D2D links. The AeNB has the capability to sense the interference in the specific channel u_n and assign uplink channels to the MMUE appropriately. We characterize the uplink interference to the AeNB in the channel u_n and propose a power control scheme to minimize the interference in the uplink transmissions.

3.7.1 Power control

We assume that the path-loss between the AeNB and the MMUE is known to MMUE by means of signal strength estimation and by the knowledge of the parameters such as AeNB's transmit power and the antenna gains. The power control algorithm is given by maximizing the ratio of signal to interference plus noise (SINR). Here, the co-channel MMUEs are denoted by $k = 1,2 \ldots K$ and K is the total number D2D links that use the same channel u_n. This technique is also subject to a constraint with an interference limit I_0 caused at the AeNB. Therefore, the algorithms can be written as

$$P = \arg\max\{\rho_k ; I_k < I_0\}$$

We characterize the performance in terms of the outage of uplink channel due to co-channel interference for the MMUE at the cell edge. We also evaluate the performance of power control by the outage probability for the D2D link. The outage probability for the uplink MMUE is given by

$$P_O^{UL} = \Pr[\gamma \leq \gamma_{min}] = F_\gamma(\gamma_{\min})$$

where $\gamma_{\min}$ is the minimum required SINR, and the outage probability for the D2D link is given by

$$P_O^{D2D} = \Pr[\rho \leq \rho_{min}] = F_\rho(\rho_{\min})$$

where $\rho_{\min}$is the minimum required signal to interference ratio at the receiver for the D2D link.

3.7.2 Performance evaluation

The proposed power control mechanism was implemented on a simulated network in MATLAB. Figure 51 shows an example network that was simulated by randomly placing nodes that engages in D2D relaying, with a serving AeNB at the centre of the area with an altitude of *L*. A single MMUE is placed at the edge of the cell (with a cell radius of $R = 1000m$). The D2D links have a maximum range of $R_{D2D} = 50m$ and a minimum of $10m$. The main aim is to clarify the outage performance of the proposed power control mechanism for (i) the D2D links and (ii) for the access link to the AeNB from the cell edge.

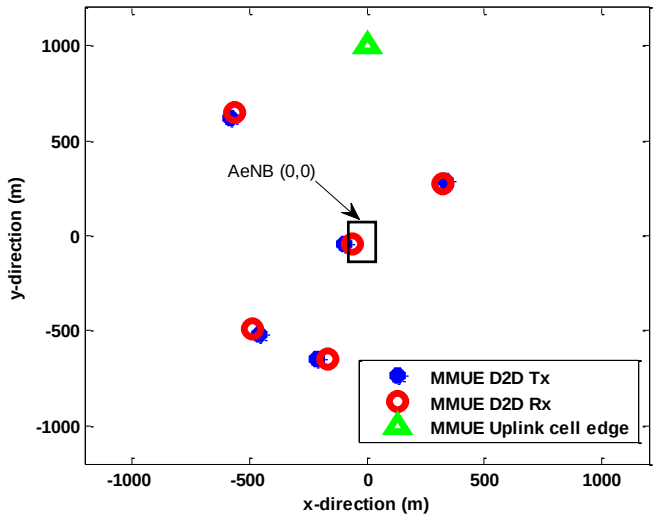

Figure 51: An example of a simulated network for D2D relaying power control.

Initially, we analyse the signal to interference distributions for the D2D transmissions and the aerial uplink access from the cell edge. Figure 52 and Figure 53 show the statistical distributions for γ and ρ, respectively, for the number of D2D users at the same channel. As we can see from Figure 52, when the number of D2D users increases, the centre of distribution (the mean of the distribution in this case) for γ is reduced. This clearly explains the increased interference in the uplink access channel with the increase in K, as same as expected. On the other hand, the distribution for the D2D signal to interference ratio ρ does not show any variation when K increases. That is because the D2D channels perform the spectrum sensing prior to using the channel u_n and only uses the unoccupied channels. The outage probabilities for P_O^{UL} for the AeNB uplink and P_O^{D2D} for the D2D links were analysed next. The outage probabilities here are the same as the cumulative distribution function (CDF) and therefore

we express the CDF in our figures. Figure 54 depicts the outage for the D2D transmissions when the terrestrial path-loss exponent α is varied, as observed from the figure the outage increases with increasing α, the outage for the uplink access does not vary with the terrestrial α because based on the power control strategy does not depend on α. A variation to the power control strategy is possible by incorporating an minimum required rate for the D2D transmissions, which in turn depends on α.

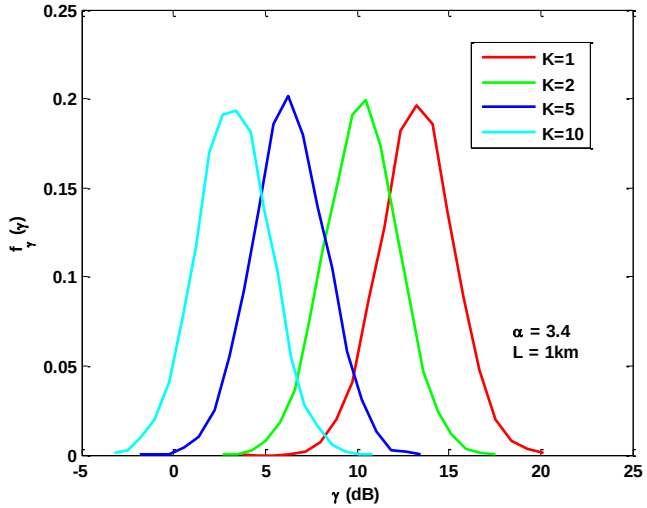

Figure 52: Distribution of the uplink SIR (γ) at the AeNB for the cell edge MMUE access, for varying number of D2D communication links.

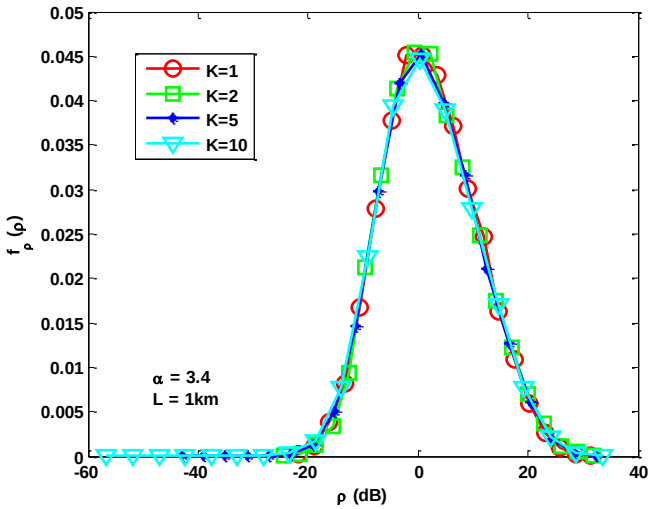

Figure 53: Distribution of the D2D link SIR (ρ) for varying number of D2D communication links.

Figure 55 depicts the outage for the uplink transmissions when the AeNB altitude L is varied. From this figure, we observe that the outage is worsened when the number L is increased due to the additional loss in the uplink transmissions and the increase in the distance between the cell edge MMUE and the AeNB. The outage in the D2D transmissions were also analysed and presented in Figure 56. From this figure, we observe that the D2D outage reduces (improves) when the AeNB altitude is increased. This is because the D2D nodes take advantage of the additional loss in the uplink due to the increase in L in increasing their transmit power levels respectively. Finally, the outage performance of the power control scheme for the D2D transmissions were compared with the case without the power control. Note that in the case of no power control, the spectrum sensing is also not

used for selecting the channel for the D2D transmissions in which case the D2D nodes do not have any knowledge of the co-channel interference. Figure 57 depicts the outage for the D2D links with the increase number K. As observed from these figures, the outage does not change with the number K for the case with power control (as discussed before). However, the outage worsens for the case without power control when K increases. Moreover, the power control in the D2D transmissions is slightly degraded due to the controlled transmit power based on the interference limit at the AeNB.

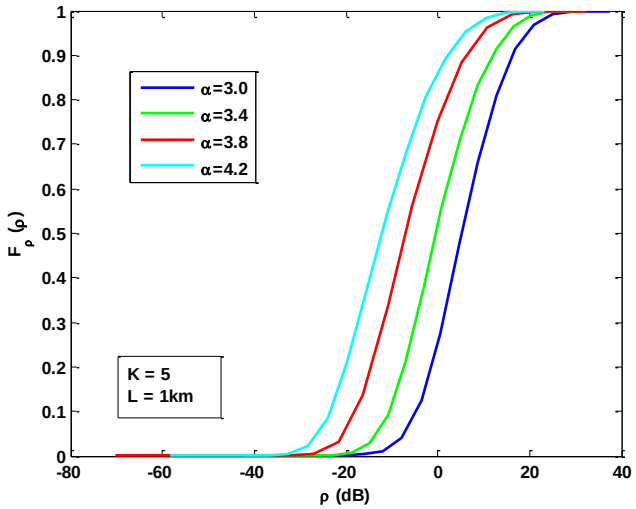

Figure 54: Outage probability variation in the D2D links for different path-loss exponents.

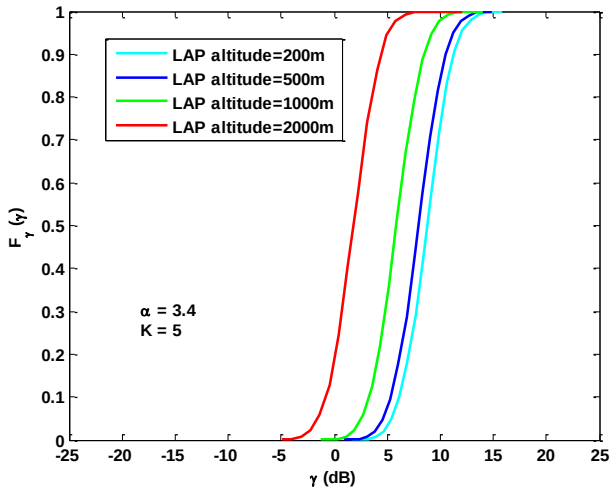

Figure 55: Outage probability variation for the uplink access with different LAP altitudes.

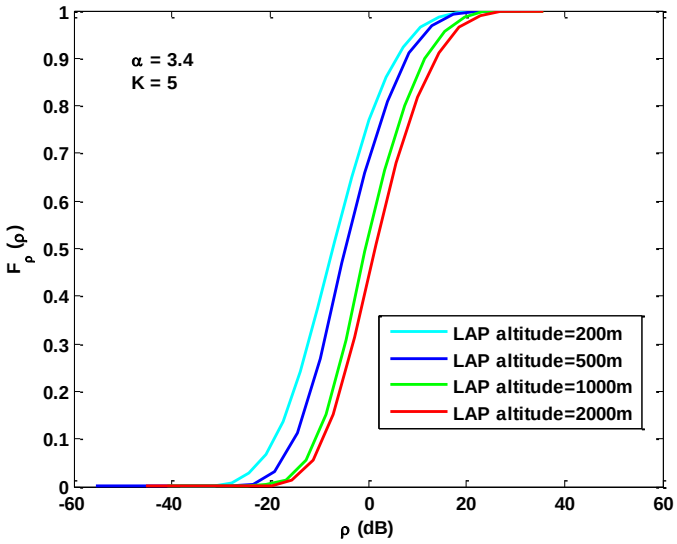

Figure 56: Outage probability variation in the D2D links for different LAP altitudes.

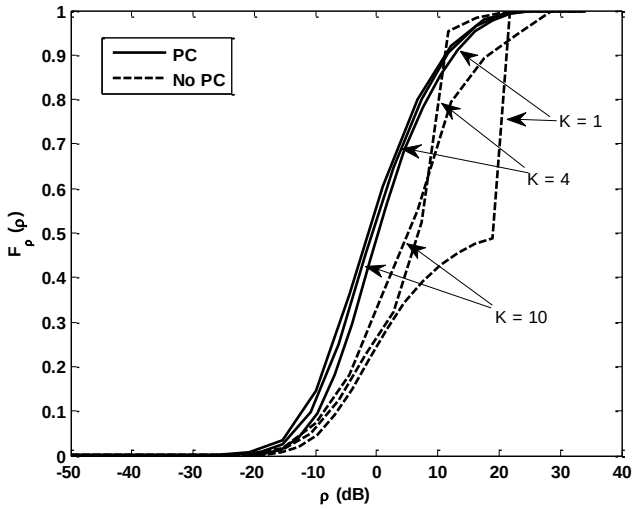

Figure 57: Outage probability for the D2D transmissions with and without power control.

Finally, we compare the outage probability for the uplink access to the AeNB with and without power control. Figure 58 depicts the outage for the uplink for different number of K. From this figure, we observe that the power control in the D2D transmissions lower the outage of cell edge, and the results show a significant improvement in the outage when power control is deployed. We observe an improvement around 14dB to achieve an outage of 0.1.

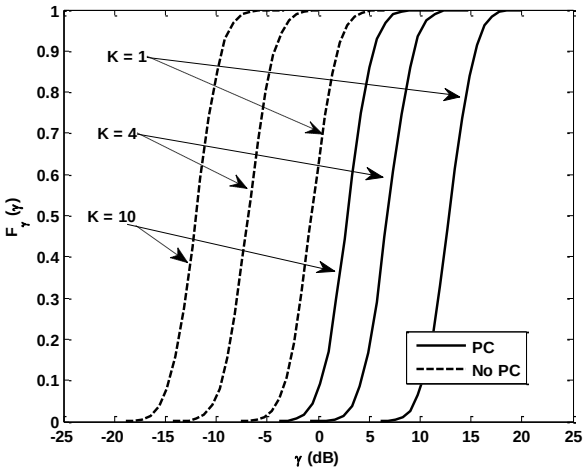

Figure 58: Outage probability for the uplink transmissions with and without power control.

3.8 **Summary**

This chapter focus on the D2D relaying. We first proposed an optimal power allocation for the opportunistic relay selection over terrestrial-aerial networks in the ABSOLUTE. The theoretical analysis and Monte-Carlo simulation corroborated that a considerable performance gain in terms of channel capacity (data rate) and outage probability (link reliability) can be achieved by such a distributed power allocation between the terminal initialling the communication and its neighbouring terminals. Based on the realistic channel models of Device-to-Device and Aerial-to-Terrestrial communication links, the impact of carrier frequencies, the number of relays, altitudes of low-altitude platform and distances among terminals on spectral efficiency are investigated. From the practical point of view, two key technical advantages of the proposed scheme can be summarized as: 1) operating in a distributed manner without any network coordination among relays; and 2) limited feedback with only a few power-control bits can achieve the near-optimal performance, which are both very encouraging. The simplicity of this scheme allows for an easy implementation in ABSOLUTE demo system and the future commercial Public Safety Communication systems.

We also propose a novel scheme coined Opportunistic Space-Time Coding (OSTC) for ABSOLUTE to combat the effect of feedback delay over the terrestrial-aerial links. When using perfect CSI, a full diversity on the number of cooperating terminals (and TeNodeBs) is achieved by the proposed scheme. In fast-fading channels, where the performance of the conventional relay selection drastically degrades and its diversity order is limited to 1 (i.e., no diversity), an order of 2 can still be achieved without any sacrifice in the spectral efficiency. To achieve a higher diversity of N, whereas Generalized Selection Combining (GSC) utilizes N orthogonal channels, only N/2 is required by OSTC thanks to the usage of Alamouti scheme. Let the spectral efficiency of GSC as a baseline, an improvement of 100% is achieved by OSTC. From the perspective of diversity-multiplexing trade-off, the proposed scheme substantially outperforms both ORS and GSC. Compared to the existing relay selection methods in opportunistic relaying, OSTC is recommended to be the best suitable method for the ABSOLUTE until now.

From the perspective of energy efficiency, we have presented an approach to find the geometrical region where placing a relay device would be optimal. Using this concept, we have developed a tractable method to estimate the energy saving gain introduced by D2D relaying. The analysis has

been based on stochastic geometry exploiting the spatial Poisson point processes' stochastic properties. Then, an analytic approach was proposed to calculate the expected coverage extension of terrestrial coverage. We showed that a relay version of the MM-UE can substantially enhance the coverage of the PLMU. This scenario will increase the coverage footprint of the deployed emergency network leading to more reliable and robust solution. Also, we proposed a game-theoretic optimal relay selection model to jointly minimize the energy consumption and the delay at the S-MM-UE. We presented the simulation results for a single S-MM-UE multiple R-MM-UEs scenario. In final, an effective power control mechanism for D2D relaying was presented. The D2D nodes also perform spectrum sensing to select the appropriate uplink channels to minimize co-channel interference. The power control technique was simulated and the outage performances were compared for the case with and without power control. The results show that a remarkable improvement in the outage performance for the uplink access to the AeNB can be achieved.

In summary, the proposed algorithms are effective, which have been verified by the realistic channel models of A2T and D2D links for ABSOLUTE: These algorithms can be applied to the ABSOLUTE use case of ABS.UC.01, ABS.UC.02, ABS.UC.18, ABS.UC.19, ABS.UC.20, ABS.UC.21, ABS.UC.22, and ABS.UC.23.

4 Protocol specifications for PLMU and D2D relaying

ABSOLUTE project aims to foster the cutting-edge technologies for public safety communication systems. The key point is the provision of 4G LTE signals over a large coverage area (several kilometres of radius) by means of the deployment of AeNBs. To leverage more stand-alone operation, the AeNB is equipped with the Flexible Management Entity (FME), which allows replacing to some extent 4G Core Network functions while giving a higher degree of flexibility. The other ABSOLUTE network entities include the terrestrial PLMU stations, satellite link and D2D-enabled MM-UEs.

The work presented in this section mainly focuses on the opportunistic relaying based on PLMU, as well as some aspect of D2D relaying that are highly correlated with PLMU-relaying, such as the cooperation and mixture of PLMU and D2D relaying for ABSOLUTE. To be specific, we investigate the interaction between D2D and PLMU relaying and the FME (see Figure 59). Procedures that will be explained hereinafter rely on the prior works already pursued in D4.1.4: "*Detailed Network and Protocol Architecture: Final Version*" [57]. However, it is necessary to detail first the possible relaying scenarios since different situations shall require the activation of different procedures and message exchange. The complete view of different relaying modes admissible within ABSOLUTE architecture is shown in Figure 60. The different cases are summarized as follows:

1. PLMU in relaying mode serving UEs camping in range,
2. PLMU with satellite backhaul serving UEs camping in range,
3. D2D relaying mode with one or more UEs served by the AeNB
4. D2D relaying mode with one or more UEs served by a PLMU connected in LTE relay mode.

Case 2 is not showed in Figure 60 since it is of less interest as it is explained hereinafter.

4.1 Protocol specifications

Relying on the work done in D4.1.4: "*Detailed Network and Protocol Architecture: Final Version*" [57] each of the different relay configurations can be distinguished. Beforehand it is anyway worth reminding that the FME is made of the *Routing Management Unit*, the *Topology Management Unit* and the *Link Management Unit*. The FME allows the AeNB (or the PLMU that is not in relaying mode) to have more autonomous behaviours replicating to some extent functions of the 4G Evolved Packet Core (EPC) network by means of a virtual EPC (vEPC) inside the Link Management Unit. vEPC functions develop through atomic blocks such as the Mobility Management Entity-Agent (MME-A), the Gateway-Agent (GW-A), the D2D-Agent (D2D-A) and the local Home Subscriber Server (HSS). In brief, the GWA manages user plane functions, whereas the MME-A manages and stores UEs information regarding their identities, mobility state and security whilst the D2D-A is responsible for UEs operating in D2D communication mode. The Routing Management Unit is responsible for finding a packet route throughout the ABSOLUTE network and it contains routing tables that are updated over time. Finally, the Topology Management Unit is responsible for the topology formation and optimization. All the units and agents inside the FME can communicate whereby suitable Application Programming Interfaces (APIs). APIs are used inside the FME to exchange different types of commands, namely Local Messaging and Remote Messaging. The former relates to any decision internal the current cell, whilst the latter relates to any decision inside another

cell (e.g., PLMU or D2D cell). As defined in D4.1.4 [57], the typical messages that can be exchanged are

a. **Cell status check message (Cell_status_check_mess):** The role of this message is to check the cell (AeNB or PLM) status.

b. **Cell activation confirmation message (Cell_activation_confirmation_mess):** The role of this message is to inform the own MME-A that the cell (AeNB or PLMU) is in active mode.

c. **Cell deactivation confirmation message (Cell_deactivation_confirmation_mess):** The role of this message is to communicate the own MME-A that the cell (AeNB or PLM) is going to be switched off.

d. **Cell activation message (Cell_activation_mess):** The role of this message is to inform a remote cell (AeNB or PLMU) that it is going to be switched on.

e. **Cell deactivation message (Cell_deactivation_mess):** The role of this message is to inform the TMU of a remote cell (AeNB or PLMU) that it is going to be switched off.

f. **Cell empty confirmation message (Cell_empty_confirmation_mess):** The role is this message is to inform the TMU that there are no MM-UEs in CONNECTED state in the cell.

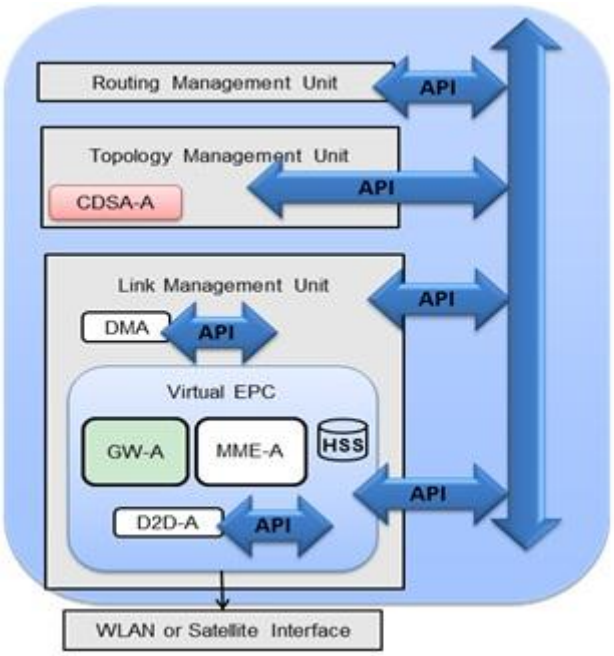

Figure 59: FME functional block diagram.

Referring to the different relay cases explained above, the following procedures are set in place.

1. PLMU in the relay mode serving UEs camping in range: Referring to Figure 60, a PLMU in the relay mode does not use an independent FME but it rather relies on control of the AeNB. Hence, the FME of the AeNB is in charge to generate activation/deactivation message for the relay network. The FME shall update correspondingly the routing tables inside the Routing Management Unit, the Topology Management Unit and the MME-A inside the vEPC. More in specific,

   a. **PLMU Relay Cell Activation Message**: this is used to inform the PLMU that the remote cell has to be activated in the relay mode

   b. **PLMU Relay Cell Deactivation Message**: this is used to inform the PLMU that the remote cell in the relay mode can be relinquished.

2. PLMU with a satellite backhaul serving UEs camping in range: In this case the PLMU is equipped with a satellite backhaul link and it performs standalone operation with respect to the AeNB and therefore it shall rely on its internal FME. Since this case is indistinguishable from a functional standpoint from that of the AeNB, it will not be analysed in the remainder of this study.

3. D2D relaying mode with one or more UEs served by the AeNB: Referring to Figure 60, a MM-UE in range of the AeNB can take the role of relay node on behalf of other MM-UEs engaged in D2D communications. Two possible situations may occur: i) MM-UEs in isolation form a D2D network and ii) MM-UEs in coverage of the AeNB start a D2D network. As already discussed in D3.4.3: "*Performance Analysis of Direct Mode LTE Communications*" [21], the two cases have to be treated differently. In this particular relay mode, the D2D-A will have an important role and interaction with the other units inside the FME. In terms of message exchange, the following can be defined

   a. **D2D Cell Activation Message**: this message is transmitted by the AeNB to the UEs that are in coverage to grant or deny permission to start a remote D2D cell.

   b. **D2D Cell Deactivation Message**: this message is transmitted by the AeNB to the UEs inside coverage that are engaged in D2D communications to relinquish the D2D network(s).

4. D2D relaying mode with one or more UEs served by a PLMU connected in LTE relay mode: This case is also showed in Figure 60 and probably represents the most complex scenario for relaying. In this particular configuration, one or more UEs that receive the signal of a PLMU with a Reference Signal Received Power (RSRP) stronger than that of the AeNB can connect to the terrestrial unit. Since the PLMU is in relay mode, it cannot rely on its own internal FME. In this case, UEs will simply carry out a standard LTE attach procedure with the PLMU including those in D2D. Therefore, no entity will have control on what occurs outside the PLMU cell although some UEs are actually camping inside the coverage area of the PLMU. This clearly highlights a difference between what occurs in a logical cell and in the physical cell. In this case no specific messages are defined and neither the D2D-A can take any active role. However, the FME shall be informed about any device through the PLMU and thus Topology and Routing Management Units can be updated still.

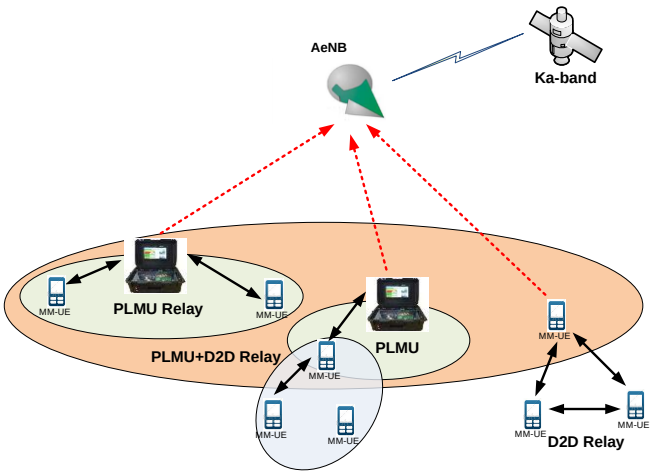

Figure 60: Different relaying mode configurations in ABSOLUTE architecture.

4.1.1 PLMU relaying

PLMU relaying is the case of a typical LTE relay mode. As explained in [58], the standard LTE relay became a part of 3GPP specifications starting from Release 10 (LTE-Advanced). Two types of relaying have been defined by 3GGP, i.e., Type I and II, with the former capable of transmitting cell specific reference signals, thus appearing to the UEs as a regular eNB and the latter unable to transmit its own reference signals, thus being transparent to the UEs. For the first case, Type I is further spit into Type Ia and Type Ib. This study focuses on relay Type Ib, which operates in-band with respect to the AeNB (donor eNB in 3GPP terminology). Since the Type Ib relay transmits its own reference signals and cell identity, UEs will be able to differentiate between being connected to a PLMU or the AeNB. For completeness, the link between a UE and the PLMU is the "access link" whereas the link from the PLMU to the AeNB is the "backhaul link".

The study that was presented in D3.2.1 "*Initial Approaches for Opportunistic Relaying for Disaster Relief and temporary Events*" [18] investigated connectivity in the relay network taking a stochastic geometry approach to model the network from a spatial standpoint. Referring to [18], the following definitions were given and reported here for the sake of subsequent explanations.

Definition 4-1 *After losing connectivity with the AeNB, the probability of connectivity is the likelihood of the event that at least one UE manages to establish a successful connection with a relay node.*

Definition 4-2 *The average degree of a relay node is the average number of UEs served by that relay.*

Definition 4-3 *The blocking probability* P_B *is the probability that an RN has no resources available for new requesting UEs.*

Definition 4-4 *The service interruption time* (SIT) *denotes the interval between the time a UE loses connectivity with the AeNB and the time it manages to establish a link with a randomly selected RN.*

The research work done in [18] relied on the assumption of modelling the distribution of relays (or PLMUs) and UEs whereby two independent homogeneous Poisson Point Processes (PPPs). The study investigated average degree of a relay node, connectivity and SIT assuming Rayleigh distributed fading without taking into account interference that might arise from the fact that LTE is a 'Frequency

Reuse 1' system. To make the study more realistic, the performance metrics mentioned above were investigated under constrained resources of the relay node. In the studies presented below similar situation is presented with the exception that now interference generated from adjacent cells will be introduced (inter-cell interference). Intra-cell interference is neglected since LTE scheduler can arbitrate resources assignment and access to the wireless channel.

As explained above, PLMU Relay Cell Activation and Deactivation messages are transmitted by the AeNB to control the start and end of the relay mode. Inside the FME, Topology Management Unit, Routing Management Unit and Link Management Unit are updated, respectively. The Topology Management Unit needs to maintain knowledge of the networks that have been deployed and their topology to create an updated view of the underlying network. The Routing Management Entity needs to update internal routing table to reach any UE at any time. The Link Management Unit requires to update the MME-A.

4.1.2 D2D relaying

The case of D2D relay mode is presented here and it was not introduced previously as well as there are no 3GPP specifications on this topic which is still an open research problem. In [21], [59], [60], [61] a novel D2D communication protocol was proposed to relief the situations of UEs in isolation and inside network coverage, although the first case was the starting point considering also activities for UEs in isolation within 3GPP. In essence, the protocol prescribes that a UE (in general the UE of the team leader of a public safety organization) can start broadcasting beacons to restore connectivity, network synchronization and enable discovery of peers in proximity (ProSe-enabled UEs as specified in 3GPP Rel. 12). Such a beaconing device is called b-UE transmitting direct-mode beacons or D-beacons. For UEs in isolation the b-UE can start broadcasting beacon frames only after a Time-of-Interruption (ToI) has elapsed and connectivity with the AeNB was not recovered. For UEs under coverage of the AeNB, the D2D network can be started only after the FME has granted the permission. A UE willing to start D2D mode shall issue a request to the AeNB, which shall grant the permission only after a cognitive process in which the decision is based on acquiring location information of the UEs deployed and building a Radio Environment Map (REM) to evaluate interference configuration (FME shall be involved in this process). D-beacons are transmitted over the uplink frequency, considering LTE in Frequency Division Duplex (FDD) mode, over Resource Blocks (RBs) in origin dedicated to the Uplink Control Channel (PUCCH). The interval between consecutive D-beacon transmissions is called D-beacon interval, assumed to be a multiple of the LTE radio frame duration (i.e. 10ms). The structure of the D-beacon interval is shown in Figure 61. Random Access Channel (PRACH) slots are used by UEs to carry out association with the b-UE whilst additional RACH (with respect to standard LTE) slots have been defined for the purpose of reserving resources in distributed fashion amongst pairs of UEs willing to communicate and without supervision of the b-UE. One resources have been reserved actual communications will take place over the Uplink Shared Channel (USCH).

D2D UEs that operate in coverage of the AeNB shall receive a D2D Cell Activation Message transmitted by the AeNB as a result of cognitive procedure done by the FME. A D2D Cell Deactivation message could be transmitted at any time by the AeNB to vanish the D2D network in case interference configuration forces to do so. The generation of the messages as well as the preliminary cognitive cycle shall be run inside the D2D-A. Furthermore, D2D UEs shall be registered inside a list maintained by the D2D-A and shall be removed from the list as soon as the D2D network

ceases operation. Clearly, for UEs in isolation the situation is different since no interaction with the AeNB is possible.

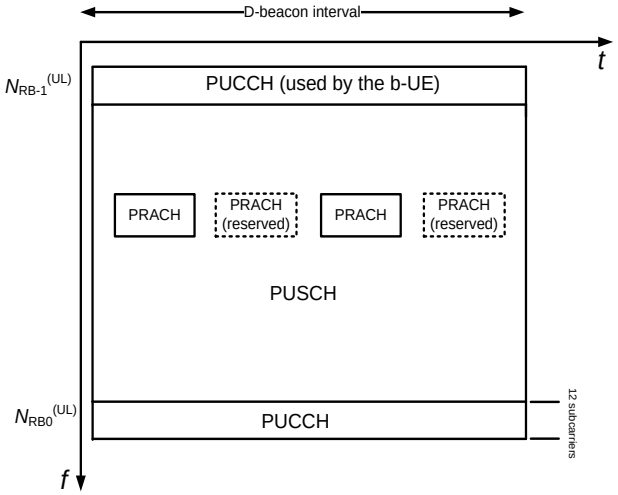

Figure 61: D-beacon interval for a network in D2D mode.

In case of D2D relay mode, D2D UEs might start in isolation but return in coverage of the AeNB due to mobility. Vice versa, the D2D network might be established with one (or more) UEs in coverage of the aerial base station since the beginning. In both cases, a user will take the role of relaying data on behalf of other peers in isolation although the two cases are not identical. For the sake of doing the relay, only the case with at least one UE in coverage of the AeNB is studied further since the case of UEs in total isolation is out of scope in this case. On the other hand, the case of D2D UEs connected to the AeNB through a two-hop relay in which the first hop is done by the PLMU is included in the study of interest from the point of view of defining protocol procedures.

The case of a D2D relay network with at least one UE in coverage of the AeNB and others in isolation will be also referred to as "mixed mode" hereinafter. Since connectivity is of utmost importance in public safety, it is worth noticing that D2D relay mode should be always permitted by the AeNB until all the UEs return in coverage. As soon as all UEs are again in coverage of the AeNB the D2D network is vanished (prior to a D2D network termination procedure [59]). A D2D network, under partial control of the AeNB should change MCS as the FME decides to adapt in relation to the spatial configuration of the interference.

Relay node other than the b-UE

In case a D2D network begins operations in isolation conditions and after some time one or more UEs return in coverage of the AeNB, D2D relay can be started. As already described in [59], UEs (including the b-UE) should periodically skip D2D mode to listen for the reference signals of the AeNB. The intention to skip D2D mode should be allowed only for UEs in idle mode (not engaged in any D2D communications). Such intention can be communicated to the b-UE sending a short message over the RACH slots already used for the association (not the RACH slots reserved for distributed resources reservation). The b-UE shall inform other D2D members whereby the D-beacon. Similarly, when the UE returns in the D2D network it should first receive the D-beacon, recover synchronization and then transmit a short command frame over the RACH. Since the D-beacon interval is assumed to last longer than an LTE radio frame, this operation could even start and end within the same D-beacon interval if connectivity with the AeNB is not recovered.

As soon as connectivity with the AeNB is recovered the UE shall start an attach procedure. However, the UE shall inform the AeNB to be member of a D2D network (e.g. defining a new preamble sequence signalling D2D mode). Consequently, the AeNB will allocate uplink/downlink resources in each radio frame. It must be noticed that resources allocated by the AeNB could conflict with the behaviour of the UE in D2D mode. In this condition the access link would conflict with the backhaul link. It is worth pointing out that

- A UE member of a D2D network which reconnects to the AeNB in regular cellular mode shall receive a D2D Cell Activation Message,
- with the AeNB aware that the particular D2D cell is in relay mode (some of the UEs are still in isolation), it should not transmit a D2D Cell Deactivation message until all UEs are again in coverage.

Furthermore, to avoid conflicts between access and backhaul links countermeasures have to be adopted. The UE that is at the same time attached to the AeNB in cellular mode and in D2D mode should inform the b-UE via the short command frame transmitted over the PRACH in which it shall notify 'dual mode' operation. The b-UE, upon recognizing the new situation, should start the D2D relay mode operation by setting an appropriate flag in the D-beacon. The b-UE will temporary shorten the D-beacon interval to the duration of an LTE radio frame and it will start a handoff procedure to handover the b-UE role to the dual mode UE. Once the handover procedure is completed the new b-UE can decide to increase again the D-beacon interval. To completely resolve the potential conflict between access and backhaul links, the new b-UE should inform other D2D members indicating in which Transmission Time Intervals (TTIs) will be unavailable for D2D mode operation. Since the b-UE cannot avoid behaving as a regular UE in cellular mode (higher priority of the AeNB), it has to communicate unavailability even though it could overlap with D-beacon transmission times. For this reason, the b-UE can adjust the D-beacon interval as well as it can decide to transmit the D-beacon frame in 'Fragmented Mode'. In Fragmented Mode, the D-beacon is simply broken down into smaller frames to adapt to the new situation.

In case the D2D Relay mode is started with some UEs under coverage of the AeNB since the beginning whilst others are in isolation, the activation of the D2D cell has to be preceded by a cognitive phase in which the D2D-A inside the FME takes the decision of whether the D2D cell can be activated and which MCS can be used. Since the UEs should notify the AeNB about their intention to engage in D2D Relay, permission to start the network should be granted by default (differently from a D2D cell without relaying functionality). In the worst case, the AeNB should notify the instructions of the D2D-A to use minimum MCS to increase communication robustness.

In both situations of UEs starting in isolation conditions or some UEs already in coverage of the AeNB, D2D Cell Activation and Deactivation messages are expected from the aerial base station conveying the necessary information (mainly MCS information) to operate the D2D cell. The role of the b-UE has to be handed-off to the UE that acts as relay point since the b-UE is the only device capable to timely notify changes in the structure of the D-beacon interval that have to be fulfilled by all other UEs. When the D2D cell finally is able to operate in relay mode, UEs will all make reservation of resources to communicate with the relay b-UE. As mentioned, the b-UE will notify the situation by enabling a flag in the D-beacon which will remain active for all the time the D2D Relay cell is in operation. The b-UE will forward communications to/from the AeNB for the D2D UEs during uplink and downlink of the cellular mode, respectively. For the rest of the D-beacon interval

the b-UE shall be in D2D mode to communicate with the other peers. The protocol described here is summarized by the structure in Figure 62.

Relay node is the b-UE

When the b-UE itself is the device skipping D2D mode to listen for the reference signals of the AeNB, it shall notify its intention in the D-beacon embedding a specific countdown. The countdown procedure can be halted at any time if D2D members require the b-UE to remain in D2D mode. More in general, the b-UE must not skip D2D mode if it is engaged in any ongoing D2D communications. In order to prevent possible disassociation from the network, the b-UE shall also inform the other UEs to reset the constant mMaxLostBeacons. mMaxLostBeacon is used by the devices as the maximum number of times a UE is allowed to avoid receiving the D-beacon consecutively prior to considering the D2D network vanished. This situation would imply disassociation with potentially dangerous isolation condition for the first responders. In case the b-UE will skip D2D mode, mMaxLostbeacons must be reset to a value higher than usual. The definition of specific values for mMaxLostBeacons is out of scope here.

The procedure described above for UEs either starting from isolation conditions or with some UEs already in coverage can be applied also to the case of the b-UE.

b-UE handoff procedure

When the UE in dual mode is not the b-UE itself, a procedure to handoff the role has to be started. The handoff procedure is done by embedding specific Handoff Information Element (HoIE) in the D-beacon including a countdown subfield before doing the handoff and the ID of the UE that will take the role of the b-UE. In case more than one UE is candidate to take the role of the b-UE, some criteria is necessary to select one with the choice under the control of the current beaconing device. Furthermore, as soon as the D2D network activates the D2D relay mode a specific bit-field shall change value to inform about the new network status. In summary, the following information shall be embedded in the D-beacon frame:

- Relay Mode bit-field: <0,1>, where ‘0’ denotes regular D2D operation and ‘1’ relay mode,
- HoIE:
    - Countdown: remaining time before swapping the b-UE role, <# of D-beacon intervals>
    - <ID of the selected UE>

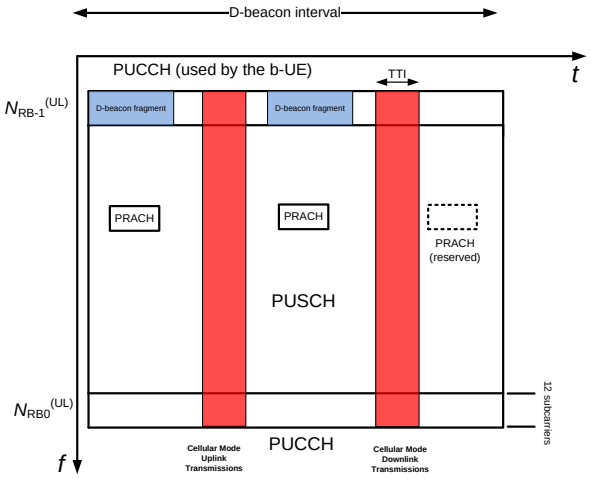

Figure 62: Modified D-beacon interval for D2D Relay Mode.

4.2 **Performance evaluation**

Public Protection & Disaster Relieve (PPDR) organizations (fire fighters, medical aid, etc) are demanded to intervene in the aftermath of a disaster or during special events to offer support to the population, rescue and security. First responders member of a PPDR organization rely on communications as an asset to carry on with different activities. So far in Europe PPDR organizations started a transition to adopt TETRA technology, thus adopting a digital communication system. Despite the improvement with respect to analogue communications, PPDR organizations cannot rely on cutting edge technologies since commercial and public safety domains do not evolve with the same pace. ABSOLUTE project is meant to fill this gap provisioning 4G LTE technology to PPDR organizations. If on the one hand first responders will be able to use not only voice based services (unicast, group call, direct mode and push-to-talk) but for example HD video as well, the fundamental prerequisite that must be guaranteed is connectivity. For the sake of this purpose the ABSOLUTE architecture prescribes using not only the AeNB to provision radio coverage but also terrestrial stations and D2D communications. Since 4G LTE is a frequency reuse 1 system, aggregate interference is a major issue to be taken into account for connectivity. In [18], connectivity study was done neglecting interference in a relay network in which the bottleneck was assumed the access link, which is the link from a UE to the PLMU configured in relay mode. To perform a realistic study, connectivity was studied under resource constrained Type Ib relay. In this way, UEs might be rejected by an overloaded relay, hence increasing the time first responders are unreachable, or the service interruption time. Definitions for connectivity and service interruption time have been provided in Definition 4-1 and Definition 4-2.

This section will show the analytical study for both PLMU and D2D relay modes when interference arising from spatially collocated networks is accounted for and modelled whereby a stochastic geometry approach. Before showing specific results a general presentation of some of the features of spatial Point Processes (PPs) will be given to provide ground for a self-contained contribution. The endeavour to model the interference in wireless networks using the theory of PPs is not new and several remarkable research contributions can be found in [62], [63], [64], [65], [66], [67], [68]. More general details on PPs can be found in [69], [70].

A Point Process is a sequence of points scattered over space that follow a specified random pattern. A more formal definition of a PP

Definition 4-5 [69]: A PP is a random variable (r.v.) taking values in the space of the integers $\mathbb{N}$.

Denoting with Φ a PP, an instantiation of the process over a subset *A* of a compact set *Ω* is denoted as

$$\varphi(A) = \sum_{x \in \Phi} 1_A(x), \tag{3}$$

where $\mathbf{1}_A(x)$ is the indicator function such that

$$1_A(x) = \begin{cases} 1, \forall x \in A \\ 0, \text{ otherwise} \end{cases}.$$

Considering now the compact space $\mathbb{R}^d$ with $A \subseteq R^d$, to a PP can be associate the concept of intensity function $\lambda_s(x)$ and an intensity measure $N(A) = E\Phi(A) = \int_A \lambda_s(x)dx$, which denotes the number of points that can be found inside *A* on average. In case of a homogeneous, stationary, isotropic PP $N(A)=\lambda_s C_d(A)$ with $C_d(A)$ denoting the volume of a *d*-dimensional ball $B_A(0,r)$ centred at zero and radius *r*. More in specific, the volume is nothing else other than the Lebesgue measure of a measurable space. The volume of the *d*-dimensional ball with unit radius ($B_A(0,1)$) has the following expression

$$C_d = \frac{\pi^{d/2}}{\Gamma(1+d/2)},$$

where Γ is the gamma function.

A PP is said to be isotropic if it is invariant to any rotation ϑ and stationary if does not depend on the particular points *y*, *z* selected over space but it rather depends on the norm ||*z*-*y*||. Furthermore, a PP is finite if the number of points in any bounded region is finite and simple if for any two points it holds that $x_i \neq x_j, \forall i \neq j$. Similarly to a simple r.v. that has moments a PP allows defining moment measures. Notably the first moment measure corresponds to the intensity measure of the PP.

Similarly to the analysis of a random process over the line (i.e. over time), it is necessary to define the concept of a 'typical' point. In this respect, Palm theory has special importance. In spatial processes a typical study case could refer to finding the distribution of the distance from a typical pint $x \in \Phi$ to another point in $\Phi \setminus \{x\}$. This clearly could be the case of interest when modelling the aggregate interference. Palm theory allows determining the properties of a PP upon conditioning on having a point of the process Φ at the location *x* as $\Pr\{\Phi \text{ has property } Y \mid x \in \Phi\}$. For a general PP the conditioning on the presence of a point of Φ at a specific location alters the properties of the PP itself but in case for example of a Poisson Point Process (PPP) this has no effect. Palm theory allows formulating the concept of the Palm distribution (P_o) and the reduced Palm distribution ($P^!_o$) depending on whether the typical point is counted or not, respectively.

A PPP is a special case of great importance since a PPP is i) simple, (ii) stationary and isotropic, (iii) points in space are independently distributed and (iv) the numbers of points in independent sets are also independent. It can be also noticed that the superposition of independent homogeneous PPPs with different intensities is again a PPP with overall intensity equal to the sum of the individual intensities. Applying an independent thinning to a PPP through a driving random measure $\Pi(x)$, the resulting point process is again Poisson but with a different intensity.

For a homogeneous PPP with intensity function λ_s, the probability to find k points within region A has the following expression

$$P\{k \text{ nodes in A}\} = \frac{\left(\lambda_s |A|\right)^k}{k!} e^{-\lambda_s |A|}, \tag{4}$$

In [71] it was proved that for a homogeneous PPP the distance to the n-nearest neighbour has the following expression

$$ED_n = \frac{\Gamma(n+1/2)}{\sqrt{\pi\lambda_s}\Gamma(n)} \sim \sqrt{\frac{n}{\pi\lambda_s}}, \tag{5}$$

where the Probability Density Function (pdf) of the distance to the 1st nearest neighbour is given by an exponential distribution $2\pi\lambda_s r \exp\left(-\lambda_s \pi r^2\right)$ for the 2-dimensional space and for the nth neighbour it can be thought as a generalization of the Erlang distribution.

In the light of Palm theory the following theorem states that for the properties of a PPP with or without conditioning on the presence of point of the process at a given location are the same.

Theorem 4-1 (Slivnyak): For a stationary PPP holds that

$$\Pr\{\Phi \text{ has property} Y \mid o\} = \Pr\{\Phi \cup \{o\} \text{has property} Y\}.$$

An immediate consequence of the Slivnyak theorem is that following Palm theory the concept of Palm measure and reduced Palm measure can be defined and for a PPP it holds that $P_o = P^!_o$.

Theorem 4-2 (Campbell): For a stationary PPP of intensity λ_s and a non-negative measurable function $f(x)$ it holds that $E(\sum_{x\in\Phi} f(x)) = \lambda \int_{R^2} f(x)dx$.
Campbell theorem is for example useful to compute the average the interference in a random network.

Theorem 4-3 (Laplace functional of a PPP): For a stationary PPP of intensity λ_s and a real-valued function $f(x)$ taking values in [0,1] the Laplace functional $L(s)$ can be written as follows

$$L(s) = E\left\{\prod_{x\in\Phi} \upsilon(x)\right\} = E^!\left\{\prod_{x\in\Phi} \upsilon(x)\right\} = \exp\left(-\lambda \int_{R^d} (1-\upsilon(x))dx\right), \tag{6}$$

where $E^!$ denotes the expectation with respect to the reduced Palm measure.

Until now some general theory of PPs was functional to understand the context and introduce homogeneous PPPs and their properties. The first modification that is necessary to introduce to model the interference in a relay network is the idea of the Matern Hard-Core (HC) Point Process. In the Matern HC process points in space are not allowed to lay closer than a certain critical distance or HC distance r_m. For this reason Matern HC PPs are particularly useful to study Carrier Sense Multiple Access (CSMA) protocols. It can be shown that the new intensity of the Matern HC process depends on the following term

$$\sigma_{HC} = \frac{1-\exp\left(-\lambda_s \pi r_m^{\ 2}\right)}{\lambda_s \pi r_m^{\ 2}}. \tag{7}$$

Previous contributions relied on the assumption of a PPP or alternatively on a Binomial Point Process (BPP), which allows already to conduct more realistic studies. Despite PPPs allows for mathematical tractability they are not inherently realistic when looking to real-world scenarios. This comes from the very simple fact that in a Poisson process the distribution of points over space is equivalent to a uniform displacement over an infinite *d*-dimensional plane with an infinite number of points as well. Furthermore, Slivnyak's theorem can be used to conclude that selecting any point in space does not change the generality of the conclusions. This is clearly not generally true and already a BPP allows distinguishing between the cases of a typical point located at the centre of an ideal reference system (e.g. in the 2-dimensional plane) and another point selected within the reference region. Anyway, even in a BPP the points are scattered uniformly over space since a PPP can be seen as the limiting case of a BPP.

Looking at the network configuration of a relay or a D2D network it can be noticed that UEs could be quite concentrated around the relay node. Despite that the two cases are different (different distance is covered), the study can be conducted in a similar manner. In other words, the modelling of the spatial point process through *cluster processes* rather than PPPs is another step forward to predict more realistic network behaviour. There are several examples of point processes more complex than Poisson explained in [69] and [70]. In the literature, Neyman-Scott is the general class of cluster point processes. One of the typical parameters adopted to study PPs is the pair correlation function $g(r)$, which highlights attraction or repulsion of points over space, thus lending to useful generalizations. For a PPP holds that $g(r)=1$, whereas this is greater than 1 for cluster processes where points show attraction and less than one for a Matern HC point process in which points exhibit repulsion.

To describe cluster processes two other processes can be defined: the process of the cluster centres and that of the daughter points around the cluster centres. Given λ_p the spatial density of the cluster centres and $\bar{c}$ the mean number of daughter points in a representative cluster C_o the total intensity is $\lambda = \lambda_p \bar{c}$. Denoting with $\Phi_p=\{x_1, x_2,...\}$ the spatial process of cluster centres, the points in the clusters are of the form $C^x=x_i+C$ and the complete process can be written as

$$\Phi = \bigcup_{x \in \Phi_p} C^x .$$

For Neyman-Scott cluster processes, the point process of cluster centres is assumed Poisson distributed. Similar to PPPs the Laplace functional can be written as follows.

Theorem 4-4 (Unconditional Laplace functional for cluster processes): The unconditional Laplace functional of a Neyman-Scott cluster process with λ_p the spatial density of the cluster centres and $\bar{c}$ the number of points in the representative cluster C_o has the following expression

$$L_o(v) = \exp\left(-\lambda_p \int_{R^d} \left(1 - M\left(\int_{R^d} \upsilon(x+y) f(y) \right) \right) dx \right), \tag{8}$$

where function $0 \le \upsilon(x) \le 1$, $f(y)$ is the pdf of a randomly selected point in the representative cluster and $M(s)$ is the generating function for the number of points in the representative cluster. It is also worth noticing that the Laplace functional has a much more complex expression than that of a PPP and to explain it more intuitively one can think to a batch arrival process over the line.

Two important types of Neyman-Scott cluster processes are the Matern cluster process in which points in the representative cluster are scattered uniformly

$$f_a(x)=\begin{cases}\frac{1}{\pi a^2}, & \|x\|\le a\\ 0, & \text{otherwise}\end{cases}, \tag{9}$$

with *a* the radius of the cluster coverage and the Thomas cluster process in which points in the representative cluster are scattered according to a normal distribution

$$f_{gauss}(x)=\frac{1}{2\pi\sigma^2}\exp\left(-\frac{\|x\|^2}{2\sigma^2}\right). \tag{10}$$

Since there is no specific pattern that can be pursued for studying the relay network more than others, the study shown hereinafter focuses only on Matern cluster processes. Hence, the number of points in the representative cluster is assumed to follow a Poisson distribution with points uniformly scattered inside the cluster.

Cluster processes, unlike PPPs, are neither isotropic nor stationary and therefore the same result obtained with Slivnyak's theorem cannot be claimed in this case. Consequently it holds that $E\left\{\prod_{x\in\Phi}\upsilon(x)\right\}\neq E^{!}\left\{\prod_{x\in\Phi}\upsilon(x)\right\}$. According to this new situation conditioning on the presence of a point at a given location in space will greatly affect both analysis and results. The Laplace functional ($L_c(s)$) for the representative cluster is the following

$$L_c(s)=M\left(\int\upsilon(x)f(x)dx\right)=\exp\left(-\bar{c}\left(1-\int_{R^2}\upsilon(x)f(x)dx\right)\right) \tag{11}$$

.

Before giving the main finding for the conditional Laplace functional of a cluster process it is necessary to give more formal definition of the reduced Palm distribution ($P^{!}_o$) for a point process that has a certain property *Y*.

$$P_o^{!}=\frac{1}{c}E\left(\sum_{x\in C_o}1_Y\left(C_{o-x}\setminus\{o\}\right)\right), \tag{12}$$

where $C_{o\text{-}x}$ is a shifted version in space of the original PP.

Theorem 4-5 (Conditional Laplace functional for cluster point processes) [72]: Let the function $0\le\upsilon(x)\le 1$, conditioning on the presence of a point of the Cluster Point Process at the origin of an hypothetical reference system, the conditional Laplace functional for Thomas and Matern cluster processes can be written as follows

$$L(v)=L_o(\upsilon)\int_{R^d}L_c\left(\upsilon(x-y)\right)f(y)dy. \tag{13}$$

Proof:

Using the Campbell-Mecke Theorem, a generalization of Theorem 4-2, focusing on the 2-dimensional space the reduced Palm distribution of the representative cluster can be written as follows

$$P_o^!(Y) = \frac{1}{c}\int_{R^2}\int_{\mathrm{N}} 1_{Yx}(C_o)P_x^!(dC_o)\bar{c}F(dx) = \int_{R^2} P(Y_x)f(x)dx \tag{14}$$

,

where to let $P_x!(dC_o) = P(Y_x)$ was used the hypothesis that points in a representative cluster are Poisson distributed. Denoting with Ψ the representative cluster and Ψ_y = Ψ +y a shifted version of the original process can be written as

$$\begin{aligned} L(v) &= \int_{\mathrm{N}}\int_{\mathrm{N}} \prod_{x\in\Phi\cup\Psi} \upsilon(x)P(d\Phi)P_o^!(d\Psi) = \int_{\mathrm{N}}\prod_{x\in\Phi}\upsilon(x)P(d\Phi)\int_{\mathrm{N}}\prod_{x\in\Psi}v(x)P_o^!(d\Psi) = \\ &= L_o(v)\int_{\mathrm{N}}\prod_{x\in\Psi}\upsilon(x)P_o^!(d\Psi) = L_o(\upsilon)\int_{\mathrm{N}}\prod_{x\in\Psi}\upsilon(x)\int_{R^2}P(d\Psi_y)f(y)dy = \\ &= L_o(v)\int_{R^2}\int_{\mathrm{N}}\prod_{x\in\Psi}\upsilon(x-y)P(d\Psi)f(y)dy = L_o(\upsilon)\int_{R^2}L_c(\upsilon(x-y))f(y)dy \end{aligned} \tag{15}$$

.

Relying on the results given in equations (8), (11) and Theorem 4-5, the conditional Laplace functional for Poisson distributed cluster process over the 2-dimensional space can be written as follows

$$L(v) = \exp\left(-\lambda_p\int_{R^2}\left[1 - M\left(\int_{R^2}\upsilon(x+y)f(y)dy\right)\right]dx\right)\times\int_{R^2}M\left(\int_{R^2}\upsilon(x-y)f(x)dx\right)f(y)dy \tag{16}$$

The result stated in equation (16) is much more complex than the Laplace functional of a Poisson Point Process and this is a direct consequence of the fact that the cluster spatial process is neither isotropic, nor stationary.

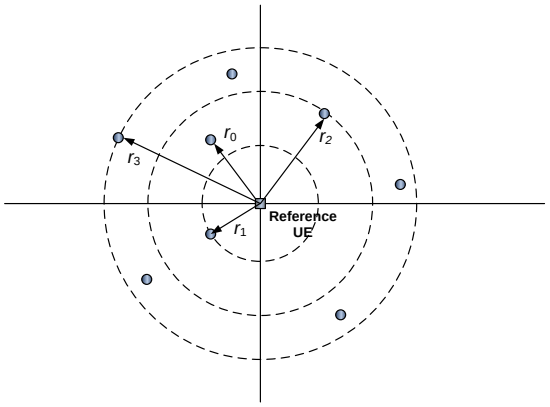

Figure 63: Scattering of points (or interferers) on the two-dimensional space.

4.2.1 Modelling aggregate interference

The modelling of the aggregated interference in wireless networks starts off with the scenario shown in Figure 63 in combination with the results obtained in the previous section. Given a transmitter at *x* and a receiver located at *y* the aggregate interference can be written as follows

$$I(x,y)=\sum_i P_{ti} g_i l_\alpha(x,y), \tag{17}$$

where P_{ti} is the transmit power of the *i*th interferer, g_i is the power fading coefficient and $l(x,y)$ is the norm defining the path-loss attenuationt of the radio signal. The interference can be written in terms of the Laplace functional as $\exp(-s\sum_i P_{ti} g_i l_\alpha(x,y)) = \prod_i \exp(-sP_{ti} g_i l_\alpha(x,y))$. In the Euclidean space and in particular for the two dimensional space the norm can be written more conveniently as $l_\alpha(x,y)=\|x-y\|^{-\alpha}$, with α the path-loss exponent and $\|\ \|$ denoting the norm. As mentioned already, interference is modelled assuming a Rayleigh distributed fading for the signal amplitude, which implies an exponentially distributed fading for the signal power. In a Rayleigh distributed fading the probability that a randomly selected test link can be successfully received by the intended receiver has the form

$$p_s = \Pr\{SINR = \frac{S}{I+N_0W} = \frac{P_{t0} g_0 l_\nu(x_0,y_0)}{\sum_{i\neq 0} g_i P_{ti} l_\nu(x_i,y_0) + N_0W} \geq \beta\} = \tag{18}$$

$$= \underbrace{\exp\left(-\beta \frac{l_\nu^{-1}(x_0,y_0)}{P_{t0}} N_0W\right)}_{\text{Noise only term}=P_{s0}} \times \underbrace{\exp\left(-\beta \frac{l_\nu^{-1}(x_0,y_0)\sum_i g_i P_{ti} l_\nu(x_i,y_0)}{P_{t0}}\right)}_{\text{Interference only term}},$$

where SINR denotes the signal-to-interference-plus-noise-ratio measured at the location of a selected receiver when the test link distance is r_0 and β denotes the threshold for detection, N_0 is one-sided noise power spectral density and W is the LTE system bandwidth.

Generality on interference modeling in wireless networks ([73]**,** [74]**)**

Referring to equation (18), the term corresponding only to interference can be computed through the Laplace functional of the interference in correspondence of a value of the transform variable $s=\beta l_\nu^{-1}(x,y)$, for some values of the parameter ν. The Laplace functional shall therefore be distinguished for the different spatial processes already mentioned above. In order to obtain the complete expression of the Laplace functional of the interference, initial conditioning upon fading realization and distance of the interferers shall be removed doing the necessary expectation operations.

A fact that will be used hereinafter to show the Laplace functional of the interference under different spatial configurations of the nodes will rely on the knowledge of the moments for a Rayleigh distributed fading

$$Eg^\nu = \Gamma(1+\nu/2)2^{\nu/2}.$$

In a simple Poisson network with a receiver located at the centre (see Figure 63**Erreur ! Source du renvoi introuvable.**), relying on the Slivnyak's theorem it can be claimed that selecting any receiver over space will allow obtaining exactly the same general conclusions in terms of the aggregate interference. Furthermore, the distance of an interfering transmitter from the centre can be modelled whereby the uniform *d*-dimensional distribution in a disk of thickness *dr* with pdf $f_R(r)=\frac{dr^{d-1}}{R^2}dr$,

where d=2 for the 2-dimensional space. For a Poisson network with initial intensity λ_s in which the density of the PLMUs follows a Matern HC process, the spatial density of the terrestrial stations is replaced with $\lambda_{HC} = \lambda_p \sigma_{HC}$ relying on the term showed in equation (7).

In a simple Poisson network the path-loss component of the signal attenuation can be written as $l(x,y) = r^{-\alpha}$, independently of the location of reference receiver and transmitter. For cluster processes instead, such a notation cannot be simplified.

The Laplace transform of a Rayleigh distributed r.v. with normalized unit power

$$L_g(sl(x,y)) = \frac{1}{1+sl(x,y)} \qquad (19)$$
$$s = \frac{\beta}{P_{t0} l(x_0, y_0)} = \frac{\beta}{P_t} r_0^{\alpha},$$

with r_0 the distance of the test link (i.e. separating the test transmitter from the reference receiver).

Theorem 4-6 (Laplace functional in a Poisson network): The Laplace functional of the aggregate interference in a Poisson network in the d-dimensional space has the following expression

$$L_p(s, \lambda_s, \nu, P_t) = \underbrace{E \exp(-sI)}_{Laplace\,functional} = \exp\left(-\lambda_s C_d (P_t s)^{\nu} E g^{\nu} \Gamma(1-\nu)\right) \qquad (20)$$
$$\nu = d/\alpha$$

.

Proof:

The calculation of the Laplace transform shall restart from $\prod_i \exp(-sP_{ti} g_i l(x,y))$. Since the interference is modelled for a homogeneous PPP, the points are uniformly distributed over space with the receiver at the centre and the pdf of the distance the d-dimensional uniform distribution. Hence, the Laplace functional has the form

$$L^{(n)}{}_p(s) = E_g E_r \prod_{i=1}^{n} \exp(-sP_{ti} g_i r_i^{-\alpha}). \qquad (21)$$

By linearity it can be further written that

$$L^{(n)}{}_p(s) = \left(E_g \int_0^R \exp(-sP_t g r^{-\alpha}) \frac{dr^{d-1}}{R^d} dr \right)^n. \qquad (22)$$

Relying now on equation (4) the Laplace functional can be rewritten as

$$L_p(s) = \exp\left\{ -\lambda_s C_d R^d \left(1 - E_g \int_0^R \exp(-sP_t g r^{-\alpha}) \frac{dr^{d-1}}{R^d} dr \right) \right\}.$$

Integrating by parts and doing the substitution $t=sgP_t r^{-\alpha}$, $dr=-\alpha sgP_t r^{-\alpha-1}$dt and letting R->∞

$$L_p(s) = \lim_{R->\infty} \exp\left\{ -\lambda_s C_d R^d \left(\frac{1}{R^d} E_g\left(sP_t g\right)^{d/\alpha} \int_0^R e^{-t} t^{-d/\alpha} dt \right) \right\} =$$

$$= \exp\left\{ -\lambda_s C_d \left(E_g\left(sP_t g\right)^{d/\alpha} \int_0^\infty e^{-t} t^{-d/\alpha} dt \right) \right\}$$

The above expression can be rewritten considering $v=d/\alpha$ and that the gamma function is $\Gamma(v) = \int_0^\infty e^{-t} t^{v-1} dt$. After few more steps the proof is completed.

Theorem 4-6 can be proved for the 2-dimensioanl plane using Theorem 4-3 and equation (19) replacing $\upsilon(r) = r^{-\alpha}$ as follows

$$L_p(s,\lambda_s,v,P_t) = \exp\left(-\lambda_s \int_{R^2} 1 - \frac{1}{1+sP_t r^{-\alpha}} d\vartheta dr \right) = \exp\left(-\lambda_s \pi \int_0^\infty \frac{2r}{1+s^{-1}P_t^{-1} r^{\alpha}} dr \right) = \quad (23)$$

$$= \exp\left(-\lambda_s (sP_t)^{2/\alpha} \frac{2\pi^2}{\alpha \sin(2\pi/\alpha)} \right)$$

The same result is obtained from equation (20) replacing the moments of the Rayleigh fading and considering that $\Gamma(1-v)\Gamma(1+v) = v\frac{\pi}{\sin(\pi v)}$ through the Eurler's reflection formula replacing d=2.

Subsequent modelling in different scenarios will rely on **[73]**, **[74]**.

Theorem 4-7 (Laplace functional of the residual interference) [74]: In a Poisson network the Laplace functional of the residual interference that the test receiver at the centre of the reference system collects due to transmitter that are located at a distance $r \geq \rho$ can be computed as follows

$$L_p(s,\lambda_s,v,P_t,\rho) = \exp\left\{ -\lambda_s \pi \left((sP_t)^v E_g\left[g^v \gamma\left(1-v, sP_t g \rho^{-\alpha}\right)\right] - \frac{sP_t \rho^{2-\alpha}}{1+sP_t\rho^{-\alpha}} \right) \right\} \quad (24)$$

where $\gamma(z,u) = \int_0^u \exp(-t) t^{z-1} dt$ is the lower incomplete gamma function.

Proof:

The proof is done considering the indicator function $1_{r>\rho}$ and distance values such that $r^{-\alpha}1_{r>\rho}$. The proof can be then completed as in Theorem 4-6.

Theorem 4-8 (Laplace functional in Matern HC process): The Laplace functional $L_p(s,\lambda_s,v,P_t)$ of the interference in a Matern HC process is obtained doing the substitution $\lambda_s = \lambda_{HC}$.

Theorem 4-9 (Laplace functional in Thomas cluster process): The conditional (on the receiver being located at a given point in the 2-dimensional space) Laplace functional of a Thomas cluster process with intensity of the cluster centres λ_p and $\bar{c}$ number of points in the reference cluster can be written as follows

$$L(s,\lambda_p,\bar{c}) = \exp\left\{-\lambda_p \int_{R^2}\left[1-\exp\left(-\bar{c}\kappa(s,z,y)\right)\right]dy\right\}\times \\ \times \int_{R^2}\exp\left(-\bar{c}\kappa(s,z,y)\,f(y)dy\right) \quad (25)$$

where $f(y)$ is the pdf of a point inside the reference cluster and

$$\kappa(z,y) = \int_{R^2}\frac{1}{1+s^{-1}\left\|x-y-z\right\|^{\alpha}}\,f(x)dx$$

Proof:

To prove this theorem it suffices to consider the Laplace transform of the conditional cluster process given in equation (16) and the expression of the Laplace functional of the reference cluster showed in equation (11). To complete the proof it is now sufficient to use the same procedure used in equation (23).

Despite the complexity of the conditional Laplace functional for the Thomas cluster process one could be tempted to conclude that with a few more manipulations it is possible to arrive at closed form expressions for equation (25). It must be noticed again that cluster processes are neither stationary nor isotropic by nature. The more complex spatial configuration prevents to obtain closed form expressions since it would be necessary to remove not only the conditioning upon the location of the interferers inside a cluster but also on the cluster centres. Complete all these operations would not yield to known closed form expressions and only numerical calculations could be done. Therefore, relying on the work done in [72], the following theorem provides lower and upper bounds to the Laplace functional in a spatial cluster process. The following results will explicitly focus on the 2-dimensional space for simplicity.

Theorem 4-10 (Upper and lower bounds for the interference in cluster processes) [72]**:** In a Thomas cluster process upper and lower bounds for the conditional Laplace functional of the interference can be written as follows

$$L_p(s,\lambda_p\bar{c},\nu,P_t)L_p\left(s,\bar{c}f_a^{*},\nu,P_t\right) \le L(s) \le L_p\left(s,\frac{\lambda_p\bar{c}}{1+\bar{c}\kappa^{*}},\nu,P_t\right) \quad (26)$$

where $\kappa^{*} = \sup_{y\in R^2}\kappa(R,y)$ and $f_a^{*} = \sup_{y\in R^2}\left(f_a \otimes f_a\right)$, where $\otimes$ is the convolution operation and f_a was given in equation (9) for the Matern cluster process.

Proof:

Referring to equation (25), the first of the two product terms can be lower bounded with

$$\exp\left\{-\lambda_p \int_{R^2}\left[1-\exp\left(-\bar{c}\kappa(s,z,y)\right)\right]dy\right\} \ge \exp\left(-\lambda_p\bar{c}\int_{R^2}\frac{1}{1+s^{-1}g(y)}\,dy\right).$$

This integral was solved already in (23). The second term in the product chain in equation (25) can be upper bounded as follows

$$\int_{R^2} \exp\left(-\bar{c}\kappa(s,z,y)\, f(y)dy\right) \geq \exp\left(-\bar{c}\int_{R^2} \kappa(R,y)\, f(y)dy\right).$$

Using the expression for the term $\kappa(z,y)$ given above, doing first a change of variable and relying on the fact that $f_a(x)=f_a(-x)$, in correspondence of $f=f_a$ it can be written that

$$\exp\left(-\bar{c}\int_{R^2} \kappa(R,y)\, f_a(y)dy\right) = \exp\left(-\bar{c}\int_{R^2} \frac{1}{1+s^{-1}g(x)} \int_{R^2} f_a(x+z-y)\, f_a(y)dydx\right)$$

Rewriting the terms in the inner integral (which is the convolution operation for the function f_a) also the second term of the conditional Laplace function is now bounded, thus proving the lower bound given in equation (26).

For the upper bound instead

$$L(s) \leq \exp\left(-\lambda_p \int_{R^2}\left[1-\frac{1}{1+\bar{c}\kappa(R,y)}\right]dy\right) = \exp\left(-\frac{\lambda_p \bar{c}}{1+\bar{c}\kappa^*}\int_{R^2}\kappa(R,y)dy\right)$$

Relying again on the result showed in equation (23) the proof is completed.

In the remainder, to model the most challenging case for PPDR organizations, only the lower bound showed in equation (26) is considered. Therefore, both terms of the lower bound will be rewritten for convenience below.

$$\underbrace{L_p(s,\lambda_p\bar{c},\nu,P_t)}_{T1}\underbrace{L_p\left(s,\bar{c}f_a^*,\nu,P_t\right)}_{T2}. \quad (27)$$

For a cluster with radius a and a Matern cluster process $f_a^* = 1/\pi a^2$. Hence, $\bar{c}f_a^*$ is nothing else than the density μ_c of points in the representative cluster.

The last cases that are shown below will be functional to derive connectivity in the relay network when CSI knowledge allows compensating for channel impairments. Two results are showed here relying on the work done in [73]. To show the effect of compensating the path-loss attenuation, the following r.v. is defined $\mathrm{P} = r^{\alpha}$, where P stands for the transmit power necessary to compensate the path-loss caused by the destination r distant away from the transmitter, given that it is capable to estimate the propagation environment materialized in the path-loss exponent α. On the other hand, in case the transmitter can estimate also the fading, it can compensate both path-loss attenuation and Rayleigh fading. This can be done introducing the following r.v. $\mathrm{P} = H \cdot r^{\alpha}$. The term H is defined as $H=g_i/g_0$, with g_0 the fading component affecting the test link and g_i the fading of the ith interfering link.

For the case of path-loss compensation only, taking the νth moment of the r.v. P in the d-dimensional space, it can be written $EP^{\nu} = Er^{d}$ since $\nu=\mathrm{d}/\alpha$. Therefore, it is necessary to compute the dth moment of the distance which, for the 2-dimensioanl space, is simply the second moment of the r.v. P.

Theorem 4-11 (Laplace functional with path-loss compensation): The Laplace functional of the interference in a Poisson network can be written as follows

$$L_{pc}(s,\lambda,\nu,P_t)=\exp\left(-\lambda C_d s^{\nu} Er^{\nu} Eg^{\nu}\Gamma(1-\nu)\right), \tag{28}$$

with λ properly replaced for each case in which the aggregate interference is studied. The Laplace functional can be rewritten in the following way

$$L_{pc}(s,\lambda,r^d,\nu,P_t)=\exp\left(-\lambda s^{\nu} Er^d \frac{\pi^2\nu}{\sin(\pi\nu)}\right). \tag{29}$$

For the case in which channel estimation allows compensating for both fading and path-loss attenuation $E\mathrm{P}^{\nu}=EH^{\nu}\cdot r^d$.

Theorem 4-12 (Laplace functional with path-loss and fading compensation): The Laplace functional of the interference in a Poisson network with compensation for both fading and path-loss attenuation has the form

$$L_{pfc}(s,\lambda,\nu,P_t)=\exp\left(-\lambda C_d s^{\nu} Er^d EH^{\nu}\Gamma(1-\nu)\right). \tag{30}$$

Since *H* is the r.v. given by the ratio between two exponentially distributed random variables (Rayleigh fading hypothesis), the *v*th moment can be written as follows

$$EH^{\nu}=Eg_i^{\nu}Eg_0^{-\nu}=\Gamma(1+\nu)\Gamma(1-\nu).$$

Using this last result the Laplace functional of the interference can be rewritten as

$$L_{pfc}(s,\lambda,r^d,\nu,P_t)=\exp\left(-\lambda C_d s^{\nu} Er^d\Gamma^2(1-\nu)\Gamma(1+\nu)\right). \tag{31}$$

To provide all the necessary elements to subsequently evaluate connectivity in both PLMU and D2D relay networks, it is necessary to generalize the concept of distance. In [21] the case in which the intended receiver is not located at the centre of the reference but elsewhere was also studied. There, by means of the Crofton fixed point theorem it was proved that the pdf of the distance for points uniformly scattered over a circle of radius *R* has the following expression

$$f_R(r)=\frac{2r}{R^2}\left[\frac{2}{\pi}\arccos\left(\frac{r}{2R}\right)-\frac{r}{\pi R}\sqrt{1-\frac{r^2}{4R^2}}\right],\ 0<r<2R \tag{32}$$

The pdf of the distance allows obtaining the moments for the r.v. of interest

$$Er^{\nu}=\frac{2\Gamma(3+\nu)}{(2+\nu)\Gamma\left(2+\frac{\nu}{2}\right)\Gamma\left(3+\frac{\nu}{2}\right)},\ \forall\,\nu>-2. \tag{33}$$

An approximation of the pdf above was obtained in [59] and [21] to model the Laplace functional in BPP network. It is worth pointing out that for a Binomial PP the numbers of points inside independent regions are not independent. This fact combined with the assumption that the reference receiver is not located at the centre justifies the study. However, for a PPP Slivniak's theorem ascertains that the particular location of a receiver does not affect the generality of the results. In this particular study spatial processes are mainly Poisson except for the cluster process. The work carried out in [59] and

[21] is used to model the general case of interference measured at the point which is not at the centre of the reference system in a cluster point process.

Theorem 4-13 (Laplace functional in a network with receiver not located at the centre): In a network in which terminals are not scattered according to a Poisson distribution, the Laplace functional of the interference with the reference receiver located at a point in space other than the reference system which is already occupied by another point can be written as follows

$$L_d(s,\lambda,\nu,P_t) = \exp\left(-\lambda\pi\left(1-D(s)\right)\right), \tag{34}$$

where

$$D(s) = E_g \frac{0.3879(\mathrm{sg})^{\frac{4}{\alpha}}\Gamma(-4/\alpha;\mathrm{sgb}^{-\alpha}) - 2.003(\mathrm{sg})^{\frac{3}{\alpha}}\Gamma(-3/\alpha;\mathrm{sgb}^{-\alpha})}{\alpha} + \tag{35}$$

$$+\frac{2.479(\mathrm{sg})^{\frac{2}{\alpha}}\Gamma(-2/\alpha;\mathrm{sgb}^{-\alpha}) - 0.088(\mathrm{sg})^{\frac{1}{\alpha}}\Gamma(-1/\alpha;\mathrm{sgb}^{-\alpha})}{\alpha}$$

It is worth pointing out that in the reminder all distance values are normalized with respect to the sensitivity range of a device in reception mode. Hence, the maximum distance between any two points is assumed for to *b*=2. The moments of the r.v. *r* which are necessary for compensating channel effects shall rely on equation (33). On the other hand, the moments of the Rayleigh distributed fading have been used extensively throughout this section.

Remark 1: Due to the difficulty to obtain closed form expressions for the Laplace functional of the interference in cluster processes, as well as that simulating the spatial process in its randomness is merely a brute force approach, in the remainder of this study the lower bound provided in Theorem 4-10 will be used to compute the success probability for uplink and downlink, distinguishing between the different cases. The lower bound will allow modelling the most difficult case of connectivity, which is not just a pessimistic assumption but rather a case of real interest for PPDR organizations.

To conclude this section, it is worth to point out that in the connectivity analysis of relay networks also the noise component showed in equation (18) will be reintroduced although relay operates in an interference dominated environment.

4.2.2 ABSOLUTE use cases

The connectivity analysis that will be showed in the next sections is tightly related to the ABSOLUTE use cases described in detail in [1]. Indeed, connectivity is a preliminary requirement of any radio network without which no meaningful task can be accomplished. This is crucial for first responders, who on one hand require improved spectral efficiency to leverage on new services supported by LTE technology, while on the other they require extremely dependable radio communications.

Referring to the full system architecture of ABSOLUTE explained in [3], the endeavour to enable first responders with a technological support which is flexible enough to cover post-disaster situations as well as temporary events could still encounter into unsatisfactory connectivity conditions. This situation might occur in case the technological advances do not fulfil the constraints provided by the actual operational scenarios. PLMU devices and D2D can greatly help in boosting up aspects such as connectivity, provided that these types of communications take place at strategic locations. Referring

to the work done in [2], placing the PLMU already at an altitude of few meters is sufficient to improve connectivity in a fading environment. However, it must be taken into account that PLMUs need to be deployed at locations in which first responders really need them and thus practical constraints arise. In this respect, it is clear that a crew of first responders must have the specific professional training to use quickly and in the best possible way ABSOLUTE technology and equipments.

The studies presented in the next sections show that when different but related radio systems operate within the same region of space, potentially in close vicinity, in a frequency reuse 1 system, problems connected with aggregate interference originated by collocated networks might arise and degrade the first requisite of PPDR organizations, which is connectivity. It will be further showed that simple power control mechanism is sufficient to improve the situation provided that channel state information is available. In order to acquire such information, channel estimation is required and quite importantly CSI must be up-to-date.

In the concluding remarks section, the link with ABSOLUTE use cases and scenarios will be completely established.

4.2.3 Connectivity analysis

This section aims to detail the connectivity analysis for a UE trying to connect to a relay network. Results given in previous sections to model interference in Rayleigh distributed fading will be used. In specific, the key idea behind this study is to model connectivity for a newcomer UE trying to join a network other than that of the AeNB in which interference configuration is non-trivial from the spatial standpoint. Similar to Section 4.1 several different cases for UEs can be specified depending also on whether knowledge of the channel state information (CSI) is assumed or not.

1. No CSI knowledge
    a. PLMU relay with interfering AeNB cellular users,
    b. D2D relay with interfering AeNB cellular users,
    c. PLMU relay with spatially collocated interfering D2D cells, PLMU cells and AeNB cellular users,
    d. D2D relay with spatially collocated interfering D2D cells, PLMU cells and AeNB cellular users.
2. Partial CSI knowledge
    a. D2D relay with spatially collocated interfering D2D cells, PLMU cells and AeNB cellular users and compensation of path-loss signal attenuation.
3. Complete CSI knowledge
    a. D2D relay with spatially collocated interfering D2D cells, PLMU cells and AeNB cellular users and compensation of fading and path-loss signal attenuation.

General system assumptions are further provided below

- All UEs and PLMUs are assumed to use the same transmit power P_t,

- All cases of interference configurations assume an infinite number of interferers to comply with the interference modelling showed in previous sections,
- The interfering transmissions that come from inside the coverage area of radius *R* are considered to give meaningful (though small) contribution, with *R* being the sensitivity range of a device in reception mode. In this study it is assumed equal for both PLMU and UE devices. Contribution of interference outside the sensitivity range has no effect,
- All distances are normalized with respect to the sensitivity range,
- *a* is the normalized (with respect to *R*) radius of the coverage for both PLMU and D2D cells,
- It holds that $a << R$, or in other words the physical range of a link is smaller than the interference range,
- In case a UE falls within the range *a* of a PLMU will try to attach to it since the RSRP is the strongest received,
- In case CSI is available (either complete or incomplete), power control is applied between test transmitter and reference receiver to compensate for channel impairments with respect to the *v*th distance neighbour computed as in equation (33),
- For the 2-dimensional case considered in remainder of this study it holds that d=2,
- Power control is applied only to links between UEs and relay nodes (either PLMU or D2D) in which UEs are already member of a network and not to newcomer device,
- The case of D2D relay mode 1.b described above with additional interference of the cellular users was mainly subject of in-depth studies in [59], [60], [61] and therefore it is not considered hereinafter, although had to be mentioned for completeness. Even though the additional interference coming from remaining cellular users is included here, this will not produce radical change in the results already provided.

As explained in [18], a UE is modelled whereby a two-state channel model shown in Figure 64. The ON state is where a UE needs to communicate in relay mode either with the PLMU or the b-UE, whereas a UE is idle in OFF state. The steady-state probability of the ON state is the following $\Pi_{on} = 1 - \Pi_{off} = \varepsilon / (\varepsilon + \tau)$.

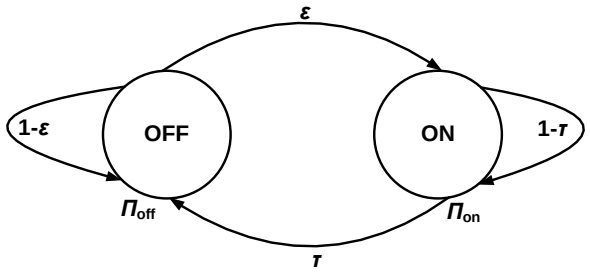

Figure 64: Two-state channel model for the behaviour of a UE.

Theorem 4-14 (Connectivity probability) [18]: The connectivity probability in a relay network (either PLMU relay mode or D2D relay mode) can be written in a very general form as follows

$$\omega = 1 - \exp\left(-(1-P_B) P_{npc} \frac{P_{UL}}{P_{DL}} \frac{\lambda_{UE}}{\lambda_{RN}} \left(1 - e^{-\lambda_{RN} P_{s0} P_{DL} |A|}\right)\right), \tag{36}$$

with P_{s0} the success probability due to the noise only term showed in equation (18), P_{UL} is the success probability under the specific interference environment and P_{DL} the success probability under the same conditions. Term P_{ncp} is the probability that a newcomer UE does not collide in the selection of one of the 64 Zadoff-Chu (ZC) preamble sequences defined by standard LTE [20]. Term P_{B} denotes the probability that a relay node (either a PLMU or a b-UE in this case) has already exhausted all the resources and the UE trying to connect is rejected by the network is trying to join. For Poisson distribution of devices over space PB has the form

$$P_B = \left(1 - \exp\left(-\lambda_{UE} P_{npc} P_{s0} P_{UL} |A| \left(1 - \left(1 - \Pi_{on}\right)^{\Pi_{on}}\right)\right)\right)^{N_{RB}},$$

where N_{RB} denotes the total number of RBs available in the LTE system. P_{UL} has to be intended as the probability of successful request to attach to a relay node (differentiating for PLMU or D2D) and P_{DL} the response over the downlink.

The number of RBs is a bandwidth dependent parameter of LTE since it grows with the system bandwidth from 6 with the minimum 1.4 MHz bandwidth up to 110 for a 20 MHz bandwidth. It is worth noticing that his holds for each of the 10 TTIs that define the LTE radio frame.

For the sake of modelling access over the PRACH slots, the standard LTE four-way handshake is used [20]. Since both PLMU and D2D relay are studied here, the same procedure applies provided that the role is logically distinguished between a terrestrial PLMU and a b-UE. According to the standard LTE procedure a newcomer UE willing to join a cell has to select first one of the 64 ZC preamble sequences at random. Following the same procedure in [20], let G denotes the normalized intensity of traffic injected over the PRACH measured in Erlangs and N_{p} denote the number of ZC sequences. As already discussed in [18], $P_{\mathrm{npc}}=\exp(-G/N_{\mathrm{p}})$.

Theorem 4-15 (Service Interruption Time) [2]: The SIT for a newcomer UE that wants to connect to a relay network (either PLMU relay or D2D relay) has the following form

$$SIT \propto \frac{1}{\omega}, \tag{37}$$

where to derive the above was assumed a geometric process in which a UE that is rejected by some relay will make the attempt to join another one. Different time constants have to be used distinguishing between D2D relaying and PLMU relaying.

Remark 2: The following results will detail how to compute connectivity probability ω and SIT for the different cases of relay mode distinguishing between the different interference configurations.

Remark 3: Since LTE is a system that employs a scheduling algorithm to resolve channel access arbitration and resources assignment, intra-cell interference does not exist. However, since LTE is a frequency reuse 1 system, inter-cell interference is the main source of transmission degradation other than propagation effects.

Although intra-cell interference does not exist in a frequency reuse 1 system inter-cell interference is an unavoidable effect. However, the transmissions originated from each relay network are not synchronized and similar to what done already in [60] time misalignment has to be taken into

consideration. Time misalignment between the interfering signals highlights the inherent robustness of the time-frequency structure of the RBs in LTE. Hence, a term taking into account for the time misalignment can be introduced distinguishing between the D2D relay and the PLMU relay assuming that interfering signals can hit the test link at any time. This mechanism is modelled with a uniform r.v. whose *ν*th moments are

$$E\delta_d{}^{\nu} = \frac{t_b}{T_D}\frac{1}{1+\nu}t_b{}^{\nu} \qquad (38)$$
$$E\delta_p{}^{\nu} = \frac{1}{N_{RB}}\frac{1}{1+\nu}T_{RF}{}^{\nu},$$

where t_b the duration of a D-beacon, T_D the duration of a D-beacon interval, T_{RF} the duration of a standard LTE radio frame and N_{RB} the number of RBs in a radio frame. It is worth pointing out that equation (38) accounts for the fact that connectivity in a D2D relay network is impaired when interference affects the reception of D-beacon frames, whereas in an PLMU relay network when interference affects downlink/uplink directions of the access link. For simplicity, to obtain the numerical results shown in the next section it is assumed that both PLMU and D2D relay networks use the same LTE system bandwidth *W* and the same path-loss exponent α is used to characterize all the links. This last assumption implies reciprocity of all the links analysed. Although this cannot be considered completely realistic it allows for mathematical tractability.

It was mentioned that the interference environment is rather complex since it includes several different interference contributions. Except for the PLMUs that form their own spatial process, UEs can only be either in

a. Cellular mode with the AeNB,
b. Cellular mode with the PLMU relay,
c. D2D mode with the b-UE relay.

To form a closed system of UEs in which mobile terminals can move around exiting and entering different networks but whose number remains the same on average, the connectivity study assumes that if the number of cellular users increases the number of D2D UEs has to decrease. In other words

$$\lambda_c + \lambda_b\bar{c} + \lambda_{HC}\bar{n} = const. = \xi\left(\lambda_p\bar{n} + \lambda_b\bar{c}\right), \qquad (39)$$

where $\xi > 1$ is a constant proportionality factor, λ_p is density of PLMUs without Matern HC repulsion, λ_c denotes the density of cellular mode UEs attached to the AeNB, λ_b denotes the density of b-UEs cluster centres and $\bar{c}$ the average number of UEs in the representative D2D cluster, $\lambda_{HC} \leq \lambda_p$ denotes the density of PLMU relays, where for $\sigma_{HC} = 1$ (or r_m->0 in equation (7)) the density of the Matern HC process coincides with that of the original process and $\bar{n}$ denotes the average number of UEs in the representative PLMU cluster. It also worth reminding that $\lambda_{HC} = \lambda_p\sigma_{HC}$.

In the following Lemmas, connectivity in different relay configurations is studied under different spatial interference configurations. Similar to [18] the attention is drawn here on the 'Access Link'. In the following lemmas, the noise only term showed in equation (18) is rewritten as

$$P_{s0} = \exp\left(-\frac{\beta}{P_t r_0^{-\alpha} / N_0 W} \right) = \exp(-\beta / \gamma_0).$$

In all cases analysed hereinafter it holds that $v=2/\alpha$ but for the sake of an analysis as general as possible v is used. Furthermore, term $D_0 = \pi v / \sin(\pi v)$ is introduced to simplify the notation whenever useful.

The transform variable s used in the remainder shall take the value $\beta / P_t r_0^{-\alpha}$, as mentioned already. Finally, L_p will denote the Laplace functional in the following lemmas with different parameters which will help studying the different cases although using a slight abuse of notation with respect to the theorems previously provided since the transmitted power is included in the transform variable s.

Lemma 4-1 (Connectivity in PLMU Relay with no CSI): In case of a relay network in which PLMUs are deployed as the only relay option, no CSI information is available and the transmitted power is assumed equal for all terminals (both PLMUs and UEs), one PLMU is assumed located at the centre of an hypothetical reference system with a UE within the normalized cluster range a doing the attempt to connect to it. Under this conditions interference contributions and the different terms of the connectivity probability ω in equation (36) can be written as follows

1. $I_{UL}=I_{PLMU}(UEs)+I_{cellular}(UEs)$ and $I_{DL}=I_{PLMU}(UEs)$, with $I_{PLMU}(UEs)$ the interference caused by other PLMU clusters and $I_{cellular}$ (UEs) the interference caused by UEs in cellular mode attached to the AeNB,
2. $\lambda_{UE} = \bar{n} / \pi a^2$ and $\lambda_{RN} = \lambda_{HC} \bar{n}$,
3. $I_{PLMU}(UEs)$: the Laplace functional of the interference is described by term $T1$ in equation (27) $\underbrace{L_p(sP_t, \lambda_{HC} \bar{n}, v)}_{T1}$,
4. $I_{cellular}(UEs)$: the Laplace functional of the interference due to UEs that are more than $\rho>a$ distant apart as in equation (24), thus the interference is $L_p(sP_t, \lambda_c, v, a)$ with $\lambda_c = \xi \lambda_p \bar{n} - \lambda_{HC} \bar{n}$.

Under these conditions, for the 2-dimensional Euclidean plane, connectivity can be studied and P_{UL} and P_{DL} to be used in Theorem 4-14 have the following expressions

$$\begin{aligned} P_{UL} &= L_p(sP_t\delta_p, \lambda_{HC}\bar{n}, v) \times L_p(sP_t, \lambda_c, v, a) = \\ &= \exp\left(-\pi\lambda_{HC}\bar{n}\left(\beta r_0^{\alpha}\delta_p\right)^v D_0(v)\right) \times \\ &\exp\left\{-\lambda_c\pi\left(\left(\beta r_0^{\alpha}\right)^v E_g\left[g^v\gamma\left(1-v, \beta r_0^{\alpha} g a^{-\alpha}\right)\right] - \frac{\beta r_0^{\alpha} a^{2-\alpha}}{1+\beta r_0^{\alpha} a^{-\alpha}}\right)\right\} \end{aligned} \quad (40)$$

where δ_p is the time misalignment for UEs in relay mode given in the second of equation (38).

$$P_{DL} = L_p(sP_t, \lambda_{HC}, v) = \exp\left(-\lambda_{HC}\pi\left(\beta r_0^{\alpha}\right)^v D_0(v)\right), \quad (41)$$

The connectivity delay is then computed $SIT = T_{RF} / \omega$ where T_{RF} is the LTE radio frame duration. In the computation of the uplink probability it was taken into account that the Laplace functional of the sum of two independent r.vs. is the product of the two individual Laplace functional.

As a remark, in case only PLMU relays are deployed, the interference can be modelled as showed above since the process of PLMUs, or cluster centres, is Poisson and hence Slivnyak's theorem can be invoked. In uplink, interference contributions are due to plink cellular users and UEs member of other PLMU clusters. In downlink, only transmission of other PLMU cluster centres can determine inter-cell interference.

Lemma 4-2 (Connectivity in PLMU+D2D Relay): In case of a relay network in which the focus in on PLMU relaying but also D2D relay is enabled, no CSI information is available and the transmitted power is assumed equal for all terminals (both PLMUs and UEs), one PLMU is assumed located at the centre of an hypothetical reference system with a UE within the normalized cluster range *a* doing the attempt to connect to it. Under this conditions interference contributions and the different terms of the connectivity probability ω in equation (36) can be written as follows

1. $I_{\mathrm{UL}}=I_{\mathrm{PLMU}}(\mathrm{UEs})+I_{\mathrm{D2D}}(\mathrm{UEs})+I_{\mathrm{cellular}}(\mathrm{UEs})$ and $I_{\mathrm{DL}}=I_{\mathrm{PLMU}}(\mathrm{UEs})$, with $I_{\mathrm{PLMU}}(\mathrm{UEs})$ is the interference caused by other PLMU clusters, $I_{\mathrm{cellular}}(\mathrm{UEs})$ is the interference caused by cellular mode UEs attached to the AeNB and $I_{\mathrm{D2D}}(\mathrm{UEs})$ is the interference caused by collocated D2D clusters,
2. $\lambda_{UE} = \bar{n} / \pi a^2$ and $\lambda_{RN} = \lambda_{HC}$,
3. $I_{\mathrm{PLMU}}(\mathrm{UEs})$: the Laplace functional of the interference is described by term $T1$ in equation (27) $\underbrace{L_p(sP_t\delta_p, \lambda_{HC}\bar{n}, \nu)}_{T1}$,
4. $I_{\mathrm{cellular}}(\mathrm{UEs})$: the Laplace functional of the interference due to UEs that are more than $\rho>a$ distant apart as in equation (24), thus the interference is $L_p(sP_t, \lambda_c, \nu, a)$ with $\lambda_c = \xi\left(\lambda_p \bar{n} + \lambda_b \bar{c}\right) - \left(\lambda_{HC} \bar{n} + \lambda_b \bar{c}\right)$
5. $I_{\mathrm{D2D}}(\mathrm{UEs})$: the Laplace functional of the interference due to D2D clusters that are $\rho>a$ can be written as $L_p(sP_t\delta_d, \lambda_b \bar{c}, \nu, a)$,
6. $I_{\mathrm{DL}}(\mathrm{UEs})$: the Laplace function of the downlink interference due to the transmission of other cluster centres or PLMUs is $L_p(sP_t, \lambda_{HC}, \nu)$

Under these conditions, for the 2-dimensional Euclidean plane, connectivity can be studied and P_{UL} and P_{DL} to be used in Theorem 4-14 have the following expressions

$$P_{UL} = L_p(sP_t\delta_p, \lambda_{HC}\bar{n}, \nu) \times L_p(sP_t\delta_d, \lambda_b\bar{c}, \nu, a) \times L_p(s, \lambda_c, \nu, a) = \quad (42)$$
$$= \exp\left(-\pi\lambda_{HC}\bar{n}\left(\beta r_0^{\alpha}\delta_p\right)^{\nu} D_0(\nu)\right) \times$$
$$\exp\left\{-\lambda_b\bar{c}\pi\left(\left(\beta r_0^{\alpha}\delta_d\right)^{\nu} E_g\left[g^{\nu}\gamma\left(1-\nu, \beta r_0^{\alpha} g a^{-\alpha}\right)\right] - \frac{\beta r_0^{\alpha} a^{2-\alpha}}{1+\beta r_0^{\alpha} a^{-\alpha}}\right)\right\} \times$$
$$\exp\left\{-\lambda_c\pi\left(\left(\beta r_0^{\alpha}\right)^{\nu} E_g\left[g^{\nu}\gamma\left(1-\nu, \beta r_0^{\alpha} g a^{-\alpha}\right)\right] - \frac{\beta r_0^{\alpha} a^{2-\alpha}}{1+\beta r_0^{\alpha} a^{-\alpha}}\right)\right\}$$

$$P_{DL} = L_p(sP_t, \lambda_{HC}, \nu) = \exp\left(-\lambda_{HC}\pi\left(\beta r_0^{\alpha}\right)^{\nu} D_0(\nu)\right), \quad (43)$$

where δ_d and δ_p are the time misalignments given in equation (38). The connectivity delay is then computed as $SIT = T_{RF}/\omega$, where T_{RF} is the LTE radio frame duration.

It is worth remarking that if a UE falls within the range of a PLMU cluster it should make the attempt to connect to it and this is the reason why D2D interference is considered only coming from a distance greater than the cluster radius.

Given the complexity of the expressions for both uplink and downlink success probabilities, in the remainder full expressions are omitted to improve the fluency of the reading.

Lemma 4-3 (Connectivity in D2D + PLMU Relay): In a relay network the focus is on D2D relaying but also PLMU relay is enabled, no CSI information is available and the transmitted power is assumed equal for all terminals (both PLMUs and UEs). One b-UE is assumed located at the centre of an hypothetical reference system with a UE within the normalized cluster range *a* doing the attempt to connect to it. The b-UE itself has a dual behaviour since it acts as relay for D2D mode UEs and it is connected to a PLMU with cluster radius *a* in range. Under this conditions interference contributions and the different terms of the connectivity probability ω in equation (36) can be written as follows

1. Link L_1 between b-UE and PLMU with connectivity probability ω_1:
    a. $I_{UL}=I_{PLMU}(UEs)+I_{cellular}(UEs)+I_{D2D}(UEs)$ and $I_{DL}=I_{PLMU}(UEs)$, with $I_{PLMU}(UEs)$ is the interference caused by other PLMU clusters, $I_{cellular}(UEs)$ is the interference caused by cellular mode UEs attached to the AeNB and $I_{D2D}(UEs)$ is the interference caused by collocated D2D clusters,
    b. $\lambda_{UE} = \bar{n}/\pi a^2$ and $\lambda_{RN} = \lambda_{HC}$,
    c. $I_{PLMU}(UEs)$: the Laplace functional of the interference is described by term $T1$ in equation (27) $\underbrace{L_p(sP_t\delta_p, \lambda_{HC}\bar{n}, \nu)}_{T1}$,
    d. $I_{cellular}(UEs)$: the Laplace functional of the interference due to UEs that are more than $\rho>a$ distant apart as in equation (24), thus the interference is $L_p(sP_t\delta_p, \lambda_c, \nu, a)$ with $\lambda_c = \xi\left(\lambda_p\bar{n} + \lambda_b\bar{c}\right) - \left(\lambda_{HC}\bar{n} + \lambda_b\bar{c}\right)$

e. I_{D2D}(UEs): the Laplace functional of the interference due to D2D clusters that are $\rho>a$ can be written as $L_p(sP_t\delta_d, \lambda_b \bar{c}, \nu, a)$,

f. I_{DL}(UEs): the Laplace function of the downlink interference due to the transmission of other cluster centres or PLMUs is $L_p(sP_t, \lambda_{HC}, \nu)$.

2. Link L_2 between a UE and b-UE with connectivity probability ω_2:

a. $I_{UL}=I_{PLMU}$(UEs)+I_{D2D}(UEs) +$I_{cellular}$(UEs) is the overall interference experienced by a b-UE during a request of a UE trying to connect,

b. $\lambda_{UE} = \bar{c}/\pi a^2$ and $\lambda_{RN} = \lambda_b$,

c. I_{PLMU}(UEs): the Laplace functional of the interference due to PLMU clusters in range of the b-UE is computed as $L_p(sP_t\delta_p, \lambda_{HC}\bar{n}, \nu)L_p\left(sP_t\delta_p, \bar{n}/\pi a^2, \nu\right)$

d. $I_{cellular}$(UEs): is computed as above,

e. I_{D2D}(UEs): the Laplace functional of the interference due other D2D networks in range of the b-UE is computed as $L_p(sP_t\delta_d, \lambda_b \bar{c}, \nu)L_p\left(sP_t\delta_d, \lambda_{UE}, \nu\right)$,

f. I_{DL}(UEs): The Laplace functional of the interference affecting a UE trying to attach to the b-UE is computed with equations (27) and (34) as $L_p(sP_t\delta_p, \lambda_b \bar{c}, \nu)L_d(sP_t\delta_d, \lambda_{UE}, \nu)$.

Under these conditions, for the 2-dimensional Euclidean plane, connectivity can be studied and P_{UL} and P_{DL} for L_1 to be used in Theorem 4-14 have the following expressions

$$P_{UL1} = L_p(sP_t\delta_p, \lambda_{HC}\bar{n}, \nu) \times L_p(sP_t\delta_d, \lambda_b \bar{c}, \nu, a) \times L_p(sP_t\delta_p, \lambda_c, \nu, a) \quad (44)$$
$$P_{DL1} = L_p(sP_t, \lambda_{HC}, \nu)$$

For L_2

$$P_{UL2} = L_p(sP_t\delta_p, \lambda_{HC}\bar{n}, \nu)L_p\left(sP_t\delta_p, \bar{n}/\pi a^2, \nu\right) \times \quad (45)$$
$$L_p(sP_t\delta_p, \lambda_b \bar{c}, \nu)L_p\left(sP_t\delta_p, \lambda_{UE}, \nu\right) \times L_p(s\delta_p, \lambda_c, \nu, a).$$
$$P_{DL2} = L_p(sP_t\delta_p, \lambda_b \bar{c}, \nu)L_d(sP_t\delta_d, \lambda_{UE}, \nu)$$

In this case the connectivity probability can be computed as $\omega = \omega_1 \times \omega_2$. The connectivity delay is then computed $SIT = T_D/\omega$ where T_D is the D-beacon interval duration.

To obtain the results for connectivity when CSI is partially or exactly known, equation (33) is used to compute the νth moment of the distance Er^d. For d=2 the second moment of the distance can be easily shown to equal a^2.

Lemma 4-4 (Connectivity in D2D + PLMU Relay + Partial CSI knowledge): In a relay network the focus is on D2D relaying but also PLMU relay is enabled, partial CSI information is available to compensate for the path-loss attenuation and the transmitted power is assumed equal for all terminals (both PLMUs and UEs). One b-UE is assumed located at the centre of a hypothetical reference system

with a UE within the normalized cluster range *a* doing the attempt to connect to it. The b-UE itself has a dual behaviour since it acts as relay for D2D mode UEs and it is connected to a PLMU in range with cluster radius *a*. Under this conditions interference contributions and the different terms of the connectivity probability ω in equation (36) can be written as follows

1. Link L_1 between b-UE and PLMU with connectivity probability ω_1:
    a. $I_{UL}=I_{PLMU}(UEs)+I_{D2D}(UEs)+I_{cellular}(UEs)$ and $I_{DL}=I_{PLMU}(UEs)$, with $I_{PLMU}(UEs)$ is the interference caused by other PLMU clusters, $I_{cellular}(UEs)$ is the interference caused by cellular mode UEs attached to the AeNB and $I_{D2D}(UEs)$ is the interference caused by collocated D2D clusters,
    b. $\lambda_{UE}=\bar{n}/\pi a^2$ and $\lambda_{RN}=\lambda_{HC}$,
    c. $I_{PLMU}(UEs)$: the Laplace functional of the interference described in equation (27) $L_{pc}(s\delta_p,\lambda_{HC}\bar{n},a^2,\nu)$,
    d. $I_{cellular}(UEs)$: the Laplace functional of the interference due to UEs that are more than $\rho>a$ distant apart as in equation (24), thus the interference is $L_p(sP_t\delta_p,\lambda_c,\nu,a)$ with $\lambda_c=\xi\left(\lambda_p\bar{n}+\lambda_b\bar{c}\right)-\left(\lambda_{HC}\bar{n}+\lambda_b\bar{c}\right)$
    e. $I_{D2D}(UEs)$: the Laplace functional of the interference due to D2D clusters that are $\rho>a$ can be written as $L_p(s\delta_d a^2,\lambda_b\bar{c},\nu,a)$,
    f. $I_{DL}(UEs)$: the Laplace function of the downlink interference due to the transmission of other cluster centres or PLMUs is $L_p(sP_t,\lambda_{HC},\nu)$.
2. Link L_2 between a UE and b-UE with connectivity probability ω_2:
    a. $I_{UL}=I_{PLMU}(UEs)+I_{D2D}(UEs)+I_{cellular}(UEs)$,
    b. $\lambda_{UE}=\bar{c}/\pi a^2$ and $\lambda_{RN}=\lambda_b$,
    c. $I_{PLMU}(UEs)$: the Laplace functional of the interference collected by the b-UE during a UE attach request due to other PLMUs that apply power control to compensate path-loss attenuation is written using equation (29) as $L_{pc}(s\delta_p,\lambda_{HC}\bar{n},a^2,\nu)L_{pc}\left(s\delta_p,\bar{n}/\pi a^2,a^2,\nu\right)$
    d. $I_{D2D}(UEs)$: the Laplace functional of the interference collected by the b-UE during the request of attach of a UE due to other D2D clusters that apply power control to compensate path-loss attenuation is written using equation (29) as $L_{pc}(s\delta_d,\lambda_b\bar{c},a^2,\nu)L_{pc}\left(s\delta_d,\lambda_{UE},a^2,\nu\right)$
    e. $I_{cellular}(UEs)$: is computed as above,
    f. $I_{DL}(UEs)$: relying on equations (29), (34) and (34) the Laplace functional of the interference collected by a receiver attempting to attach to a b-UE due to other D2D clusters is given by $L_{pc}(s\delta_p,\lambda_b\bar{c},a^2,\nu)L_d(s\delta_d,\lambda_{UE},Er^d a^d,\nu)$, with d=1,2,3,4 and the moments computed whereby equation (33).

Under these conditions, for the 2-dimensional Euclidean plane, connectivity can be studied and P_{UL} and P_{DL} for L_1 to be used in Theorem 4-14 have the following expressions

$$P_{UL1} = L_{pc}(s\delta_p, \lambda_{HC}\bar{n}, a^2, \nu) \times L_p(s\delta_d a^2, \lambda_b \bar{c}, \nu, a) \times L_p(sP_t\delta_p, \lambda_c, \nu, a) \times \quad (46)$$
$$P_{DL1} = L_p(sP_t, \lambda_{HC}, \nu)$$

.

For L_2

$$P_{UL2} = L_{pc}(s\delta_p, \lambda_{HC}\bar{n}, a^2, \nu) L_{pc}\left(s\delta_p, \bar{n}/\pi a^2, a^2, \nu\right) \times \quad (47)$$
$$L_{pc}(s\delta_d, \lambda_b \bar{c}, a^2, \nu) L_{pc}\left(s\delta_d, \lambda_{UE}, a^2, \nu\right) \times L_p(sP_t\delta_p, \lambda_c, \nu, a).$$
$$P_{DL2} = L_{pc}(s\delta_p, \lambda_b \bar{c}, a^2, \nu) L_d(s\delta_d, \lambda_{UE}, Er^d a^d, \nu)$$

Similar to the previous case the connectivity probability can be computed as $\omega = \omega_1 \times \omega_2$. The delay is then computed as $SIT = T_D / \omega$, where T_D is the D-beacon interval duration.

Lemma 4-5 (Connectivity in D2D + PLMU Relay + Perfect CSI knowledge): In a relay network the focus is on D2D relaying but also PLMU relay is enabled, perfect CSI information is available to compensate for the path-loss attenuation and fading and the transmitted power is assumed equal for all terminals (both PLMUs and UEs). One b-UE is assumed located at the centre of a hypothetical reference system with a UE within the normalized cluster range *a* doing the attempt to connect to it. The b-UE itself has a dual behaviour since it acts as a relay for D2D mode UEs and it is connected to a PLMU with cluster radius *a* in range. Under this conditions interference contributions and the different terms of the connectivity probability ω in equation (36) can be written as follows

1. Link L_1 between b-UE and PLMU with connectivity probability ω_1:
    a. I_{UL}=I_{PLMU}(UEs)+I_{D2D}(UEs)+$I_{cellular}$(UEs) and I_{DL}=I_{PLMU}(UEs), with I_{PLMU}(UEs) is the interference caused by other PLMU clusters, $I_{cellular}$(UEs) is the interference caused by cellular mode UEs attached to the AeNB and I_{D2D}(UEs) is the interference caused by collocated D2D clusters,
    b. $\lambda_{UE} = \bar{n}/\pi a^2$ and $\lambda_{RN} = \lambda_{HC}$,
    c. I_{PLMU}(UEs): the Laplace functional of the interference is described in equation (27) $L_{pfc}(s\delta_p, \lambda_{HC}\bar{n}, a^2, \nu)$,
    d. $I_{cellular}$(UEs): the Laplace functional of the interference due to UEs that are more than $\rho>a$ distant apart as in equation (24), thus the interference is $L_p(sP_t\delta_p, \lambda_c, \nu, a)$ with $\lambda_c = \xi\left(\lambda_p \bar{n} + \lambda_b \bar{c}\right) - \left(\lambda_{HC}\bar{n} + \lambda_b \bar{c}\right)$
    e. I_{D2D}(UEs): the Laplace functional of the interference due to D2D clusters that are $\rho>a$ can be written as $L_p(s\delta_d \Gamma(1-\nu)\Gamma(1+\nu)a^2, \lambda_b \bar{c}, \nu, a)$,
    f. I_{DL}(UEs): the Laplace function of the downlink interference due to the transmission of other cluster centres or PLMUs is $L_p(sP_t, \lambda_{HC}, \nu)$.

2. Link L_2 between a UE and b-UE with connectivity probability ω_2:
    a. $I_{UL}=I_{PLMU}(UEs)+I_{D2D}(UEs)+I_{cellular}(UEs)$,
    b. $\lambda_{UE}=\bar{c}/\pi a^2$ and $\lambda_{RN}=\lambda_b$,
    c. $I_{PLMU}(UEs)$: the Laplace functional of the interference collected by the b-UE during a UE request of attach due to other PLMUs that apply power control to compensate path-loss attenuation and fading is written using equation (31) as $L_{pfc}(s\delta_p,\lambda_{HC}\bar{n},a^2,\nu)L_{pfc}\left(s\delta_p,\bar{n}/\pi a^2,a^2,\nu\right)$
    d. $I_{D2D}(UEs)$: the Laplace functional of the interference collected by the b-UE during the a UE request of attach due to other D2D clusters that apply power control to compensate path-loss attenuation and fading is written using equation (31) as $L_{pfc}(s\delta_d,\lambda_b\bar{c},a^2,\nu)L_{pfc}\left(s\delta_d,\lambda_{UE},a^2,\nu\right)$
    e. $I_{cellular}(UEs)$: is computed as above,
    f. $I_{DL}(UEs)$: relying on equations (31), (34) and (34) the Laplace functional of the interference collected by a receiver attempting to attach to a b-UE due to other D2D clusters is given by $L_{pfc}(s\delta_d,\lambda_b\bar{c},a^2,\nu)L_d(s\delta_d\Gamma(1-\nu)\Gamma(1+\nu),\lambda_{UE},Er^d a^d,\nu)$, with d=1,2,3,4 and the moments computed whereby equation (33).

Under these conditions, for the 2-dimensional Euclidean plane, connectivity can be studied and P_{UL} and P_{DL} for L_1 to be used in Theorem 4-14 have the following expressions

$$\begin{aligned}&P_{UL1}=L_{pfc}(s\delta_p,\lambda_{HC}\bar{n},a^2,\nu)\times L_p(s\delta_d\Gamma(1-\nu)\Gamma(1+\nu)a^2,\lambda_b\bar{c},\nu,a)\times\\&L_p(sP_t\delta_p,\lambda_c,\nu,a)\\&P_{DL1}=L_p(sP_t,\lambda_{HC},\nu)\end{aligned}\quad(48)$$

For L_2

$$\begin{aligned}&P_{UL2}=L_{pfc}(s\delta_p,\lambda_{HC}\bar{n},a^2,\nu)L_{pfc}\left(s\delta_p,\bar{n}/\pi a^2,a^2,\nu\right)\times\\&L_{pfc}(s\delta_d,\lambda_b\bar{c},a^2,\nu)L_{pfc}\left(s\delta_d,\lambda_{UE},a^2,\nu\right)\times L_p(sP_t\delta_p,\lambda_c,\nu,a)\\&P_{DL2}=L_{pfc}(s\delta_d,\lambda_b\bar{c},a^2,\nu)L_d(s\delta_d\Gamma(1-\nu)\Gamma(1+\nu),\lambda_{UE},Er^d a^d,\nu)\end{aligned}\quad(49)$$

Similar to the previous case the connectivity probability can be computed as $\omega=\omega_1\times\omega_2$. The \delay is then computed as $SIT=T_D/\omega$, where T_D is the D-beacon interval duration.

Table 8: Numerical parameters for simulations

Parameter	**Description**	**Value**
P_t	Transmit power	23 dBm
R_{max}	Maximum sensitivity range	1000 m
B	Detection threshold	3 dB

α	Path-loss exponent	{2.01, 4}
a	Normalized cluster radius for both PLMU and D2D	0.8
T_{RF}	LTE radio frame duration	10 ms
T_{D}	D-beacon interval	80 ms
t_{b}	D-beacon overhead with respect to D-beacon interval	10%
W	LTE system bandwidth	10 MHz
G	Normalized PRACH traffic intensity	0.1
N_{p}	Number of ZC preamble sequences	64
Π_{on}	Steady-state probability a UE is active	[0,1]
τ	Transition probability a UE returns in idle state	{0.3,0.6}
ξ	Scale factor for cellular users density computation	1.05
λ_{HC}	Matern HC intensity	[0,1]
λ_{p}	Density of b-UEs	1.8
λ_{b}	Density of PLMUs	0.2
$\bar{n}$	Number of UEs in a PLMU cluster	20
$\bar{c}$	Number of UEs in a D2D cluster	15

4.2.4 Numerical results

Numerical values used for the connectivity analysis in both PLMU and D2D relay networks are showed in Table 8. The duration of D-beacon interval and LTE radio frame are normalized to milliseconds for the sake of producing results. All distance ranges which are used for numerical evaluations are normalized with respect to the values of $R_{\max}$ given in the table above. The thermal noise power spectral density equals N_0=-174 dBm/Hz. The link budget for computing the SNR γ_0 which is used in the probability P_{s0} is computed as

$$\gamma_0 = P_t - \alpha \times 10\log_{10}(r_0) - \alpha \times 10\log_{10}(R_{\max}) - (N_0 + 10\log_{10}(W[Hz])). \quad (50)$$

Results for the case of D2D connectivity will be shown with and without applying power control on the basis of the CSI knowledge. As mentioned already above, when power control is applied, it is assumed that the size of the link between the test transmitter and the reference receiver (UE trying to attach to the selected b-UE) corresponds to the dth moment of distance computed whereby equation (33) for d=2. Furthermore, UEs which are already attached as well as the relay stations can apply power control whereas a newcomer UE trying to connect is assumed to perform operations at maximum power since it might not have sufficient channel information. The SIT, which is inversely proportional to the connectivity probability ω, is computed for the D2D network considering the duration of the D-beacon interval T_{D}. On the other hand, for PLMU relay, the SIT is computed using the duration of the LTE radio frame T_{RF}.

The results presented hereinafter are a selection of the whole set of possible results which can be obtained whereby the general analysis showed above in order to provide a better understanding of the connectivity problem for PPDR organizations that operate in critical conditions. Therefore, results will not be showed for all the cases presented until here but a selection is functional to provide more focused discussion as well as to avoid reproducing an excessive amount of similar figures which would reduce the readability of the contribution.

PLMU relaying

Numerical results for connectivity probability ω and SIT are given respectively in Figure 65 and Figure 66 for α=2.01 and Π_{on}=0.8 for the case in which PLMUs are the only relay options. Similar results are showed for α=4 in Figure 67 and Figure 68, respectively. Results are plot with respect to the normalized test link distance r_0 and for different values of the Matern HC probability r_m (which affects σ_{HC}) or in other words reducing the spatil density of the PLMUs. To completely understand the results, it must be taken into account that not only the aggregate interference (collocated PLMUs and cellular users in this case) contributes but also the event that the (randomly) selected relay node is in overloading conditions and consequently the attach request is rejected. The results show behaviour similar to what already highlighted by the study done in [18]. In [18] it was evident that there exist values of the normalized test link distance r_0 for which connectivity probability is maximized. In particular, the figures highlight the complexity and the dependence from the spatial configuration of the interference and noise which is further mixed with relay overloading conditions. Indeed, three regions can be identified. In the first region (region on the left hand side of the maximum) connectivity is small but it shows to grow quickly with r_0. In the middle region connectivity is maximized and in the third region (on the right hand side of the maximum) connectivity goes rapidly to zero as the normalized distance r_0 increases. The effect of increasing the path-loss α is to shift the optimal region towards higher values of r_0 moving from α=2.01 to α =4. This shows that in propagation conditions near to free space the useful signal can be received with a higher power but the same holds true also for the interfering signals, thus mixing the effects in a non trivial manner. In both propagation conditions, increasing the test link distance, the SIT grows without bound (in the order of tens seconds in Figure 66 and Figure 68), thus highlighting a dangerous condition of first responders operating in isolation conditions. The study presented here completes what was done already in [18] for the case without interference. The figures show also the non-obvious effect of the Matern HC distance r_m. Increasing the hard core distance (or reducing the spatial density of the PLMUs) the connectivity probability increases but on the other hand the whole connectivity becomes more sensitive to the link distances r_0 (the distance range values that maximizes connectivity becomes narrower). This effect can be explained thinking that reducing the spatial density of PLMUs the opportunity to attach to one which is not overloaded reduces. The results show also that selecting a high value of the probability Π_{on} (as it could be during talk sparks) that UEs are active greatly affects connectivity. Concluding, PLMUs will be really effective to relieve connectivity holes only under certain spatial configurations, whereas an excessive amount of PLMUs deployed or the wrong spatial collocation of these network elements could reduce the effectiveness of the solution.

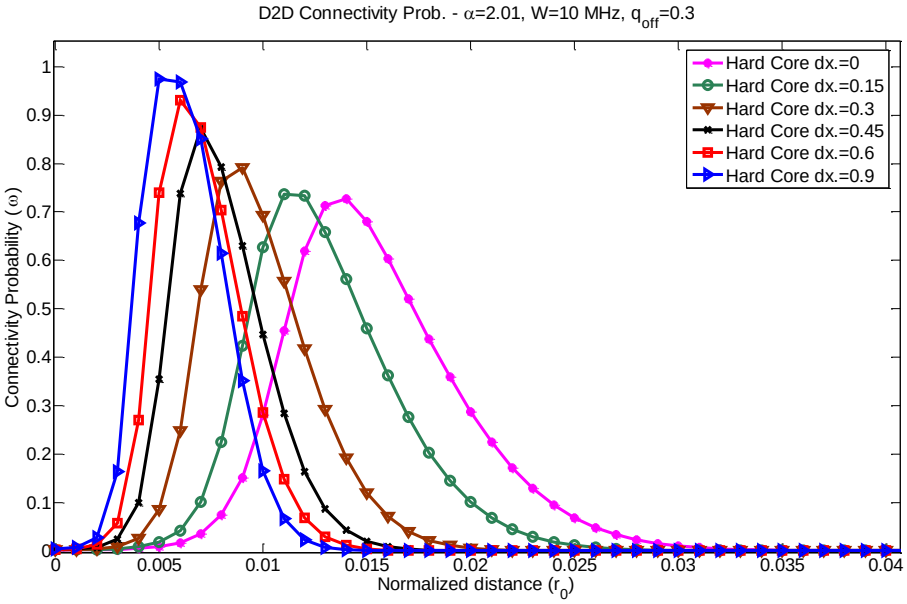

Figure 65: PLMU relaying with no CSI knowledge. Connectivity probability ω for α=2.01, Π_{on}=0.8 vs. normalized test link distance r_0 and for different values of the Matern HC distance of the spatial PLMU process.

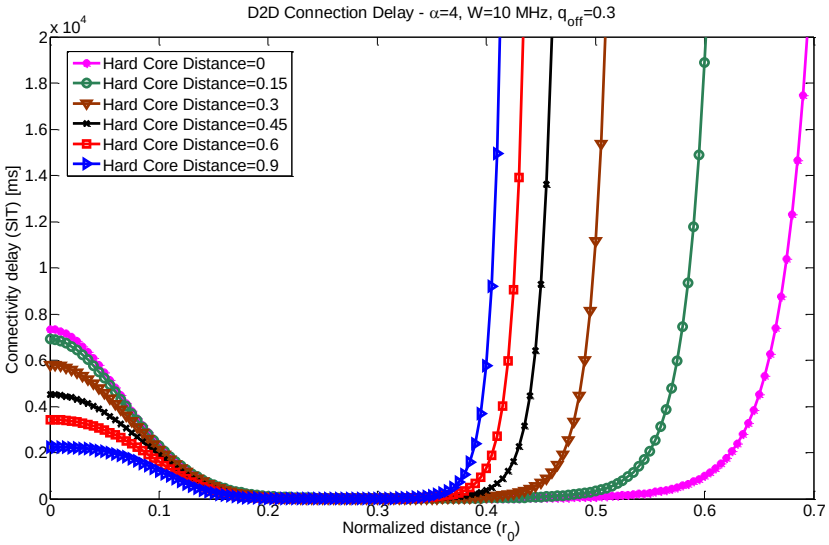

Figure 66: SIT for a UE trying to attach to a PLMU relay with no CSI knowledge, α=2.01, Π_{on}=0.8 vs. normalized test link distance r_0 and for different values of the Matern HC distance for the spatial PLMU process.

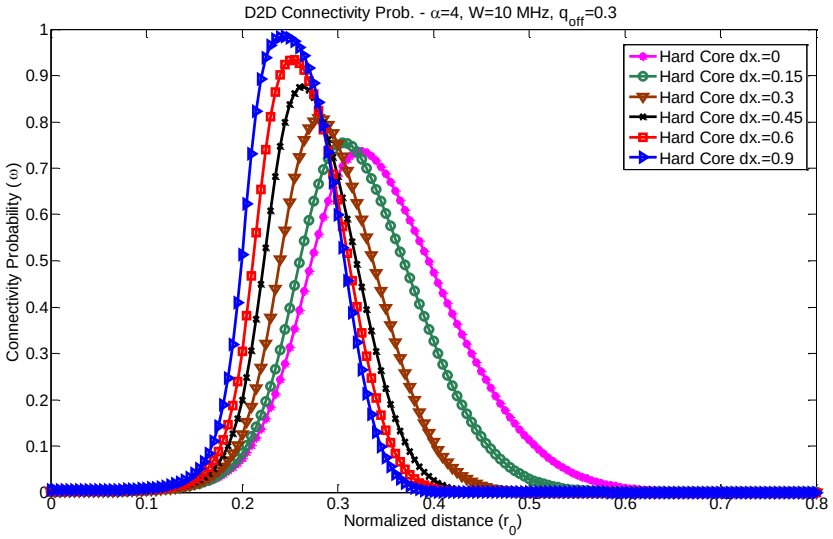

Figure 67: PLMU relaying with no CSI knowledge. Connectivity probability ω for α=4, Π_{on}=0.8 vs. Test link distance r_0 and different values of the Matern HC distance for the spatial PLMU process.

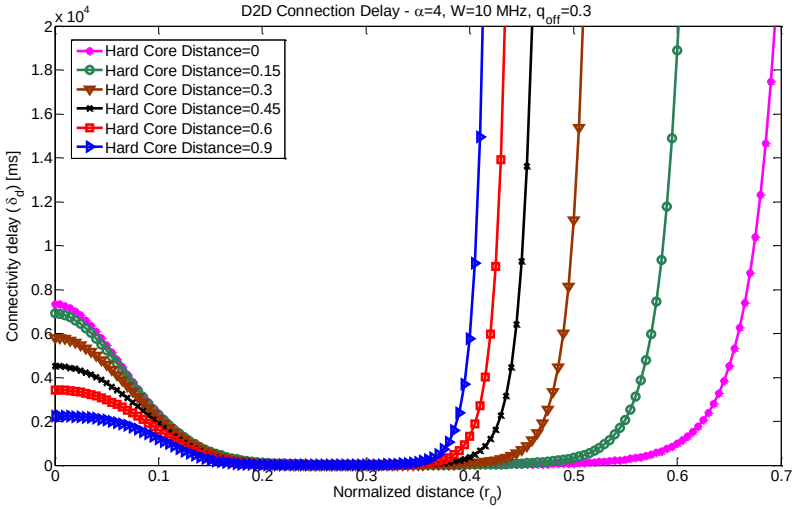

Figure 68: SIT for a UE trying to attach to a PLMU relay with no CSI knowledge, α=4, Π_{on}=0.8 vs. normalized test link distance r_0 and different values of the Matern HC distance of the spatial PLMU process.

PLMU+D2D relaying

The results for this case are not reported since they are very similar to the previous one. For this particular case of relay mode operation it can be concluded that the addition of an external source of interference does not change the results dramatically.

D2D+PLMU relaying

Results for the case in which both D2D and PLMU are deployed (along with cellular mode UEs) are shown in Figure 69 and Figure 70 for connectivity probability ω and SIT, respectively. Results are showed for α=4 and a normalized hard core distance r_m=0.03 for different values of the probability Π_{on}

a UE is active. Considering that the HC distance is selected to be a small value, the interference configuration is non-trivial given the possibly dense spatial distribution of terrestrial stations contributing to the interference environment. As discussed in detail already, the density of PLMUs depends on the original spatial density λ_p. The study pursues connectivity for a newcomer UEs doing the attempt to attach to a D2D network.

Figure 71 shows the connectivity probability versus the normalized test link distance r_0 as well as with respect to the Matern HC distance r_m. This result is presented here to give complete understanding of the connectivity probability ω with respect to all the system parameters. This figure shows that the case of D2D and PLMU relaying together is spatially more complex than what showed in Figure 65 - Figure 68 since a UE can connect to the AeNB only through a two-hop communication link. In specific, a UE can attach to a b-UE which is connected to a PLMU relay before reaching the AeNB. However, it must be noticed that the connectivity probability is still maximized in correspondence of a range of r_0 values. Such a range of values is similar to what showed in Figure 67 but in correspondence of Π_{on}=0.8 the connectivity probability is much smaller. In this case either the PLMU or the b-UE (or even both) could be in overloading conditions. Hence, three regions can be identified for connectivity also in this case. On the left hand side of the maximum, the connectivity probability grows but it is substantially higher than in the previous case in which only PLMUs are available as connectivity option. On the right hand side of the maximum, the connectivity probability decreases although with a less steep slope compared to the previous case. Furthermore, it is worth to point out that for small values of Π_{on} the connectivity probability is significantly high and it remains high across a large interval of r_0 values. The service interruption time SIT, which reflects the period of time a UE is forced to operate in complete isolation, behaves in way that depends on the connectivity probability. The SIT grows without bound and it becomes of order of tens of seconds. The main difference with respect to the case of PLMU only is that D2D networks could operate near the edge of the coverage area of the AeNB or in indoors, thus receiving potentially lower levels of interference on the access link (either with PLMU or b-UE) compared to other spatial configurations with the test receiver positioned in other locations of the area of interest. This evidence is also reflected by the hypothesis that in case UEs fall within the normalized cluster radius a of a PLMU they should try to attach to it.

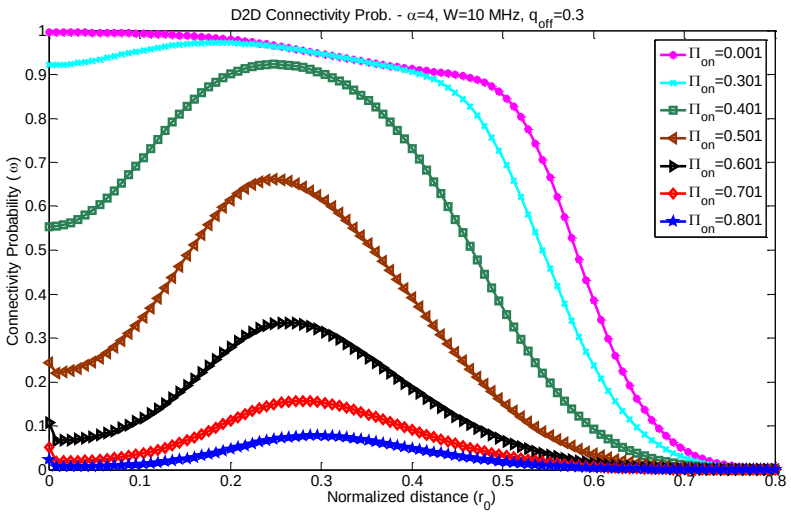

Figure 69: D2D and PLMU relaying with no CSI knowledge. Connectivity probability ω for the D2D network vs. normalized test link distance r_0, α=4, W=10 MHz and Matern HC distance r_m=0.03.

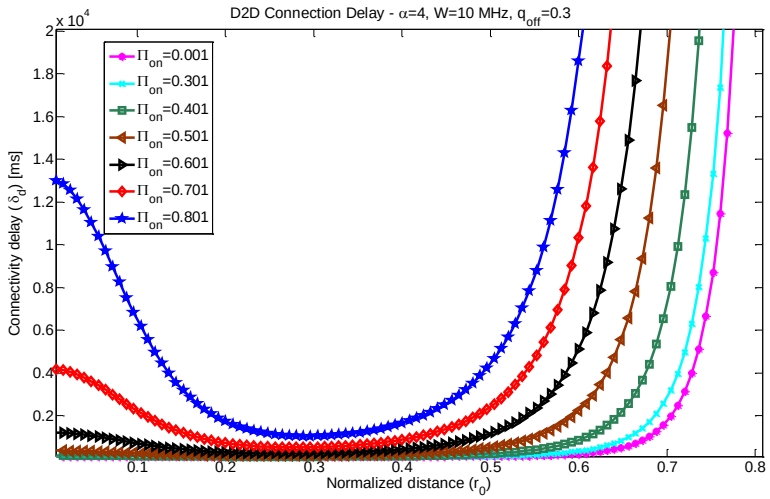

Figure 70: SIT for D2D and PLMU relaying with no CSI knowledge of a UE trying to attach to a D2D network vs. normalized test link distance (r_0), α=4, W=10 MHz and Matern HC distance r_m=0.03.

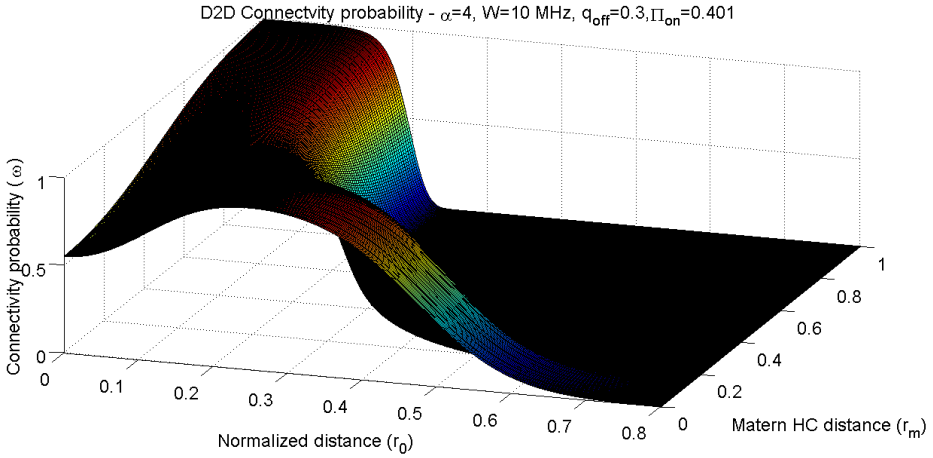

Figure 71: D2D and PLMU relaying with no CSI knowledge: probability ω versus the normalized test link distance (r_0) and Matern HC distance (r_m).

D2D+PLMU relaying+partial CSI knowledge

Results are shown in Figure 72 and Figure 73 for connectivity probability ω and SIT with path-loss exponent α=4 and normalized Matern hard core distance r_m=0.03, respectively. Figure 74 shows the connectivity probability versus the normalized test link distance r_0 and the Matern HC distance r_m. The latter figure is considered for completeness to show sensitivity to system parameters but also to highlight the difference with respect to the previous case of D2D and PLMU relying combined together without CSI knowledge. On the other hand, in this particular study case, it is assumed that both UEs and PLMUs have partial CSI knowledge in opposition to the previous cases in which no CSI information was available. The study pursues connectivity for a newcomer UE attaching to a D2D network. It is worth stressing that power control is applied by the devices already member of a network and not by newcomer UEs trying to attach for the first time to a b-UE. For the first two figures is assumed that PLMUs can be spatially dense depending on the initial intensity of the spatial PLMU process λ_p. CSI information is used here to apply power control and compensate the path-loss

attenuation of the radio signal between test transmitter and reference receiver (i.e. the UE trying to attach and a b-UE) but not the fading. Furthermore, CSI here is assumed to be perfectly up-to-date although incomplete. The only UEs which do apply any form of power control are those attached to the AeNB in cellular mode. Referring to Figure 72, it is important to emphasize that the shape of the connectivity probability ω is completely different from the previous cases. Indeed, if the previous cases highlighted the presence of three regions for connectivity, with power control, the connectivity probability is monotonically decreasing with the normalized test link distance r_0. Therefore, the probability is not any more maximized but it rather decreases as the distance inside the D2D cluster increases. The SIT in Figure 73 behaves accordingly to the connectivity probability but the figure shows that, depending on the value of the probability Π_{on} and for ample ranges of r_0, the delay can be reduced from tens of seconds (as showed in previous study cases for relay) to few seconds. Hence, power control, if applied by all interested parties, will greatly improve coexistence and will contribute to dramatically lower the SIT (at least up to some values of r_0). As soon as the probability UEs are active Π_{on} grows high, when power control is not applied, path-loss attenuation affecting the reference link and blocking events become predominant. It is clear that during the phase of attach a UE does not have sufficient information to tune the transmit power. The figures shown here provide an interesting and remarkable result which allows concluding that in complex scenarios in which interference would affect connectivity in a non-trivial manner due to the spatial configuration of radio transmitters, power control is essential to relieve problems connected with interference. This would require channel estimation operations possibly combined with location information as discussed in previous sections for the cognitive cycle performed by the FME. This operation, despite the clear benefits, might result complex although LTE provides specific reference signals that can facilitate its accomplishment.

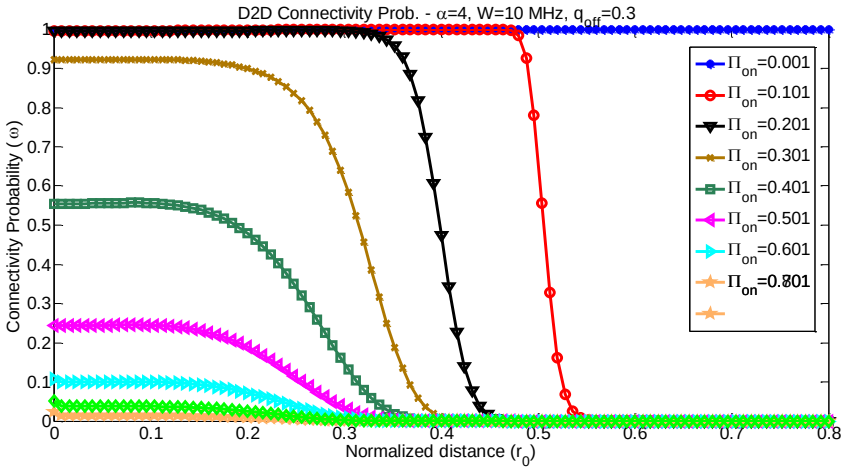

Figure 72: D2D and PLMU relaying with <u>partial</u> CSI knowledge for path-loss compensation. D2D network connectivity probability ω vs. normalized test link distance (r_0) with α=4, W=10 MHz and Matern HC distance r_m=0.03.

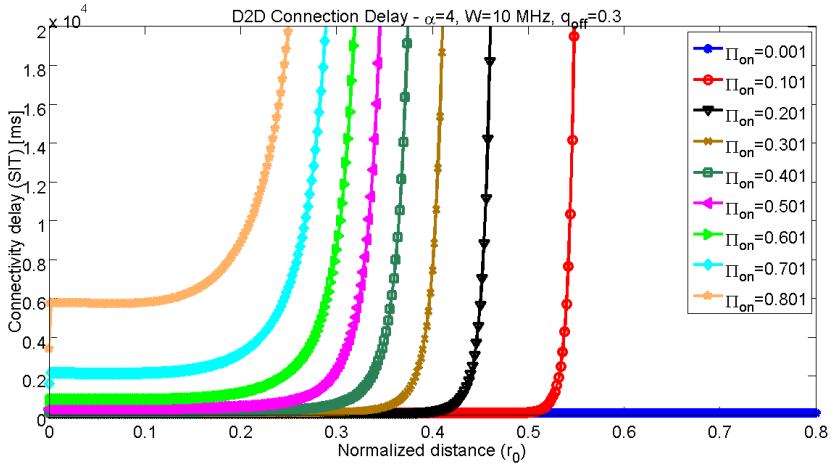

Figure 73: SIT for D2D and PLMU relaying with <u>partial</u> CSI knowledge and path-loss compensation for a UE trying to attach to a D2D network vs. normalized test link distance (r_0), α=4, W=10 MHz and Matern HC distance r_m=0.03.

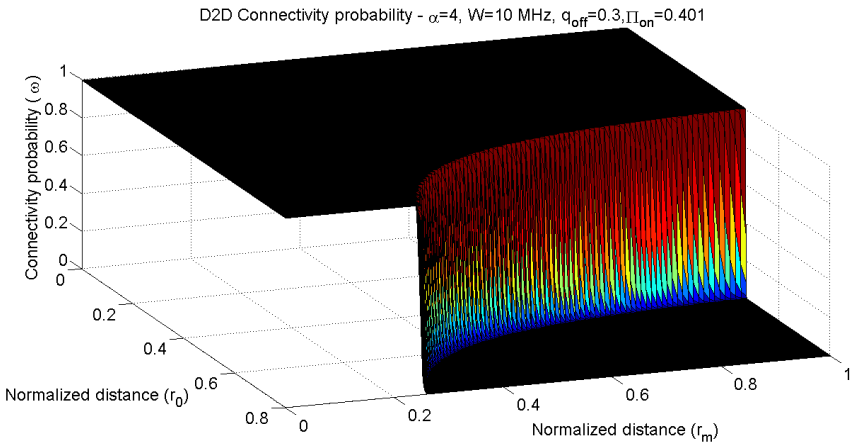

Figure 74: D2D and PLMU relaying with <u>partial</u> CSI knowledge for path-loss compensation: probability ω versus the normalized test link distance (r_0) and Matern HC distance (r_m).

<u>D2D+PLMU relay+perfect CSI knowledge</u>

For this case results are shown in Figure 75 and Figure 76 for the connectivity probability ω and SIT, respectively. The path-loss exponent is assumed α=4 and the normalized Matern hard core distance is assumed r_m=0.03. As before, results are showed varying the normalized test link distance r_0. Unlike the previous study in which only incomplete CSI knowledge was assumed, in this case PLMUs and UEs have complete and up-to-date CSI knowledge. Hence, power control is applied to compensate not only for the path-loss attenuation of the radio signal but for the Rayleigh fading as well. The study pursues connectivity for a newcomer UE attaching to a D2D network. As mentioned already, newcomer UEs do not apply power control since they might not possess all necessary information to do so. Power control is instead applied by UEs and PLMUs already engaged in relay networks but not by UEs attached to the AeNB in cellular mode. As it can be seen from the figures below, the behaviour is similar to what showed already in Figure 72 - Figure 74. The connectivity probability ω monotonically decreases with the increase of normalized distance r_0, whilst the SIT behaves

accordingly. Improvements can be observed in terms of connectivity probability and SIT, with the latter dropping from tens of seconds down to few seconds for some values of the probability Π_{on} UEs are active and for an ample range of r_0 values. For the particular numerical parameters selected, it can be observed that compensating also the fading brings small improvements with respect to the case in which only path-loss compensation is applied. This effect denotes that the path-loss attenuation of the radio signal affects significantly both interfering and useful signals, with this behaviour revealed also by the tight dependence from the choice of the path-loss exponent. Therefore, estimation of the channel possibly in combination with location information of the radio terminals can greatly improve communication performance through simple but effective power control mechanism. Such inputs could be fed into the cognitive cycle performed by the FME. It is however worth noticing that the acquisition of accurate location information is definitively not trivial and also channel estimation is quite a complex operation. Clearly, this latter aspect highlights the need of more fundamental research along this direction.

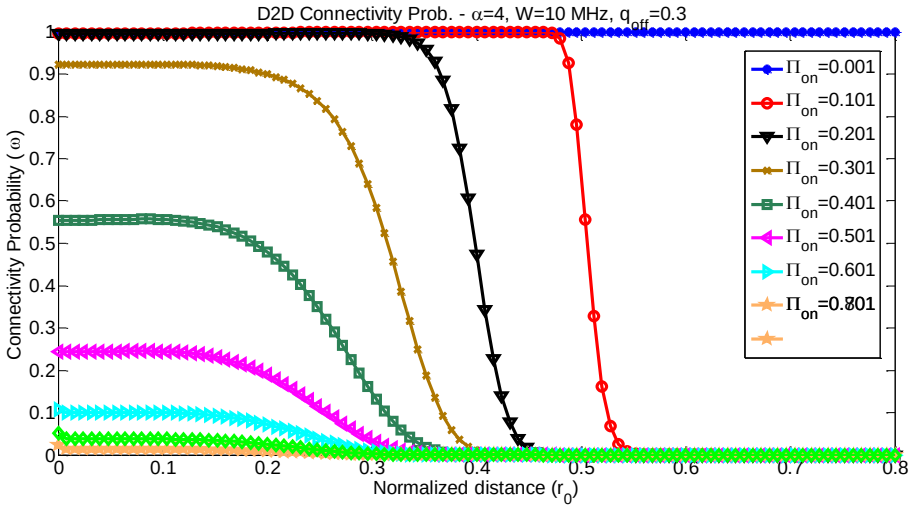

Figure 75: D2D and PLMU relaying with <u>perfect</u> CSI knowledge for path-loss and fading compensation. D2D network connectivity probability ω vs. the normalized test link distance with α=4, W=10 MHz and Matern HC distance r_m=0.03.

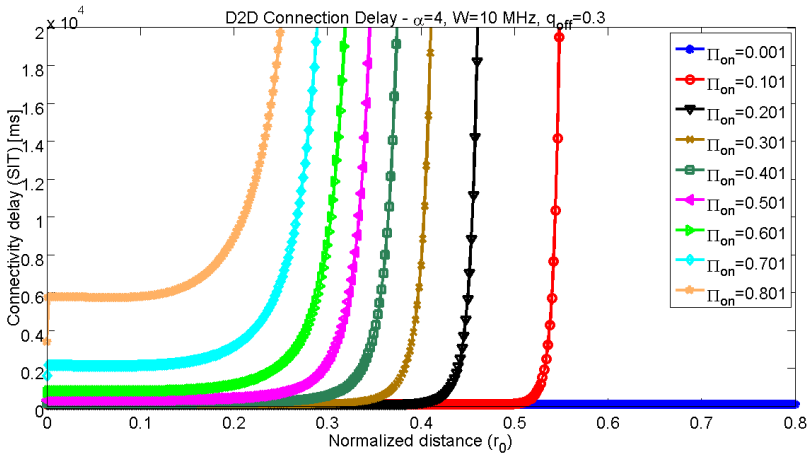

Figure 76: SIT for D2D and PLMU relaying with <u>perfect</u> CSI knowledge for path-loss and fading compensation for a UE trying to attach to a D2D network vs. normalized test link distance (r_0), α=4, W=10 MHz and Matern HC distance r_m=0.03.

4.3 **Conclusions**

In this section, we have presented protocol details for 4G relay networks deployed for the needs of first responders in ABSOLUTE scenarios. Two types of relay mode have been considered, namely PLMU relay mode (3GPP Type Ib) and D2D relay. Particular attention was paid to protocol additions for the D2D relay mode with respect to D2D protocol specifications provided in other ABSOLUTE deliverables. Meaningful interactions between the D2D-A inside FME, the activation and deactivation messages of D2D relay mode as well as interactions with other functional units of the Flexible Management Unit have been described. Starting from the obvious fact the LTE is a frequency reuse-1 system and that ABSOLUTE system prescribes the deployment of several options for bringing connectivity to the first responders, an in-depth study of the impact of the aggregate interference on the connectivity of both PLMU and D2D mode relay networks was conducted relying on the tool of stochastic geometry and in particular on the enlightening results shed by cluster point processes. The study showed that interference configuration is non-trivial in frequency reuse-1 radio systems. Using the interference characterization, connectivity analysis for both PLMU and D2D relay modes was done under different deployment conditions. In particular, the study showed connectivity probability and service interruption time for all the relevant cases. The study clearly showed that in complex spatial configurations even simple power control (in addition more advanced 3GPP self-organizing network techniques such as eICIC could be applied) on concurrent communications taking place in adjacent networks (i.e. inter-cell interference) can greatly help to improve overall connectivity inside a region of space.

Relay Mode	**Scenarios** [1]	**Use-cases** [1]	**Subsystem Architecture** [3]
PLMU Relay (no CSI)	Public Safety (Sect. 4.1) Temporary Events (Sect. 4.2)	ABS.UC.02/04/05/15/16	Public Safety Scenarios: Phases 3 and 4 Temporary Events Scenarios
PLMU+D2D relay (no CSI)	Public Safety (Sect. 4.1) Temporary Events (Sect. 4.2)	ABS.UC.02/04/05/15/16 + ABS.UC.21/22	Public Safety Scenarios: Phase 3 and 4 Temporary Events Scenario
D2D+PLMU Relay (with partial and perfect CSI)	Public Safety (Sect. 4.1) Temporary Events (Sect. 4.2)	ABS.UC.21/22 + ABS.UC.02/04/05/15/16	Public Safety Scenarios: Phases 3 and 4 Temporary Events Scenario

Table 9: Mapping of relays modes selected for connectivity analysis with ABSOLUTE use cases.

The general lesson that can be learned from previous studies is that ABSOLUTE equipment and communication networks other than the AeNB can be used after evaluating the conditions in each use case for both PLMU and D2D. In general, the maximization of the benefits for each solution is location and time dependent, it requires professional roll out of the equipment and automatic interference management techniques. The different ABSOLUTE use cases in which the study shown

throughout previous sections can be conveniently applied are extracted from [1] and summarized below.

- *Public Safety*: ABS.UC.02, ABS.UC.04, ABS.UC.05, ABS.UC.21 (D2D)
- *Temporary events*: ABS.UC.15, ABS.UC.16
- *Public Safety and temporary events*: ABS.UC.22 (D2D)

A more in-depth explanation of the relay modes studied in previous sections with ABSOLUTE use cases and subsystem architecture is shown in **Erreur ! Source du renvoi introuvable.**. In both public safety and temporary event use cases, PLMU and D2D communications and a combination thereof can be conveniently exploited with the primary goal of bringing connectivity to the first responders. The number of PLMU and D2D networks can be different and a fairly large number could be used concurrently. Both networks are subject to the constraints of each specific scenario. In all use cases that have been identified, as mentioned already, on top of identifying the best possible conditions (e.g., location) in which PLMU and D2D based communications can maximize their benefit, any time the interference environment becomes complex, interference management techniques are essentials. Indeed this includes D2D communication and PLMU based-communications as well as their mix within the same physical region.

5 Conclusions

As the follow-up work of the first deliverable D3.2.1 "*Initial Approaches for Opportunistic Relaying for Disasetr Relief and temporary Events*", the performance evaluation of the opportunistic relaying has been carried out and been presented in this deliverable. First, the models of Aerial-to-Terrestrial and Device-to-Device channels have been investigated. The ABSOLUTE channel model has been proposed for Aerial-to-Terrestrial links based on the ray-tracing methods, while WINNER II channel model has been selected to be applied for Device-to-Device communications according to the theoretical analyses and the real-world experimental measurements. Taking advantage of these channel models, the performance evaluation of the proposed algorithms was carried out and the performance results were obtained. According to the system architecture, the opportunistic relaying in ABSOLUTE can be categorized into D2D relaying and PLMU relaying. The former is based on the cooperation among D2D-enabled mobile terminals and the latter is more similar to the infrastructure-based relaying specified in LTE-A. Different technical aspects of opportunistic relaying have been studied in order to apply this technique for the disaster relief and emergency events in the ABSOLUTE scenarios. To be specific, the distributed power allocation between the source and relays has been proposed to maximize the end-to-end channel capacity over the cascaded relaying channel. The impact of feedback delay over Aerial-Terrestrial channel on the performance of opportunistic relaying has been analysed, and the results reveal that it substantially degrade the system performance. To combat the effect of feedback delay, a novel opportunistic relaying scheme, called the opportunistic space-time coding, has been proposed. The analytical and numerical results justified that the proposed scheme can effectively alleviate the impact of feedback delay with a reasonable cost. Besides, the game-theoretic relay selection method with the joint minimization of energy consumption and feedback delay, the power-control scheme to mitigate co-channel interference, have been proposed and been evaluated. And, the energy efficiency and the coverage area of the opportunistic relaying in the ABSOLUTE scenarios have been analysed. In final, the integration of LTE-A system and the proposed opportunistic relaying scheme has been discussed. The required modifications on the specifications of LTE/LTE-A standards were depicted in this deliverable, which are useful to the standardization in 3GPP and the implementation works.

In summary, the analytical, simulated and experimental results reveal that the opportunistic relaying can play the key role in ABSOLUTE to improve the reliability and resilience of communication links in the scenarios of disaster relief and temporary events. The proposed algorithms are well fit for the application scenarios and can achieve the good performance.

Bibliography

[1] FP7-ICT-2011-8-318632-ABSOLUTE, "D2.1: Use Cases Definition and Scenarios Description," ABSOLUTE project, March 2014.

[2] FP7-ICT-2011-8-318632-ABSOLUTE, "D3.2.1: Initial Approaches for Opportunistic Relaying for Disasetr Relief and temporary Events," ABSOLUTE Project, 2013.

[3] FP7-ICT-2011-8-318632-ABSOLUTE, "D2.5.2: Architecture Reference Model," ABSOLUTE project, Nov. 2013.

[4] FP7-ICT-2011-8-318632-ABSOLUTE, "D2.6.1: System-wide simulations planning document," in *ABSOLUTE project*, 2013.

[5] FP7-ICT-2011-8-318632-ABSOLUTE, "D2.3: Aerial Platforms Study," in *ABSOLUTE project*, 2013.

[6] FP7-ICT-2011-8-318632-ABSOLUTE, "D5.1.1: LTE-A AeNodeB related implementation requirement specifications for cognitive LTE extension," in *ABSOLUTE project*, 2013.

[7] FP7-ICT-2011-8-318632-ABSOLUTE, "D5.2.1: Portable land mobile rapid deployment unit specification," in *ABSOLUTE project*, 2013.

[8] FP7-ICT-2011-8-318632-ABSOLUTE, "D3.4.3: Performance Analysis of Direct Mode LTE Communications," in *ABSOLUTE project*, 2014.

[9] FP7-ICT-2011-8-318632-ABSOLUTE, "D3.1.1: Requirements and Specification for Spectrum Awareness," in *ABSOLUTE project*, 2013.

[10] FP7-ICT-2011-8-318632-ABSOLUTE, "D3.3.1: Initial approaches for Cognitive Spectrum Assignment using Distributed Artificial Intelligence," in *ABSOLUTE project*, 2013.

[11] A. Al-Hourani, S. Chandrasekharan and S. Kandeepan, "Path Loss Sudy for Millimeter Wave Device-to-Device Communications in Urban Environment," in *IEEE International Conference on Communications Workshops (ICC)*, Sydney, 2014.

[12] A. Al-Hourani, S. Kandeepan and A. Jamalipour, "Modeling air-to-ground path loss for low altitude platforms in urban environments," in *Global Communications Conference (GLOBECOM)*, Austin, 2014.

[13] ITU-R, "Propagation data and prediction methods required for the design of terrestrial broadband millimetric radio access systems operating in a frequency range of about 20-50 GHz," International Telecommunication Union, 2003.

[14] J. Holis and P. Pechac, "Elevation Dependent Shadowing Model for Mobile Communications via High Altitude Platforms inBuilt-Up Areas," *IEEE TRANSACTIONS ON ANTENNAS AND PROPAGATION*, vol. 56, no. 4, pp. 1078-1084, 2008.

[15] A. Saakian, Radio Wave Propagation Fundamentals, Artech House, 2011.

[16] Intel, "Discussion on UE-UE channel model for studies on D2D proximity services," 3GPP R1-130924, Chicage, USA,, Apr. 2013.

[17] W. I. Project, "Matlab SW Documentation of WIM 2 Model," Aug. 2008.

[18] W. Jang, L. Goratti, A. Hourani, O. Araft and S. Kandeepan, "Initial Approaches for Opportunistic Relaying for Disasetr Relief and temporary Events," FP7 ABSOLUTE Project, 2013.

[19] W. I. Project, "D1.1.1: WINNER II Interim Channel Models," Nov. 2006.

[20] S. Sesia, I. Toufik and B. Matthew, LTE The UMTS Long Term Evolution: From Theory to Practice, Second Edition, Wiley, 2011.

[21] L. Goratti, I. Bucaille, T. Rasheed and k. Gomez, "D3.4.3: Performance Analysis of Direct Mode LTE Communications," FP& ABSOLUTE Project, Oct. 2014.

[22] S. Cotton, "A statistical characterization of shadowed device-to-device communications in an indoor environment," in *IEEE 8th European Conference on Antennas and Propagation (EuCAP)*, 2014.

[23] S. Cotton, "Channel measurements of device-to-device communications in an urban outdoor environment," in *IEEE XXXIth General Assembly and Scientific Symposium (URSI GASS)*, 2014.

[24] S. Cotton, "Human Body Shadowing in Cellular Device-to-Device Communications: Channel Modeling Using the Shadowed k-mew Fading Model," *IEEE Journal on Selected Areas in Communications*, vol. PP, no. 99, pp. 1-9, 2015.

[25] T. Rappaport, Wireless Communication: Principles and Practice, New Jersey: Prentice Hall, 1996.

[26] M. Gudmundson, "Correlation model for shadow fading in mobile radio systems," *IEEE Electronic Letters*, vol. 27, no. 23, pp. 2145-2146, 1991.

[27] J. Karedal, F. Tufvesson, N. Czink, A. Paier, C. Dumard, T. Zemen, C. Mecklenbrauker and A. Molisch, "A Geometry-based stochastic MIMO model for Vehicle-to-Vehicle communications," *IEEE Transactions on Wireless Communications*, vol. 8, no. 7, pp. 3646-3657, July 2009.

[28] R1-130924, "Discussion on UE-UE channel model for studies on D2D proximity services," Intel, Chicage, USA, Apr. 2013.

[29] Wei Jiang, Hanwen Cao, and Thomas Kaiser, "Power Optimal Allocation in Decode-and-Forward Opportunistic Relaying," in *Proc. of IEEE WCNC 2014*, Istanbul, 2014.

[30] Wei Jiang, Hanwen Cao, L. Goratti, M. Wiemeler, and Thomas Kaiser, "Opportunistic Relaying over Aerial-to-Terrestrial and Device-to-Device Radio Channels," in *Proc. of IEEE ICC 2014*, Sydney, 2014.

[31] D. J. L. e. al., "An overview of limited feedback in wireless communication systems," *IEEE J.*

Sel. Areas Commun., vol. 26, no. 8, p. 1341–1365, Oct. 2008.

[32] Wei Jiang, Hanwen Cao, and Thomas Kaiser, "An MGF-Based Performance Analysis of Opportunistic Relay Selection with Outdated CSI," in *Proc. of IEEE VTC 2014 spring*, Seoul, South Korea, 18-21th May 2014.

[33] Y. Ma and S. Pasupathy, "Efficient performance evaluation for generalized selection combining on generalized fading channels," *IEEE Trans. Wireless Commun.,* vol. 3, no. 1, p. 29–34, Jan. 2004.

[34] M.-S. Alouini and M. K. Simon, "An MGF-based performance analysis of generalized selection combining over Rayleigh fading channels," *IEEE Trans. Commun.,* vol. 48, no. 3, p. 401–415, Mar. 2000.

[35] S. S. Ikki and M. H. Ahmed, "Performance analysis of generalized selection combining for decode-and-forward cooperative-diversity networks," in *IEEE 72nd Vehicular Tech. Conf. (VTC)'2010-Fall*, Ottawa, Canada, 2010.

[36] S. S. Ikki and M. H. Ahmed, "Performance analysis of generalized selection combining for amplify-and-forward cooperative-diversity networks," in *IEEE Int. Commun. Conf. (ICC'09)*, Dresden, Germany, 2009.

[37] Wei Jiang, Hanwen Cao, and Thomas Kaiser, "Analysis of Generalized Selection Combining in Cooperative Networks with Outdated CSI," in *Proc. of IEEE WCNC 2014*, Istanbul, Turkey, 6-9th April 2014.

[38] L. Xiao and X. Dong, "Unified analysis of generalized selection combining with normalized threshold test per branch," *IEEE Trans. Wireless Commun.,* vol. 5, no. 8, p. 2153–2163, Aug. 2006.

[39] S. M. Alamouti, "A simple transmit diversity technique for wireless communications," *IEEE J. Sel. Areas Commun.,* vol. 16, no. 8, p. 1451–1458, Oct. 1998.

[40] Wei Jiang, Hanwen Cao, and Thomas Kaiser, "Opportunistic Space-Time Coding to Exploit Cooperative Diversity in Fast-Fading Channels," in *Proc. of IEEE ICC 2014*, Sydney, Australia, 10-14th June 2014.

[41] Wei Jiang, Hanwen Cao, Mielemer Wiemeler, and Thomas Kaiser, "Achieving High Reliability in Aerial-Terrestrial Networks: Opportunistic Space-Time Coding," in *Proc. of EuCNC*, Bologne, Italy, 23-25th June, 2014.

[42] A. Al-Hourani, S. Kandeepan and E. Hossain, "Relay-Assisted Device-to-Device Communication: A Stochastic Analysis of Energy Saving," *Submitted to IEEE Transcations on Wireless Communications,* 2015.

[43] A. Al-Hourani, S. Kandeepan and A. Jamalipour, "Stochastic Geometry Study on Device to Device Communication as a Disaster Relief Solution," *Submitted to IEEE Transactions on Vehicular Technology,* 2015.

[44] L. Daewon, G. Y. Li and T. Suwen, "Intercell Interference Coordination for LTE Systems," *IEEE*

Transactions on Vehicular Technology, vol. 62, no. 9, p. 4408–4420, 2013.

[45] D. Lopez-Perez, I. Guvenc, G. de la Roche, M. Kountouris, T. Quek and J. Zhang, "Enhanced Intercell Interference Coordination Challenges in Heterogeneous Networks"," *IEEE Wireless Communications,* vol. 18, no. 3, pp. 22-30, 2011.

[46] M. Z. Win, P. C. Pinto and a. L. A. Shepp, "A Mathematical Theory of Network Interference and Its Applications," *Proceedings of the IEEE,* vol. 97, pp. 205-230, 2009.

[47] M. Haenggi, Stochastic Geometry for Wireless Networks, Cambride, 2013.

[48] S. Kandeepan, S. Jayaweera and R. Fedrizzi, "Power-Trading in Wireless Communications: A Cooperative Networking Business Model," *IEEE Transactions on Wireless Communications,* vol. 11, no. 5, pp. 1872-1880, May 2012.

[49] S. Kandeepan, C. Saradhi, M. Filo and R. Piesiewicz, "Delay Analysis of Cooperative Communication with Opportunistic Relay Access," in *Vehicular Technology Conference (VTC Spring)* , Yokohama, 2011.

[50] R. Chen, A. J.G, H. R.W and G. A., "Uplink Power Control in Multi-Cell Spatial Multiplexing Wireless Systems," *IEEE Transactions on Wireless Communications, Volume:6 , Issue: 7,* pp. 2700-2711, 2007.

[51] V. Chandrasekhar, J. G. Andrews, T. Muharemovict, Z. Shen and A. Gatherer, "Power control in two-tier femtocell networks," *IEEE Transactions on Wireless Communications, Volume:8 , Issue: 8,* pp. 4316-4328, 2009.

[52] Hui Yu, Lin Gao, Z. Li, X. Wang and E. Hossain, "Pricing for Uplink Power Control in Cognitive Radio Networks," *IEEE Transactions on Vehicular Technology, , Volume:59 , Issue: 4,* pp. 1769-1778, 2010.

[53] M. Monemi, Neyriz, M. Rasti and E. Hossain, "On Joint Power and Admission Control in Underlay Cellular Cognitive Radio Networks," *IEEE Transactions on Wireless Communications, Volume:14 , Issue: 1,,* pp. 265-278, 2014.

[54] S. Kandeepan, S. Jayaweera and R. Fedrizzi, "Power-Trading in Wireless Communications:A Cooperative Networking Business Model," *IEEE TRANSACTIONS ON WIRELESS COMMUNICATIONS, VOL. 11, NO. 5,,* pp. 1872-1880, MAY 2012.

[55] G. Fodor and N. Reider, "A Distributed Power Control Scheme for Cellular Network Assisted D2D Communications," in *IEEE GLOBECOM,* Houston, 2011.

[56] A. Padani, G. Fodor, G. Miao and M. Belleschi, "Near-Optimal Practical Power Control Schemes for D2D Communications in Cellular Networks," in *EuCNC,* Bologna, 2014.

[57] A. Project, "D4.1.4: Detailed Network and Protocol Architecture: Final Version," March 2015.

[58] C. Hoymann, W. Chen, J. Montojo, A. Golitschek, C. Koutsimanis and X. Shen, "Relaying Operation in 3GPP LTE: Challenges and Solutions," *IEEE Commun. Magazine,* vol. 50, no. 2, pp. 156 - 162, Feb. 2012.

[59] I. Bucaille, L. Goratti and T. Rasheed, "Algorithms and Protocol SPecifications for LTE D2D Communications," FP7 ABSOLUTE Project, Nov. 2013.

[60] K. G. R. F. a. T. R. L. Goratti, "A novel Device-to-Device Communication Protocol for Public Safety Applications," in *in Proc., Intl Workshop on D2D With and Without Infrastructure, GLOBECOM*, 2013.

[61] G. S. K. G. a. G. B. L. Goratti, "Connectivity and Security in a D2D Communication Protocol for Public Safety Applications," in *in Proc., IEEE Intl. Conf. ISWCS*, Aug. 2014.

[62] E. Sousa and J. Silvester, "Optimum Transmission Ranges in a Direct-Sequence Spread-Spectrum Multihop Packet Radio Network," *IEEE J. on Sel. Areas in Commun.*, vol. 8, no. 5, pp. 762-771, june 1990.

[63] R. Nelson and L. Kleirock, "The Spatial Capacity of a Slotted ALOHA Multihop Packet Radio Network with Capture," *IEEE Trans. on Commun.*, Vols. vol. COM-32, no. 6, pp. 684-694, June 1984.

[64] J. Ilos and D. Hatzinakos, "Analytic Alpha-Stable Noise Modeling in a Poisson Field of Interferers or Scatterers," *IEEE trans. on Signal Processing*, vol. 46, no. 6, pp. 1601-1611, June 1984.

[65] M. Haenggi, J. G. Andrews, F. Baccelli, O. Dousse and M. Franceschetti, "Stochastic geometry and random graphs for the analysis and design of wireless networks," *IEEE J. Sel. Areas in Commun.*, vol. 27, no. 7, pp. 1029-1046, Sept. 2009.

[66] M. Z. Win, C. P. Pinto and L. A. Shepp, "AMathematical Theory of Network Interference and Its Applications," *Proceeding fo the IEEE*, vol. 97, no. 2, pp. 205-230, Feb. 2009.

[67] S. Srinivasa and M. Haenggi, "MODELING INTERFERENCE IN FINITE UNIFORMLY RANDOM NETWORKS," *IEEE Trans. on Veh. Technol.*, vol. 59, no. 2, pp. 940-949, 2009.

[68] M. Wildemeersch, T. Quek, C. Slump and A. Rabbachin, "Cognitive Small Cell Networks: Energy Efficiency and Trade-Offs," *IEEE Trans. on Commun.*, vol. 61, no. 9, pp. 4016-4029, Sept. 2013.

[69] D. J. Daley and D. Vere-Jones, An Introduction to the Theory of Point Processes: Volume I: Elementary Theory and Methods, Second Edition, Springer, 2002.

[70] D. Stoyan, W. S. Kendall and J. Mecke, Stochastic Geometry and its Applications, Second Edition, John Wiley and Sons , 2008.

[71] M. Haenggi, "On Distances in Uniformly Random Networks," *IEEE Trans. on Inf. Theory*, vol. 51, no. 10, pp. 3584-3586, Oct. 2005.

[72] R. K. Ganti and M. Haenggi, "Interference and Outage in CLustered Wireless Ad Hoc Networks," *IEEE Trans. on Inf. Theory*, vol. 55, no. 9, pp. 4067-4086, Sept. 2009.

[73] M. Haenggi and G. R. Krishna, "Interference in Large Wireless Networks," *Foundations and Trends in Networking*, vol. 3, no. 2, 2008.

[74] C.-H. Lee and M. Haenggi, "Interference and Outage in Poisson Cognitive Networks," *IEEE Trans. on Wireless Commun.*, vol. 11, no. 4, pp. 1392-1401, April 2012.

[75] L. Reynaud and e. al, "D2.1: Use Cases Definition and Scenarios Description," March 2014.

Acknowledgement

This document has been produced in the context of the ABSOLUTE project. ABSOLUTE consortium would like to acknowledge that the research leading to these results has received funding from the European Commission's Seventh Framework Programme (FP7-2011-8) under the Grant Agreement FP7-ICT-318632.